

RESEARCH



SIMPLIFIED CPT PERFORMANCE-BASED ASSESSMENT OF LIQUEFACTION AND EFFECTS: TASKS 8, 9, & 10

Prepared For:

Utah Department of Transportation
Research and Innovation Division

Submitted By:

Brigham Young University
Department of Civil and Environmental
Engineering

Authored By:

Kevin W. Franke
Jingwen He
Jenny L. Blonquist

**Year 2, Quarter 3 Update Report for the
TPF-5(338) Technical Advisory Committee
September 2019**

DISCLAIMER

The authors alone are responsible for the preparation and accuracy of the information, data, analysis, discussions, recommendations, and conclusions presented herein. The contents do not necessarily reflect the views, opinions, endorsements, or policies of the Utah Department of Transportation or the U.S. Department of Transportation. The Utah Department of Transportation makes no representation or warranty of any kind, and assumes no liability therefore.

ACKNOWLEDGMENTS

The authors acknowledge the Utah, Oregon, South Carolina, and Connecticut Departments of Transportation for funding this research for pooled fund study TPF-5(338). The views and opinions presented in this report represent those of its authors, and may not represent those of the state agencies funding this research.

TECHNICAL REPORT ABSTRACT

1. Report No. NA	2. Government Accession No. NA	3. Recipient's Catalog No. NA	
4. Title and Subtitle SIMPLIFIED CPT PERFORMANCE-BASED ASSESSMENT OF LIQUEFACTION AND EFFECTS: TASKS 8, 9, & 10		5. Report Date September 2019	
		6. Performing Organization Code NA	
7. Author(s) Kevin W. Franke, Jingwen He, Jenny L. Blonquist		8. Performing Organization Report No. NA	
9. Performing Organization Name and Address Brigham Young University Department of Civil and Environmental Engineering 368 Clyde Building Provo-UT 84602-4009		10. Work Unit No. 4207415D	
		11. Contract or Grant No. 16-9826	
12. Sponsoring Agency Name and Address Utah Department of Transportation 4501 South 2700 West P.O. Box 148410 Salt Lake City, UT 84114-8410		13. Type of Report & Period Covered Year 2 TAC Report April 2019 – September 2019	
		14. Sponsoring Agency Code PIC No. UT15.402	
15. Supplementary Notes Prepared in cooperation with the Utah Department of Transportation and the U.S. Department of Transportation, Federal Highway Administration			
16. Abstract The purpose of the research being performed is to provide the benefit of the full performance-based probabilistic earthquake hazard analysis, without requiring special software, training, and experience. To do this, simplified models of liquefaction triggering, post-liquefaction settlement, and lateral spread displacement that approximate the results of the full probabilistic analysis were developed. The goal of these simplified methods are to be user-friendly, requiring only simple calculations and a liquefaction parameter map. The simplified procedures are based on the Boulanger and Idriss (2014) probabilistic liquefaction triggering model, the Ku et. al (2010) (probabilistic version of Robertson and Wride (2009)) for liquefaction triggering; Juang et al. (2013) for post-liquefaction settlements; and lastly, Zhang et al (2004) for lateral spread displacement. This report details the development of the liquefaction parameter maps and provides a comparison of the simplified method and pseudo-probabilistic method.			
17. Key Words Lateral Spread Displacements, Liquefaction Triggering, Post-Liquefaction Settlements, Performance-based Engineering Reference Maps, Simplified Models, Seismic Hazards		18. Distribution Statement Not restricted. Available through: UDOT Research Division 4501 South 2700 West P.O. Box 148410 Salt Lake City, UT 84114-8410 www.udot.utah.gov/go/research	
23. Registrant's Seal NA			
19. Security Classification (of this report) Unclassified	20. Security Classification (of this page) Unclassified	21. No. of Pages 123	22. Price NA

TABLE OF CONTENTS

LIST OF TABLES	6
LIST OF FIGURES	7
UNIT CONVERSION FACTORS	9
LIST OF TERMS.....	10
EXECUTIVE SUMMARY	11
1.0 INTRODUCTION.....	12
1.1 Problem Statement	12
1.2 Objectives	12
1.3 Scope	12
2.0 REFERENCE PARAMETER MAPS	14
2.1 Reference Profile.....	14
2.2 Development of Reference Parameter Maps	15
2.3 Grid Spacing Study	15
2.4 Create a List of Grid Points	20
2.5 Perform Full Performance-Based Analysis at the Grid Points	21
2.6 Create Contours Based on Interpolated Values	21
2.7 Summary.....	23
3.0 COMPARISON STUDY.....	23
3.1 Overview.....	23
3.2 Locations and Profiles	23
3.3 Comparison with the Pseudo-Probabilistic Procedure	24
3.4 Liquefaction Triggering Comparison.....	25
3.4.1 Ku et al. (2012) Comparison Results.....	25
3.4.2 Boulanger and Idriss (2014) Comparison Results	25
3.5 Post-Liquefaction Settlement Comparison	29
3.5.1 Post-Liquefaction Settlement Comparison Results using Boulanger and Idriss (2014)	29
3.5.2 Post-Liquefaction Settlement Comparison Results using Ku et al. (2012).....	31
3.6 Discussion.....	32
3.7 Lateral Spread Comparison Results	35

3.7.1 Lateral Spread Comparison Results using Zhang et al. (2004) with Boulanger and Idriss (2004).....	35
3.7.2 Lateral Spread Comparison Results using Zhang et al. (2004) with Ku et al. (2012)..	37
3.8 Comparison with the Deterministic Procedure	39
3.8.1 Locations and Profiles.....	39
3.8.2 Liquefaction Triggering Comparison	41
3.8.3 Robertson and Wride Comparison Results	42
3.8.4 Boulanger and Idriss (2014) Comparison Results	43
3.8.5 Post-Liquefaction Settlement Comparison (Ishihara and Yoshimine (1992))	44
3.8.6 Lateral Spread Comparison Results (Zhang et al. (2004)).....	45
3.9 Summary	46
4.0 CONCLUSIONS.....	47
4.1 Summary	47
4.2 Limitations and Challenges	47
REFERENCES	48
A. APPENDIX.....	49

LIST OF TABLES

Table 2-1. Proposed Optimum Grid Spacings within a <i>PGA</i> Range for a) <i>CSR%</i> , b) q_{req} , and c) ϵ_v and γ_{max}	20
Table 3-1. Sites Selected for Comparison Study	24
Table 3-2. NGA model weights used in the deterministic procedure.	40
Table 3-3. Input variables used in the deterministic models (a_{max} calculated using F_{pga} from AASHTO code).	41

LIST OF FIGURES

Figure 2-1. Reference Soil Profile	14
Figure 2-2. PGA Hazard Map ($T_R=2475$ years) after USGS 2014.....	16
Figure 2-3. Range of <i>PGA</i> Values for Cities Included in Grid Spacing Study	16
Figure 2-4. Layout of Grid Points Centered on a City’s Anchor Point (Ulmer, 2015).....	17
Figure 2-5. Correlation between <i>PGA</i> and Optimum Grid Spacing for <i>CSR%</i> [Boulanger and Idriss (2014)]	18
Figure 2-6. Correlation between <i>PGA</i> and Optimum Grid Spacing for q_{req} [Ku et al. (2012)]	18
Figure 2-7. Correlation between <i>PGA</i> and Optimum Grid Spacing for ϵ_v and γ_{max} [Boulanger and Idriss (2014)]	19
Figure 2-8. Correlation between <i>PGA</i> and Optimum Grid Spacing for ϵ_v and γ_{max} [Ku et al. (2012)].....	19
Figure 2-9. Location of Grid Points for Oregon with <i>PGA</i> Color Zones in Background.....	21
Figure 2-10. Sample Kriging Raster for Oregon	22
Figure 2-11. Sample Contour map for Oregon.....	22
Figure 3-1. Comparison Results for the Ku et al. (2012) Triggering Model for (a) q_{req} , (b), FS_L , and (c) <i>CSR%</i>	27
Figure 3-2. Comparison Results for the Boulanger and Idriss (2014) Triggering Model for (a) <i>CSR%</i> , (b), FS_L , and (c) q_{req}	28
Figure 3-3. Settlement Comparison Results using the Boulanger and Idriss (2014) Triggering Model for Sites with $PGA < 0.2 g$ (for All Return Periods)	30
Figure 3-4. Settlement Comparison Results using the Boulanger and Idriss (2014) Triggering Model for Sites with $PGA \geq 0.2g$ (for All Return Periods).....	30
Figure 3-5. Settlement Comparison Results using the Ku et al. (2012) Triggering Model for Sites with $PGA < 0.2 g$ (for All Return Periods)	31
Figure 3-6. Settlement Comparison Results using the Ku et al. (2012) Triggering Model for Sites with $PGA \geq 0.2g$ (for All Return Periods).....	32
Figure 3-7. Ishihara and Yoshimine (1992) Method for Determining Volumetric Strain	33
Figure 3-8. Lateral Spread Comparison Results using the Boulanger and Idriss (2014) Triggering Model for Sites with $PGA < 0.2g$ (for All Return Periods).....	35

Figure 3-9. Lateral Spread Comparison Results using the Boulanger and Idriss (2014) Triggering Model for Sites with $PGA \geq 0.2g$ (for All Return Periods).....	36
Figure 3-10. Lateral Spread Comparison Results using the Ku et al. (2012) Triggering Model for Sites with $PGA < 0.2g$ (for All Return Periods)	38
Figure 3-11. Lateral Spread Comparison Results using the Ku et al. (2012) Triggering Model for Sites with $PGA \geq 0.2g$ (for All Return Periods)	38
Figure 3-12. Soil Profile used for the deterministic comparison study.....	40
Figure 3-13. Comparison of deterministic and simplified performance-based values of q_{req}	42
Figure 3-14. Comparison of deterministic and simplified performance-based values of FS_L	42
Figure 3-15. Comparison of deterministic and simplified performance-based values of $CSR\%$..	42
Figure 3-16. Comparison of deterministic and simplified performance-based values of q_{req}	43
Figure 3-17. Comparison of deterministic and simplified performance-based values of FS_L	43
Figure 3-18. Comparison of deterministic and simplified performance-based values of $CSR\%$..	43
Figure 3-19. Comparison of deterministic and simplified performance-based vertical strains using the Robertson and Wride (2009) model.	44
Figure 3-20. Comparison of deterministic and performance-based vertical strains using the Boulanger and Idriss (2014) model.....	44
Figure 3-21. Comparison of deterministic and simplified performance-based maximum strains using the Robertson and Wride (2009) model.	45
Figure 3-22. Comparison of deterministic and simplified performance-based maximum strains using the Boulanger and Idriss (2014) model.....	45

UNIT CONVERSION FACTORS

SI* (MODERN METRIC) CONVERSION FACTORS				
APPROXIMATE CONVERSIONS TO SI UNITS				
Symbol	When You Know	Multiply By	To Find	Symbol
LENGTH				
in	inches	25.4	millimeters	mm
ft	feet	0.305	meters	m
yd	yards	0.914	meters	m
mi	miles	1.61	kilometers	km
AREA				
in ²	square inches	645.2	square millimeters	mm ²
ft ²	square feet	0.093	square meters	m ²
yd ²	square yard	0.836	square meters	m ²
ac	acres	0.405	hectares	ha
mi ²	square miles	2.59	square kilometers	km ²
VOLUME				
fl oz	fluid ounces	29.57	milliliters	mL
gal	gallons	3.785	liters	L
ft ³	cubic feet	0.028	cubic meters	m ³
yd ³	cubic yards	0.765	cubic meters	m ³
NOTE: volumes greater than 1000 L shall be shown in m ³				
MASS				
oz	ounces	28.35	grams	g
lb	pounds	0.454	kilograms	kg
T	short tons (2000 lb)	0.907	megagrams (or "metric ton")	Mg (or "t")
TEMPERATURE (exact degrees)				
°F	Fahrenheit	5 (F-32)/9 or (F-32)/1.8	Celsius	°C
ILLUMINATION				
fc	foot-candles	10.76	lux	lx
fl	foot-Lamberts	3.426	candela/m ²	cd/m ²
FORCE and PRESSURE or STRESS				
lbf	poundforce	4.45	newtons	N
lbf/in ²	poundforce per square inch	6.89	kilopascals	kPa
APPROXIMATE CONVERSIONS FROM SI UNITS				
Symbol	When You Know	Multiply By	To Find	Symbol
LENGTH				
mm	millimeters	0.039	inches	in
m	meters	3.28	feet	ft
m	meters	1.09	yards	yd
km	kilometers	0.621	miles	mi
AREA				
mm ²	square millimeters	0.0016	square inches	in ²
m ²	square meters	10.764	square feet	ft ²
m ²	square meters	1.195	square yards	yd ²
ha	hectares	2.47	acres	ac
km ²	square kilometers	0.386	square miles	mi ²
VOLUME				
mL	milliliters	0.034	fluid ounces	fl oz
L	liters	0.264	gallons	gal
m ³	cubic meters	35.314	cubic feet	ft ³
m ³	cubic meters	1.307	cubic yards	yd ³
MASS				
g	grams	0.035	ounces	oz
kg	kilograms	2.202	pounds	lb
Mg (or "t")	megagrams (or "metric ton")	1.103	short tons (2000 lb)	T
TEMPERATURE (exact degrees)				
°C	Celsius	1.8C+32	Fahrenheit	°F
ILLUMINATION				
lx	lux	0.0929	foot-candles	fc
cd/m ²	candela/m ²	0.2919	foot-Lamberts	fl
FORCE and PRESSURE or STRESS				
N	newtons	0.225	poundforce	lbf
kPa	kilopascals	0.145	poundforce per square inch	lbf/in ²

*SI is the symbol for the International System of Units. (Adapted from FHWA report template, Revised March 2003)

LIST OF TERMS

Liquefaction Triggering Terms

CSR^{ref}	uniform hazard estimate of CSR associated with the reference soil profile
CSR^{site}	site-specific uniform hazard estimate of CSR
FS_L	factor of safety against liquefaction triggering
M_w	mean moment magnitude
q_{req}	CPT resistance required to resist or prevent liquefaction
q_{req}^{ref}	uniform hazard estimate of q_{req} associated with the reference soil profile
P_a	atmospheric pressure (1 atm, 101.3 kPa, 0.2116 psf)
PGA	peak ground acceleration
CPT	Cone Penetration Test

Post-Liquefaction Settlement Terms

ε_v	vertical strain
ε_v^{ref}	vertical strain for the reference soil profile

Lateral Spread Displacement Terms

γ_{max}	maximum cyclic shear strain
γ_{max}^{ref}	horizontal strain for the reference soil profile
γ_{max}^{site}	site-specific horizontal strain

EXECUTIVE SUMMARY

The purpose of the research presented is to provide the benefit of the full performance-based probabilistic liquefaction hazard analysis with the cone penetration test (CPT), but without requiring special software, training in performance-based earthquake engineering, or experience with probabilistic methods. To accomplish this purpose, simplified performance-based procedures for predicting liquefaction triggering, post-liquefaction settlement, and lateral spread displacements and that approximate the results of the full probabilistic analysis are developed. These simplified procedures are based on a few governing predictive models and a liquefaction reference parameter map that has been developed through this research. In the previous report, the derivation and validation of these simplified procedures were presented (Tasks 5, 6, and 7). This report discusses and presents the development of the liquefaction reference parameter maps and a comparison of the simplified and pseudo-probabilistic (i.e., conventional) procedures to the full performance-based procedure, addressing Tasks 8, 9, & 10 of the TPF-5(338) research contract.

A major component of the simplified procedure is the use of liquefaction reference parameter maps. A grid spacing study is conducted to understand how the spacing of points could potentially bias the predicted results from the procedure. Once the optimum grid spacing is identified, *CPTLiquefY* is used to perform full-probabilistic calculations for a reference soil profile at each grid point. The maps are then developed in ArcMap. Using the completed reference maps, a comparison study between the simplified procedure and pseudo-probabilistic procedure is conducted for points throughout Utah, South Carolina, Connecticut, and Oregon.

1.0 INTRODUCTION

1.1 Problem Statement

The purpose of Tasks 8 through 10 of this project are to develop the liquefaction reference parameter maps for the states involved in this study, evaluate the simplified performance-based procedures against conventional (i.e., pseudo-probabilistic) and full performance-based procedures, and create a practical design methodology for incorporating the simplified procedures.

1.2 Objectives

The objective of this report is to detail the creation of the reference parameter maps and compare the results of the simplified procedure to the pseudo-probabilistic and full performance-based procedures. The main objectives of this report include:

- Describe the development of the reference parameter maps
- Compare the simplified procedure and the pseudo-probabilistic procedure to the full performance-based procedure.
- Provide a recommended methodology for implementing the simplified procedure in practice

These objectives specifically address Tasks 8, 9, & 10 of the TPF-5(338) research contract.

1.3 Scope

This phase of research focuses on the development of the reference parameter maps and a comparison study of the simplified procedure to the pseudo-probabilistic procedure. The completed maps are presented in the appendix.

This report is organized to include the following Sections:

- Development of Reference Parameter Maps
- Comparison of Simplified Procedure and Pseudo-Probabilistic Procedure
- Recommended Methodology for Applying the Simplified Procedure
- Conclusions

- Appendices

2.0 REFERENCE PARAMETER MAPS

The purpose of this Section is to detail the steps to develop the reference parameter maps. These maps provide values for a reference soil profile at a set of grid points for a return period of interest.

2.1 Reference Profile

Liquefaction parameter maps are an important part of the simplified procedure because they provide the same benefits of a site-specific, full performance-based analysis, but do not require the user to perform the associated probabilistic calculations. The maps are based on a reference soil profile that is presented in Figure 2-1. This soil profile was used for the simplified procedure in Tasks 5-7 and is similar to the one originally introduced by Mayfield et al. (2010). The goal of the liquefaction parameter maps is to allow users to interpolate reference values for use in the simplified performance-based procedures developed through this research. For the simplified liquefaction triggering procedures using Boulanger and Idriss (2014) and Ku et al (2012), respective reference values for q_{req} and CSR are mapped in this study. For the simplified settlement and lateral spread procedures using Juang et al. (2013) and Zhang et al. (2004), respectively, respective reference values of ε_v (%) and γ_{max} (%) are mapped in this study. These computed reference parameter values are distinguished using the terms q_{req}^{ref} , CSR^{ref} , ε_v^{ref} (%), and γ_{max}^{ref} (%) .

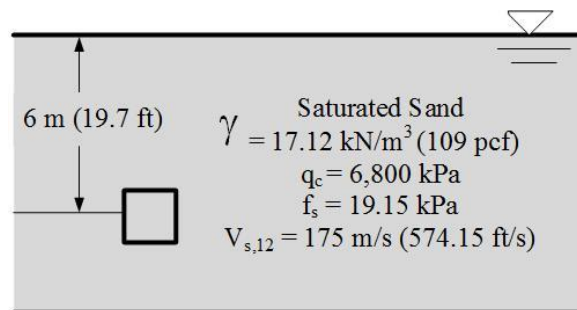


Figure 2-1. Reference Soil Profile

2.2 Development of Reference Parameter Maps

The reference parameter maps are created following these steps:

1. Perform grid spacing study
2. Create a list of grid points
3. Run full performance-based analysis on grid points using *CPTLiquefY*
4. Create contours based on interpolated values

Steps 2 and 4 are accomplished using software developed by ESRI, ArcMap. The following Sections will describe each step.

2.3 Grid Spacing Study

The distance between grid points is important in determining the accuracy of the parameter maps. From the grid points, contours are developed by interpolating the values between grid points. If the grid points are too far apart, the maps may not be able to capture potential seismic gradients over areas with complex seismic sources. If the grid points are too close, the maps become computationally expensive to develop. Therefore, a study to optimize the grid spacing to an acceptable maximum interpolative error through correlation with mapped probabilistic seismic hazard (i.e., ground motions) is warranted.

Based on previous research involving simplified procedures for the SPT (Ulmer, 2015; Ekstrom, 2015; Error, 2017), researchers observed that areas of high mapped *PGA* hazard would require smaller grid spacing, and areas of low mapped *PGA* hazard would allow larger grid spacing. We also evaluated if this observation was true for the CPT. The USGS 2014 *PGA* hazard map (Figure 2-2) is chosen for this study. The map divides the United States into areas of different *PGA* ranges that are represented by different color bins. Thirty-six cities representing different *PGA* ranges are chosen from various locations across the United States as part of the study and are presented in Figure 2-3 with their corresponding *PGA* values corresponding to a return period of 2475 years. The goal of the grid spacing study is to find an optimal grid spacing for each *PGA* color bin on the map.

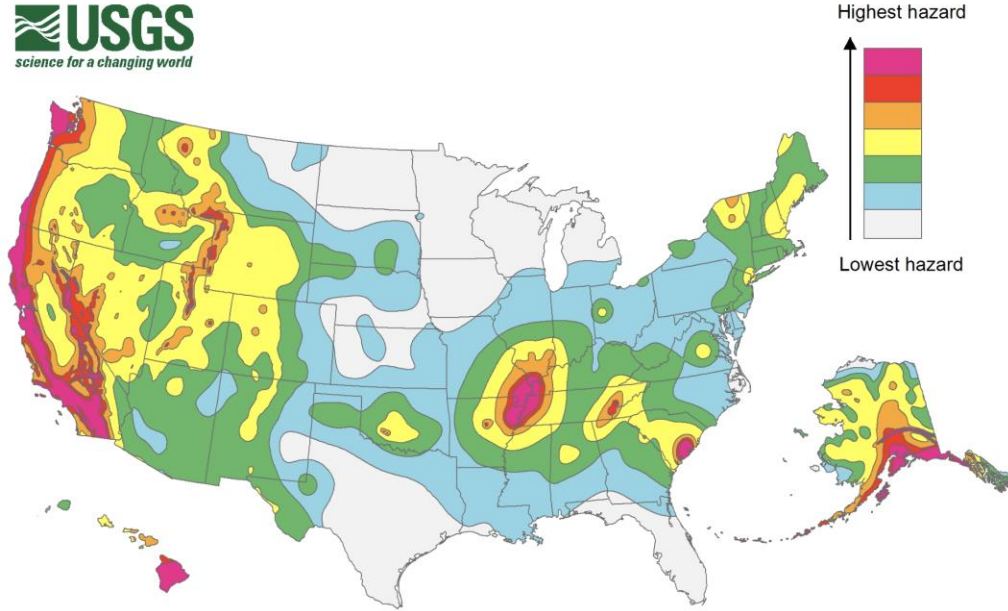


Figure 2-2. PGA Hazard Map ($T_R=2475$ years) after USGS 2014

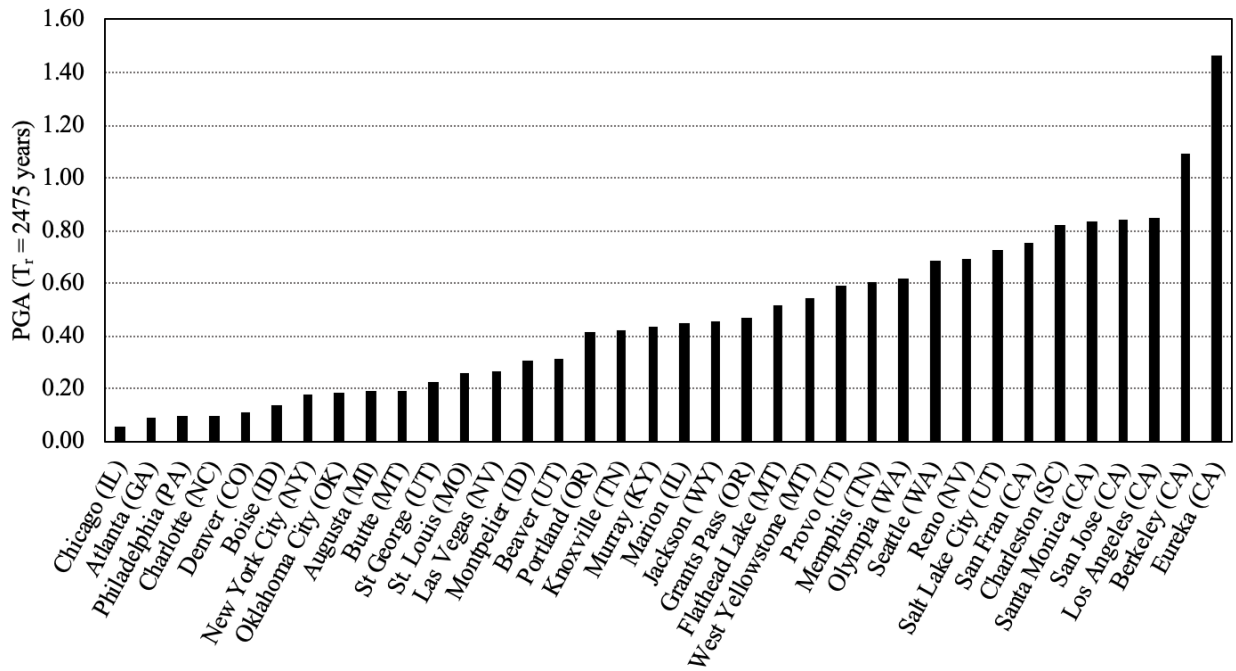


Figure 2-3. Range of PGA Values for Cities Included in Grid Spacing Study

Following the framework and methodology described by Ulmer (2015), the grid spacing study is preformed using square grids with the site of interest as the anchor (or center) point in the center, as shown in Figure 2-4. To determine the maximum grid spacing, corner points are created with spacings of 1, 2, 4, 8, 16, 25, and 50 km.

Full performance-based analyses are performed at the center point and four corner points using *CPTLiquefy*. The average of the four corner points are then compared to the center point. An error is then calculated as the absolute difference between the interpolated and the anchor value. For this study, the optimum grid spacing is defined as the smallest grid spacing that yields a selected maximum percent error. The maximum percent error is selected as 5% (for *CSR%* and q_{req}) and 0.1% (for e_v and γ_{max}) based on engineering judgment.

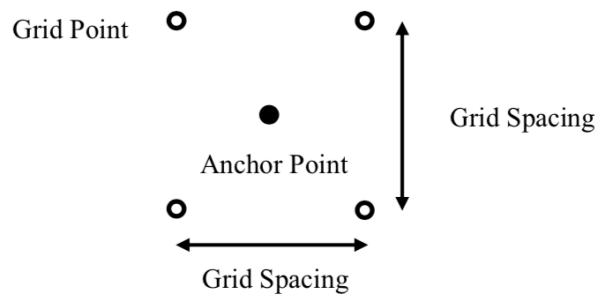


Figure 2-4. Layout of Grid Points Centered on a City’s Anchor Point (Ulmer, 2015)

The resulting correlations between optimum grid spacing and *PGA* for all the evaluated cities are shown for the Boulanger and Idriss (2014) and Ku et al. (2012) triggering models in Figure 2-5 through Figure 2-8. The vertical dashed lines indicate different *PGA* ranges (or color bins) from the USGS 2014 *PGA* hazard map. The horizontal blue lines are chosen to define the apparent lower bound of the grid spacing for each range. Table 2-1a, b, and c summarize the optimum grid spacing of each *PGA* range for *CSR%*, q_{req} , e_v , and γ_{max} , respectively

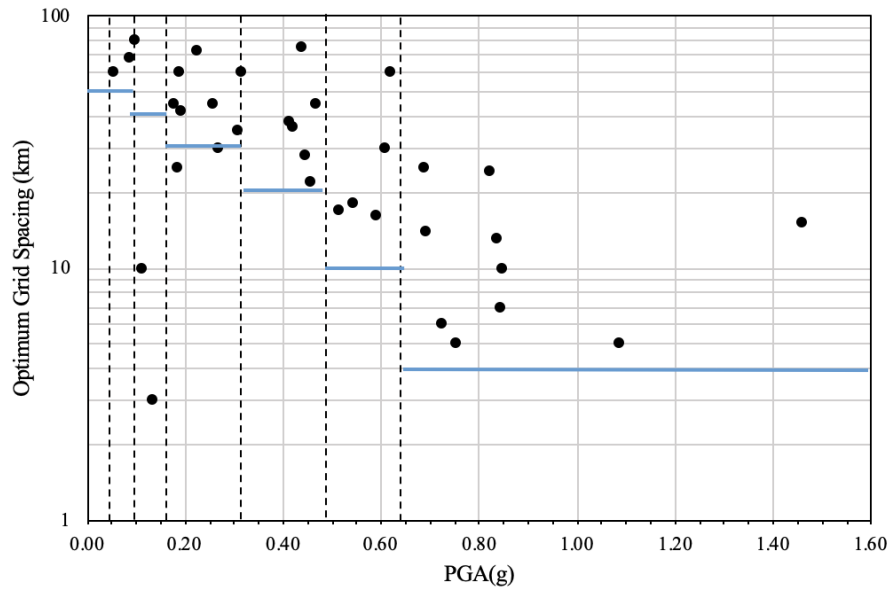


Figure 2-5. Correlation between PGA and Optimum Grid Spacing for CSR% [Boulanger and Idriss (2014)]

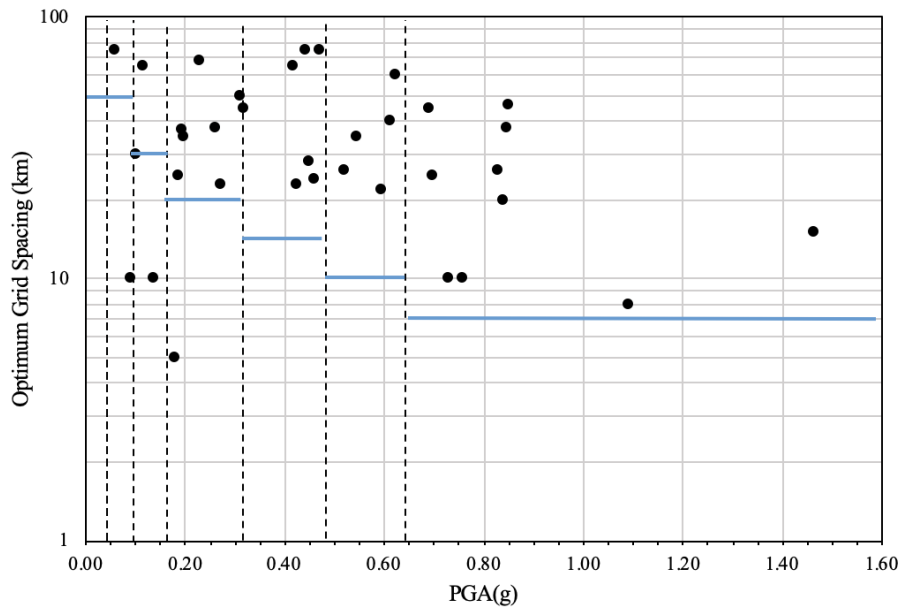


Figure 2-6. Correlation between PGA and Optimum Grid Spacing for q_{req} [Ku et al. (2012)]

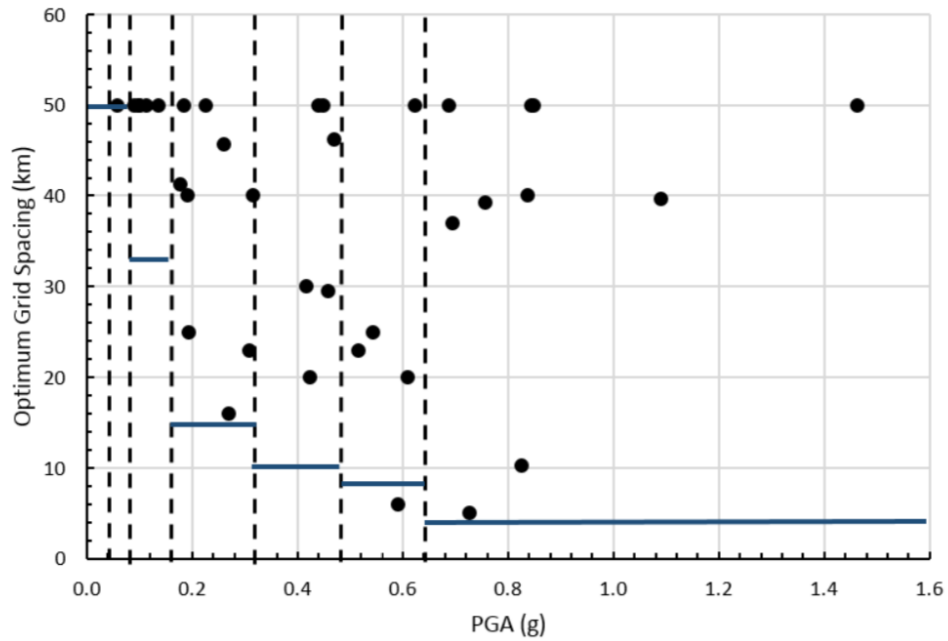


Figure 2-7. Correlation between PGA and Optimum Grid Spacing for ϵ_v and γ_{max}
[Boulanger and Idriss (2014)]

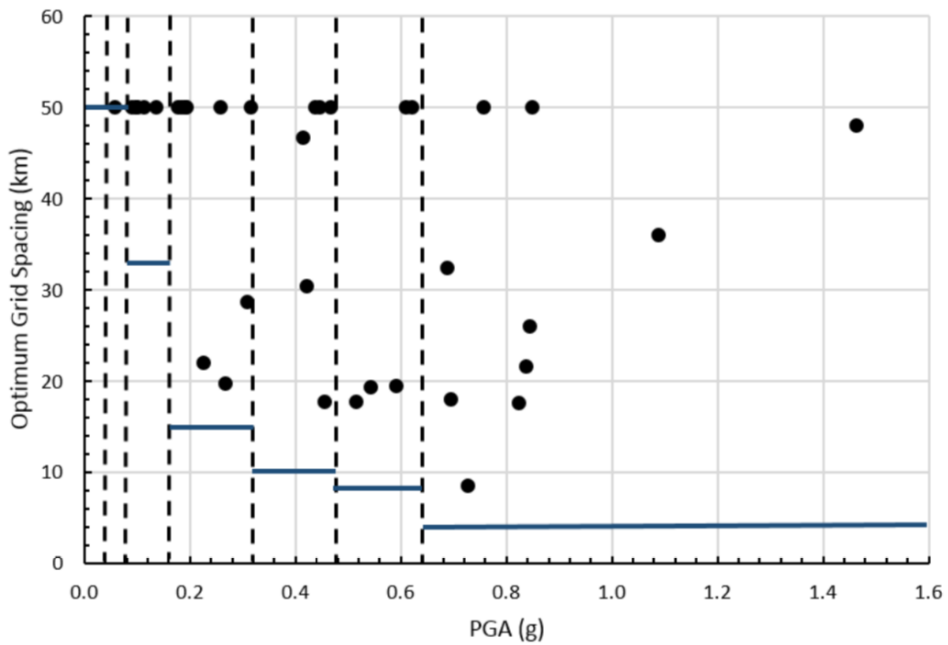


Figure 2-8. Correlation between PGA and Optimum Grid Spacing for ϵ_v and γ_{max} [Ku et al. (2012)]

Table 2-1. Proposed Optimum Grid Spacings within a *PGA* Range for a) *CSR%*, b) q_{req} , and c) ϵ_v and γ_{max}

a) <i>CSR%</i>				b) q_{req}			
PGA	Color	Spacing (km)	Spacing (mi)	PGA	Color	Spacing (km)	Spacing (mi)
0-0.04	Gray	50	31.1	0-0.04	Gray	50	31.1
0.04-0.08	Blue	50	31.1	0.04-0.08	Blue	50	31.1
0.06-0.16	Green	40	24.9	0.06-0.16	Green	30	18.6
0.16-0.32	Yellow	30	18.6	0.16-0.32	Yellow	20	12.4
0.32-0.48	Orange	20	12.4	0.32-0.48	Orange	15	9.3
0.48-0.64	Red	10	6.2	0.48-0.64	Red	10	6.2
0.64+	Pink	4	2.5	0.64+	Pink	8	5.0

c) ϵ_v and γ_{max}			
PGA	Color	Spacing (km)	Spacing (mi)
0-0.04	Gray	50	31.1
0.04-0.08	Blue	50	31.1
0.06-0.16	Green	33	20.5
0.16-0.32	Yellow	15	9.3
0.32-0.48	Orange	10	6.2
0.48-0.64	Red	8	5
0.64+	Pink	4	2.5

2.4 Create a List of Grid Points

In ArcMap, polygons are created to represent each *PGA* range or color bin presented in Figure 2-2. Within each polygon, the *Fishnet* tool is used to create the grid points based on the determined grid spacing. The latitude and longitude of each of these grid points are combined into one text file to be analyzed. Figure 2-9 shows an example of Oregon with optimally spaced grid points and the corresponding USGS *PGA* color zones.

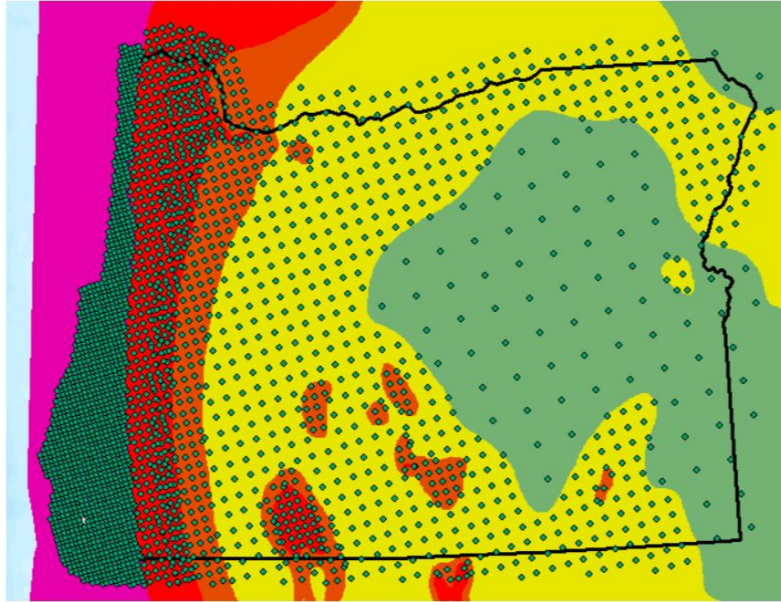


Figure 2-9. Location of Grid Points for Oregon with PGA Color Zones in Background

2.5 Perform Full Performance-Based Analysis at the Grid Points

Using *CPTLiquefY* (Franke et al., 2017), full performance-based liquefaction hazard analysis calculations are performed at each of the mapped grid points using the reference soil profile presented in Figure 2-1. These analyses are performed at return periods of 475, 1039, and 2475 years for both the Boulanger and Idriss (2014) and Ku et al. (2012) triggering models. Resulting liquefaction hazard curves computed at the grid points are then compiled and formatted in preparation for map creation.

2.6 Create Contours Based on Interpolated Values

Before creating the contours, the values from Section 2.5 must be interpolated. Using the *Kriging* tool in ArcMap, values between the grid points are interpolated to generate a raster that can be used to create contours. An example of a raster for Oregon is shown in Figure 2-10 where varying shades of grey represent higher or lower values. Darker shades represent lower relative reference parameter values.

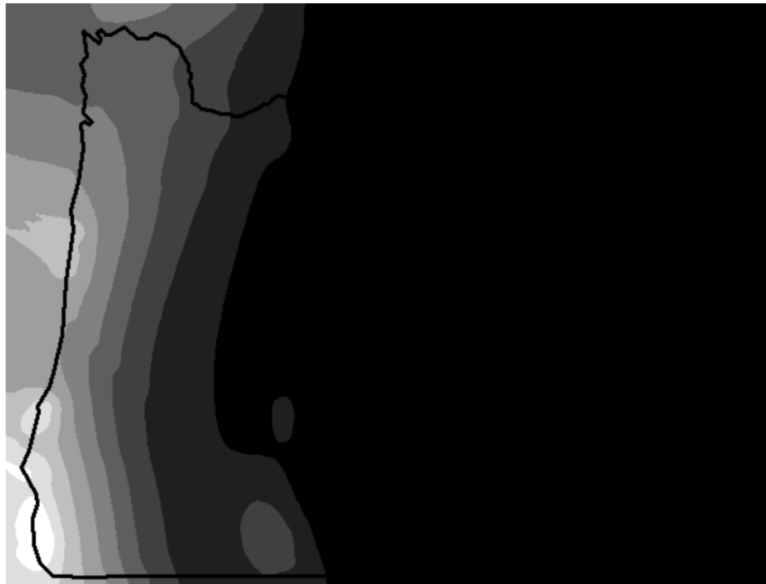


Figure 2-10. Sample Kriging Raster for Oregon

Once the raster is created, the *Contour* tool is used to create contour lines at any specified interval. For higher seismicity areas, smaller contour intervals are used to show the detailed changes, while lower seismicity areas used larger contour intervals. Figure 2-11 shows an example contour map for Oregon.

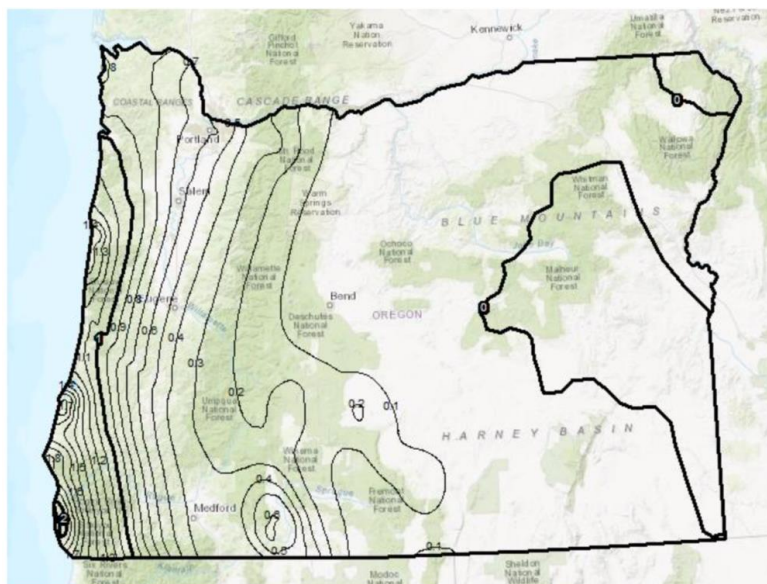


Figure 2-11. Sample Contour map for Oregon

2.7 Summary

Using the steps outlined in Section 2.2, reference parameter maps are created for Utah, South Carolina, Oregon, and Connecticut for the return periods of 475, 1039, and 2475 years. These maps are a crucial part of the simplified liquefaction hazard analysis procedure for the CPT because they provide a user-friendly process to quantify seismic loading at a targeted return period and they allow for the close approximation of values computed using the sophisticated full performance-based liquefaction hazard analysis.

3.0 COMPARISON STUDY

3.1 Overview

This section presents the comparison between the simplified performance-based liquefaction hazard analysis developed through this research, the deterministic, and conventional pseudo-probabilistic liquefaction hazard analysis routinely applied in engineering practice and currently prescribed by AASHTO code. The ultimate goal of these comparisons is to demonstrate that the simplified performance-based analysis is a much more reliable and accurate approximation of the full performance-based analysis than the conventional deterministic and pseudo-probabilistic analyses. This section compares the accuracy between the simplified performance-based analysis results and the conventional pseudo-probabilistic analysis results.

3.2 Locations and Profiles

Twelve locations were chosen at random from among cities in the four participating states (Utah, South Carolina, Connecticut, and Oregon), resulting in three selected sites in each state. Out of the 12 sites, 8 sites have a *PGA* less than 0.2g, with the remaining sites having *PGA* values greater than 0.2g. We have defined low seismicity areas as cities with a *PGA* less than 0.2g and areas of moderate to high seismicity as cities with a *PGA* greater than or equal to 0.2g. Table 3-1 presents a list of the 12 sites and their corresponding latitudes and longitudes, *PGA*, and mean

magnitude at the 2475-year return period (from the deaggregation results of the 2014 USGS seismic hazard maps). For the simplified performance-based analyses in this study, the developed reference parameter maps are used to interpolate reference parameter values rather than calculate them directly at each of the selected sites. Such interpolation allows for evaluation of the potential bias that could be introduced through interpolation with the reference parameter maps.

Table 3-1. Sites Selected for Comparison Study

State	City	Latitude	Longitude	PGA	Mw
Utah	Salt Lake City	40.755	-111.898	0.726	6.8
	Fillmore	38.964	-112.339	0.178	6.31
	Moab	38.598	-109.547	0.1	5.74
Oregon	Eugene	44.075	-123.132	0.398	8.68
	Bend	44.079	-121.306	0.175	7.13
	Mt. Vernon	44.405	-119.113	0.139	6.24
Connecticut	Hartford	41.779	-72.666	0.099	5.64
	Stamford	41.077	-73.565	0.161	5.49
	New Haven	41.317	-72.963	0.111	5.58
South Carolina	Charleston	32.821	-79.943	0.945	6.77
	Columbia	34.037	-81.038	0.189	6.14
	Florence	34.222	-79.754	0.161	6.81

3.3 Comparison with the Pseudo-Probabilistic Procedure

This section will present the results of the comparison study for the Boulanger and Idriss (2014) and Ku et al. (2012) models. For each plot, computed results for the full performance-based procedure that we are attempting to approximate are plotted on the x-axis. Computed results for the pseudo-probabilistic and simplified performance-based procedures are plotted on the y-axis. The comparison between the simplified performance-based procedure and the pseudo-probabilistic procedure is based on two main criteria: the slopes of the trend line and the R^2 values. The data with a trend line slope closer to 1.0 is considered to better approximate the full-performance based procedure on average, and the data with the larger R^2 value is more consistent in its predictions. This section will present the plots for liquefaction triggering, settlement, and lateral spread.

3.4 Liquefaction Triggering Comparison

3.4.1 Ku et al. (2012) Comparison Results

The comparison results for the Ku et al. (2012) triggering model are presented in Figure 3-1 using different representations of liquefaction triggering hazard: q_{req} (a), FS_L (b), and $CSR\%$ (c). Each plot contains the results of all three analyzed return periods. An initial observation of the comparison plots shows that the pseudo-probabilistic procedure exhibits much greater scatter than the simplified procedure. For all three parameters shown, the simplified procedure achieved a much higher R^2 value than the pseudo-probabilistic procedure. The average R^2 values are 0.7 (pseudo-probabilistic) and 0.975 (simplified), suggesting that, on average, the simplified performance-based procedure is a better overall approximation of the full performance-based procedure. For the slope of the trend lines, the average slopes are 1.04 (pseudo-probabilistic) and 0.981 (simplified). This means, on average, the pseudo-probabilistic procedure over-predicts the full performance-based procedure by 4% (with the exception of the FS_L) and the simplified procedure is underpredicting by 1.9%. Based on the results, the proposed simplified performance-based procedure incorporating the Ku et al (2012) triggering model provides a more consistent and precise approximation of the full performance-based procedure than the conventional pseudo-probabilistic procedure.

3.4.2 Boulanger and Idriss (2014) Comparison Results

The comparison results for the Boulanger and Idriss (2014) triggering model are presented in Figure 3-2 for $CSR\%$ (a), FS_L (b), and q_{req} (c), also showing all three return periods. Similar to the Ku et al. (2012) comparison results, the pseudo-probabilistic procedure also visually exhibits much greater scatter than the simplified procedure. By comparing average R^2 values, the simplified procedure had a higher average R^2 value (0.987) than the pseudo-probabilistic procedure (0.921). In the case of q_{req} , the pseudo-probabilistic has a slightly greater R^2 value (0.977) than the simplified procedure (0.975), however such small differences are negligible. The average slopes of the trendlines are 1.016 (pseudo-probabilistic) and 0.996 (simplified), meaning the pseudo-probabilistic procedure overestimates the full performance-based method by 1.62% and the simplified procedure underpredicts by 0.42%. Overall, a similar conclusion can be made that the

proposed performance-based procedure incorporating the Boulanger and Idriss (2014) triggering model also provides a more consistent and equally precise approximation of the full performance-based procedure as the conventional pseudo-probabilistic procedure.

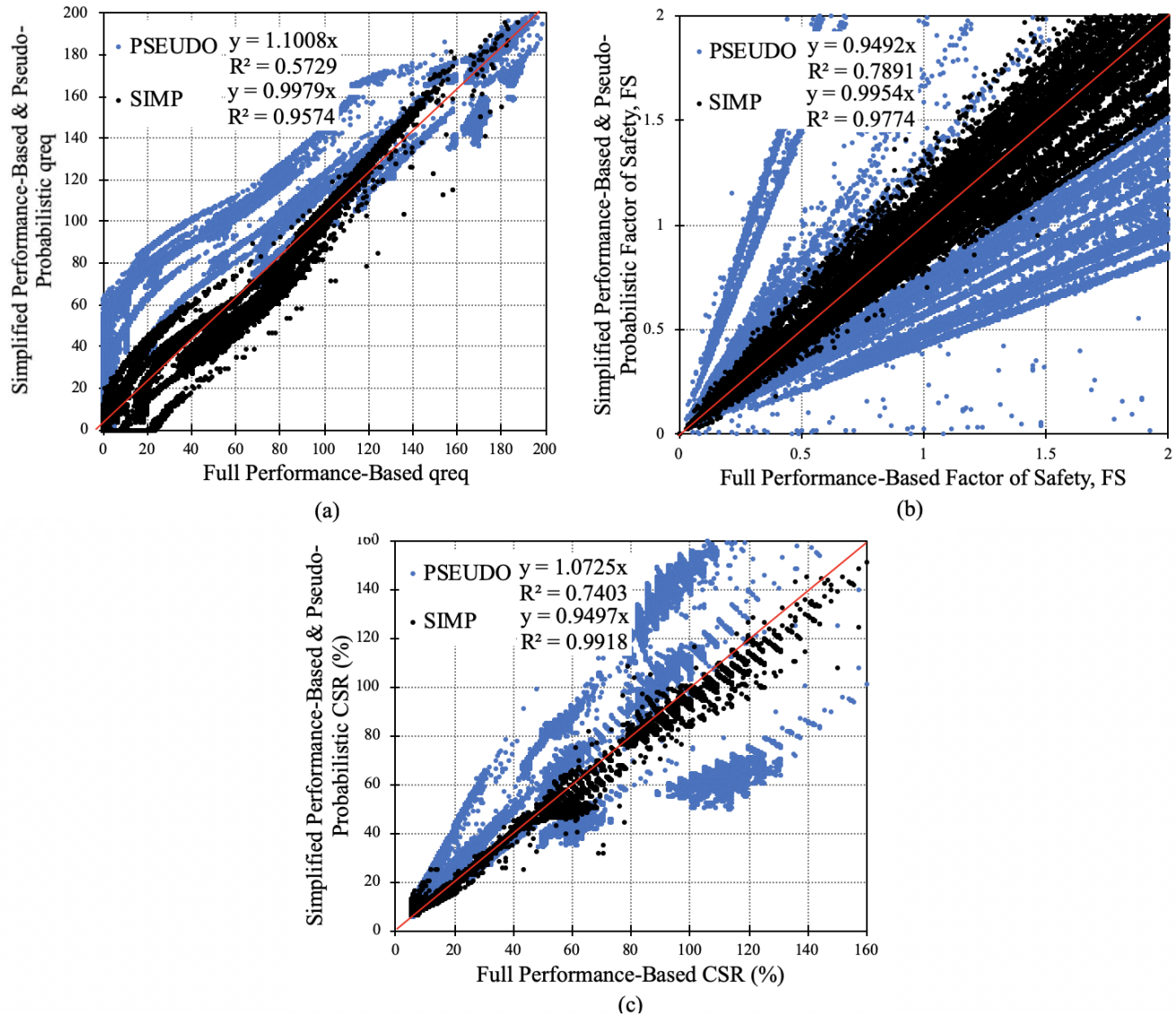


Figure 3-1. Comparison Results for the Ku et al. (2012) Triggering Model for (a) q_{req} , (b) FS_L , and (c) $CSR\%$

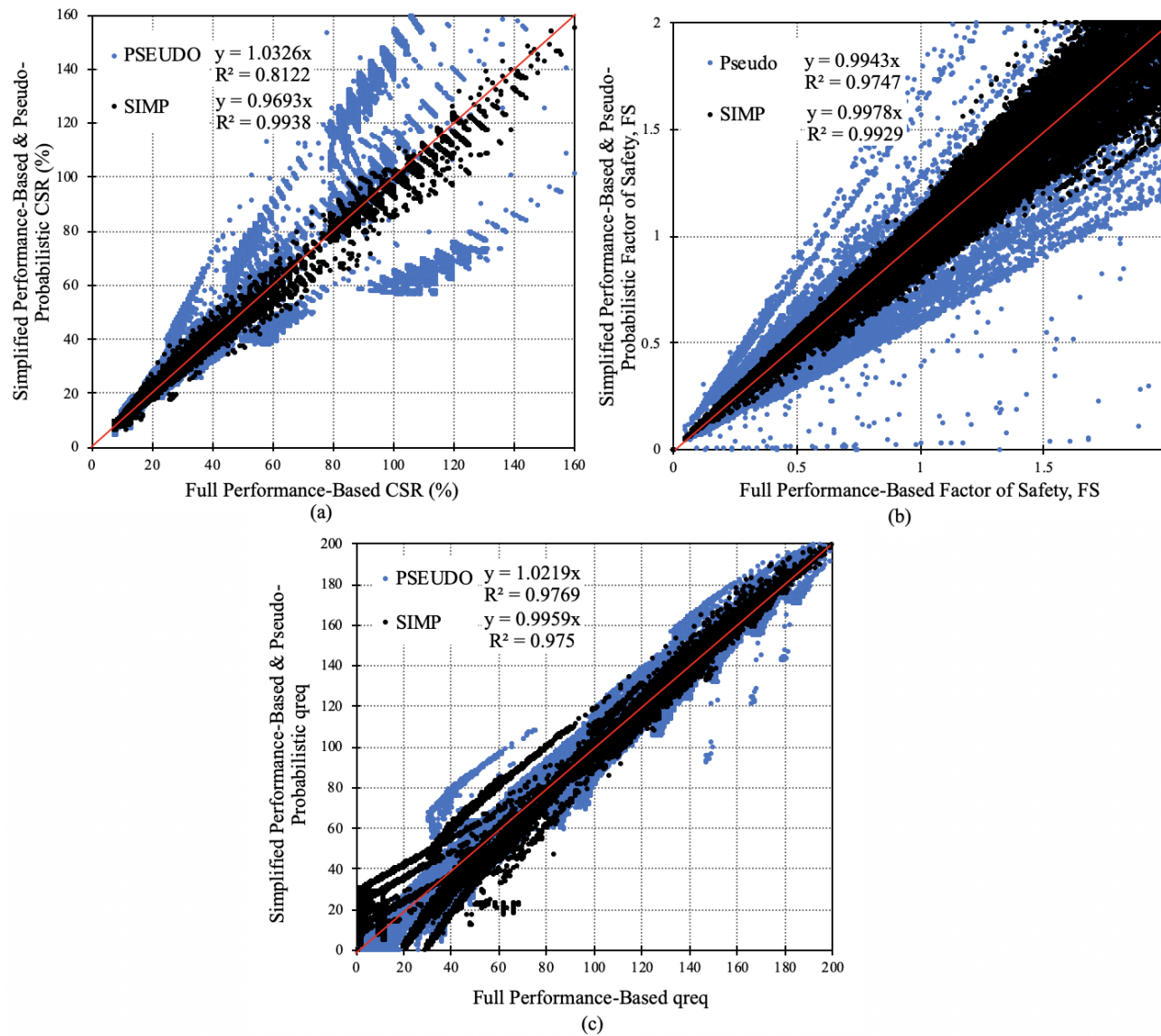


Figure 3-2. Comparison Results for the Boulanger and Idriss (2014) Triggering Model for (a) CSR%, (b) FS_L , and (c) q_{req}

3.5 Post-Liquefaction Settlement Comparison

3.5.1 Post-Liquefaction Settlement Comparison Results using Boulanger and Idriss (2014)

The comparison results of all three return periods for the Boulanger and Idriss (2014) triggering model are shown Figure 3-3 and Figure 3-4. Figure 3-3 contains sites with PGA less than 0.2g and Figure 3-4 contains sites with PGA higher than 0.2g.

For all return periods and for both the simplified performance-based and the pseudo-probabilistic procedures, more scatter is observed for sites with PGA less than 0.2g (Figure 3-3). This observation agrees with the validation study presented in Task 7. At sites with $PGA < 0.2g$ (Figure 3-3) the slopes of the trend lines are 1.0545 and 1.2398 for the simplified performance-based procedure and the pseudo-probabilistic procedure, respectively, meaning that the simplified procedure overestimates the full performance-based procedure by 5.5% and the pseudo-probabilistic procedure overestimates by 24% on average. As for the R^2 values, both the simplified performance-based procedure and the probabilistic procedure have R^2 values near 0.925, suggesting comparable consistencies between the two procedures. For sites with $PGA \geq 0.2g$ (Figure 3-4), the plot shows that the simplified performance-based procedure underestimates the full performance-based procedure by 3.2% on average, and the pseudo-probabilistic procedure overestimates the full performance-based procedure by 10.3% on average. Additionally, the simplified performance-based procedure has a slightly higher R^2 value of 0.9729, which is greater than the value of the pseudo-probabilistic procedure at $R^2 = 0.9515$, though such small differences in R^2 are likely insignificant.

Overall, both the simplified performance-based procedure and the pseudo-probabilistic procedure overestimate the full performance-based procedure for sites with $PGA < 0.2g$ (i.e., low seismicity areas), and underestimate for $PGA \geq 0.2g$ (i.e., moderate to high seismicity areas). However, the simplified performance-based procedure more accurately approximates the full performance-based procedure on average and is slightly more consistent and precise than the pseudo-probabilistic procedure based on the comparisons performed in this study.

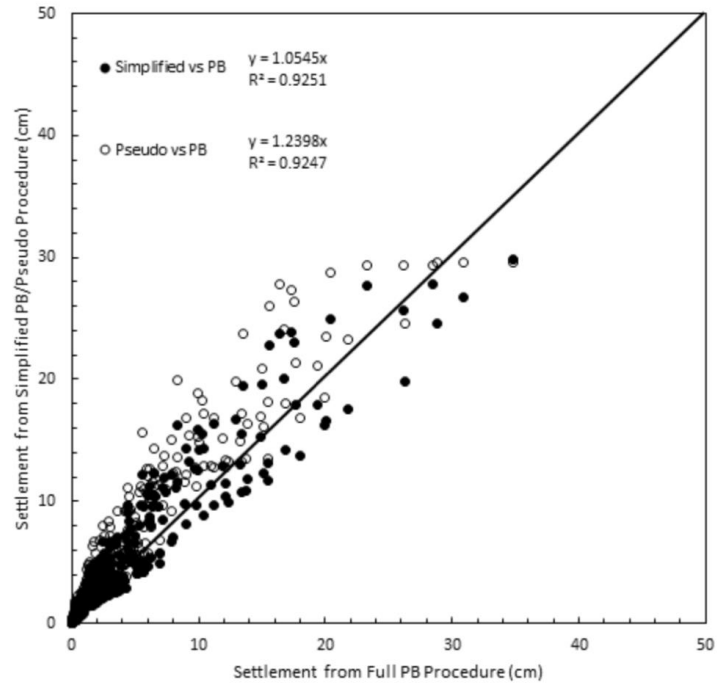


Figure 3-3. Settlement Comparison Results using the Boulanger and Idriss (2014) Triggering Model for Sites with $PGA < 0.2 g$ (for All Return Periods)

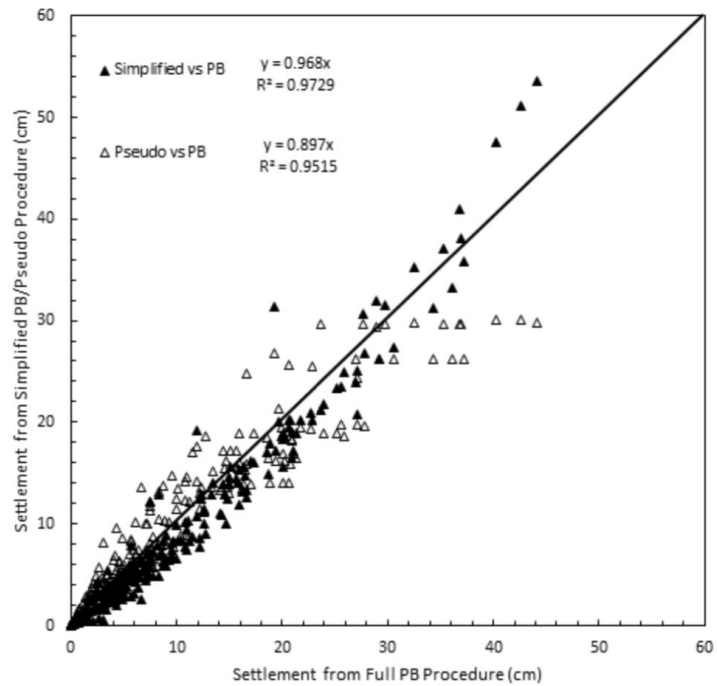


Figure 3-4. Settlement Comparison Results using the Boulanger and Idriss (2014) Triggering Model for Sites with $PGA \geq 0.2g$ (for All Return Periods)

3.5.2 Post-Liquefaction Settlement Comparison Results using Ku et al. (2012)

The comparison plots based on the Ku et al. (2012) triggering model are shown in Figure 3-5 and Figure 3-6, with Figure 3-5 containing sites with $PGA < 0.2g$ and Figure 3-6 containing sites with $PGA \geq 0.2g$.

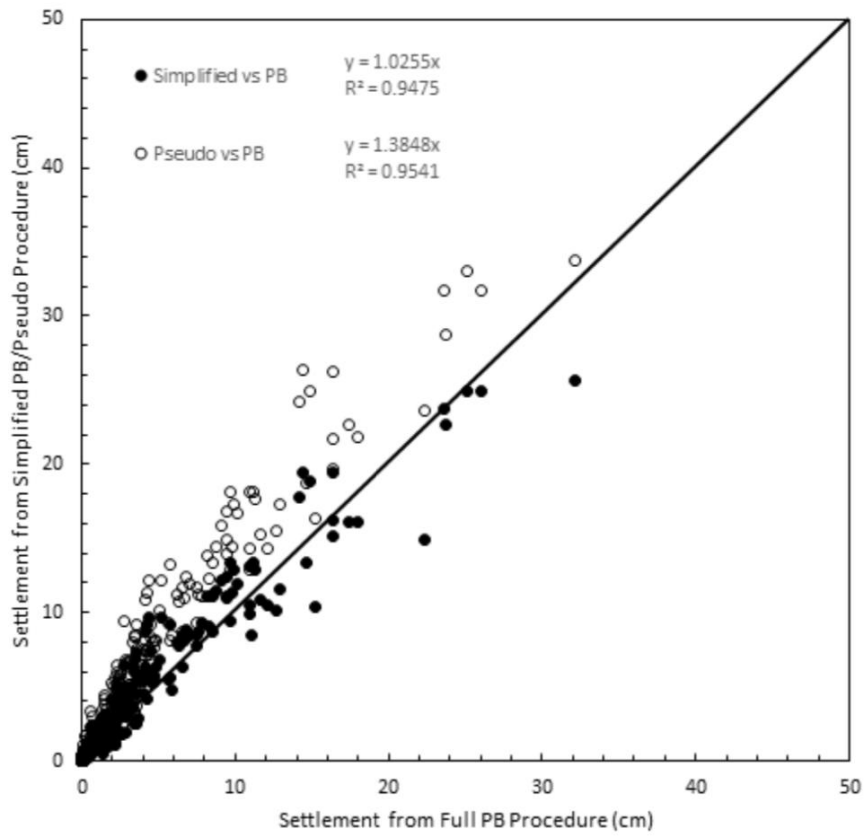


Figure 3-5. Settlement Comparison Results using the Ku et al. (2012) Triggering Model for Sites with $PGA < 0.2 g$ (for All Return Periods)

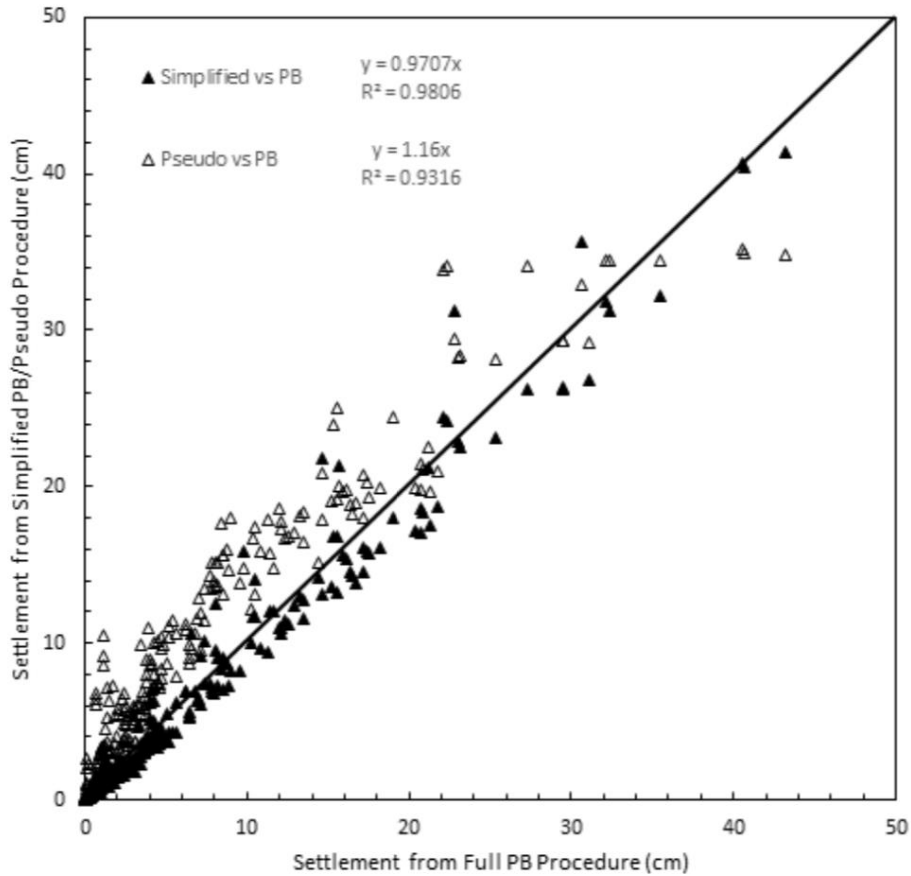


Figure 3-6. Settlement Comparison Results using the Ku et al. (2012) Triggering Model for Sites with $PGA \geq 0.2g$ (for All Return Periods)

As observed with the Boulanger and Idriss (2014) model, the simplified performance-based procedure with the Ku et al (2012) model produced better approximations of the full performance-based procedure and was slightly more consistent and precise than the pseudo-probabilistic procedure.

3.6 Discussion

From a visual observation of the comparison plots, the plots do not show an obvious visual difference between the simplified procedure and the pseudo-probabilistic procedure. However, the trend line slopes and R^2 values presented in Section 3.5 suggest that the simplified performance-based procedure can consistently provide better approximations of the full performance-based procedure than the pseudo-probabilistic procedure.

The apparent similarities between the simplified performance-based and pseudo-probabilistic procedures for post-liquefaction settlement can be explained. Studies have shown that the performance-based procedure generally deviates significantly from the pseudo-probabilistic procedure in liquefaction triggering (Kramer and Mayfield, 2007; Franke et al., 2013). However, these significant differences in computed FS_L are not fully transferred to the resulting volumetric strains, which are computed using the Ishihara and Yoshimine (1992) method.

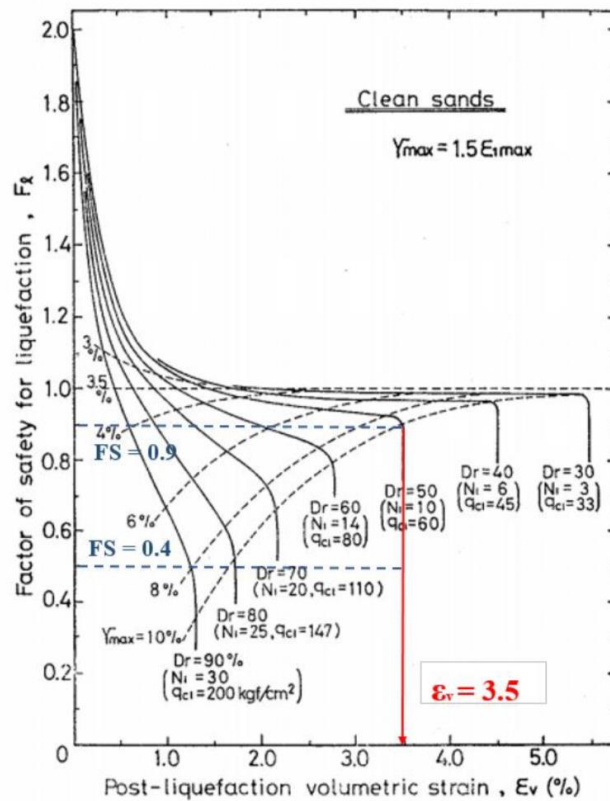


Figure 3-7. Ishihara and Yoshimine (1992) Method for Determining Volumetric Strain

Consider, for example, two different values of FS_L (0.9 and 0.4) and the resulting volumetric strains from Ishihara and Yoshimine (1992) presented in Figure 3-7. Each of the FS_L values, although significantly different, is predicted to result in approximately the same amount of volumetric strain: 3.5%. As such, significant differences in the computed FS_L between the simplified performance-based procedure and the pseudo-probabilistic procedure may not translate directly to significant differences in volumetric strain when using the Ishihara and Yoshimine

(1992) volumetric strain curves. Consequently, the resulting post-liquefaction settlements computed using the two different procedures can appear quite similar.

Regardless, engineers in practice may question why the simplified procedure should be used over the pseudo-probabilistic procedure when no visually obvious improvements have been achieved. In response to this question, the simplified performance-based procedure clearly demonstrates trend line slopes that are closer to 1.0 and larger R^2 values than the conventional pseudo-probabilistic approach. This indicates that the simplified approach is better at approximating the full performance-based approach. However, engineers may choose if they would like to benefit from the increased accuracy, consistency, and precision of the simplified performance-based approach or continue using the approach they are already familiar with. Continued use of the pseudo-probabilistic approach in computing post-liquefaction settlements will not produce substantially inaccurate estimates of the full performance-based post-liquefaction settlements.

3.7 Lateral Spread Comparison Results

3.7.1 Lateral Spread Comparison Results using Zhang et al. (2004) with Boulanger and Idriss (2004)

The comparison of predicted lateral spread displacements using Zhang et al. (2004) for all three return periods using the Boulanger and Idriss (2014) triggering model are presented in Figure 3-8 and Figure 3-9. Figure 3-8 contains sites with $PGA < 0.2g$, and Figure 3-9 contains sites with $PGA \geq 0.2g$.

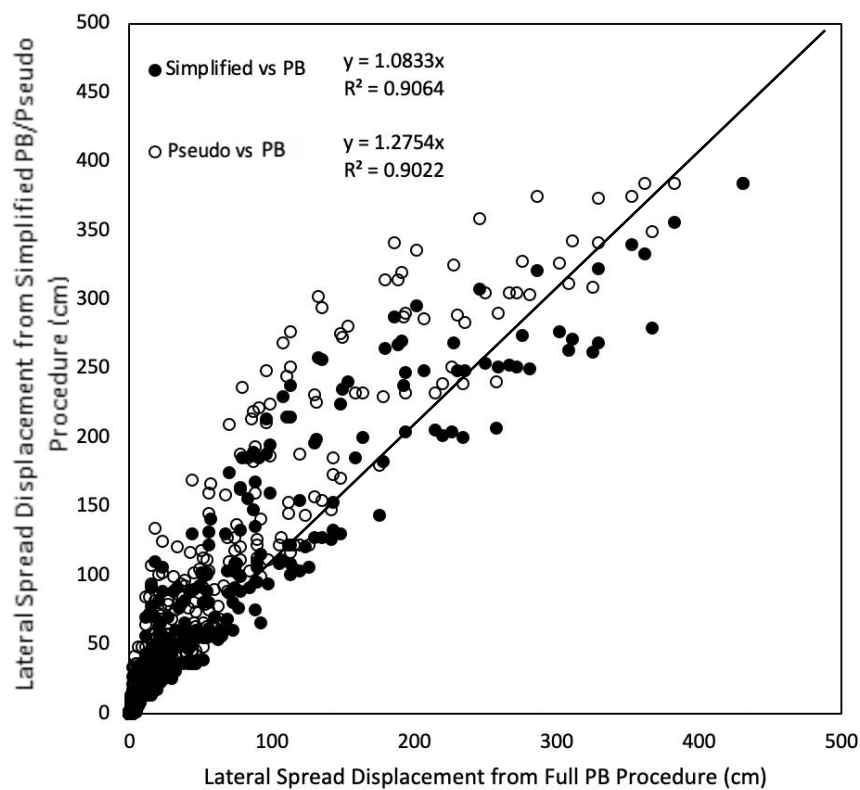


Figure 3-8. Lateral Spread Comparison Results using the Boulanger and Idriss (2014) Triggering Model for Sites with $PGA < 0.2g$ (for All Return Periods)

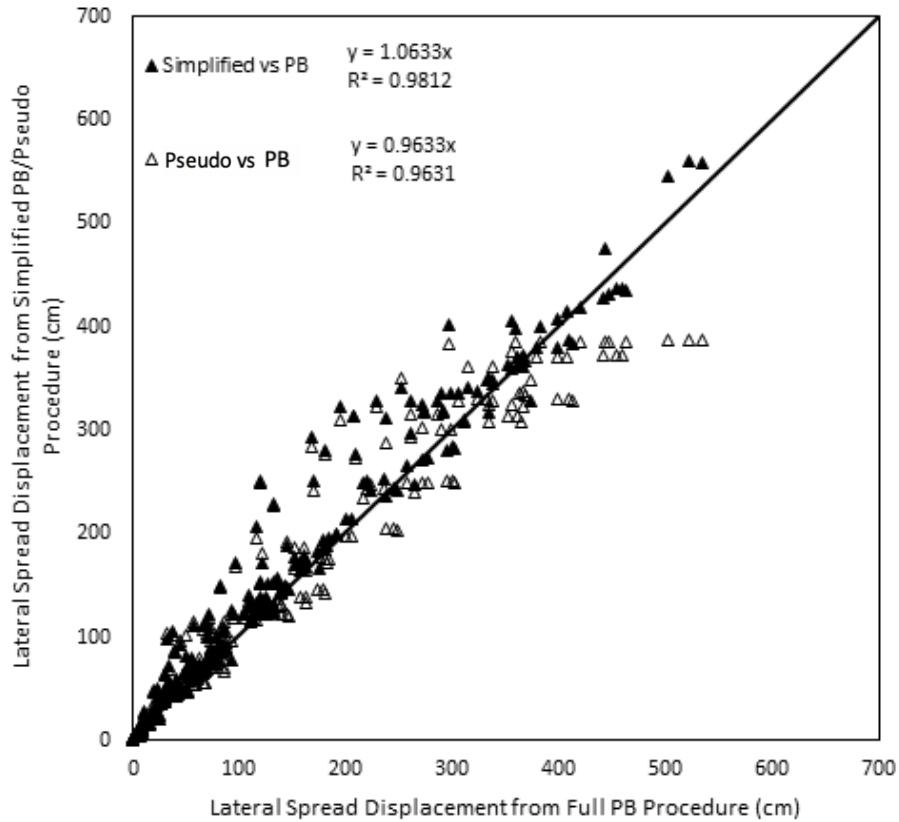


Figure 3-9. Lateral Spread Comparison Results using the Boulanger and Idriss (2014) Triggering Model for Sites with $PGA \geq 0.2g$ (for All Return Periods).

For both the simplified performance-based procedure and the pseudo-probabilistic procedure, more scatter is observed for sites with $PGA < 0.2g$ (Figure 3-8). At sites with $PGA < 0.2g$ (Figure 3-8), slopes of the trend lines are 1.0833 and 1.2754 for the simplified procedure and the pseudo-probabilistic procedure, respectively, suggesting that, on average, the simplified performance-based procedure is over-predicting the full performance-based procedure by 8.3% and the pseudo-probabilistic method is over-predicting by 27.5%. Considering the R^2 values, both the simplified performance-based procedure and the pseudo-probabilistic method produce R^2 values around 0.90. Similarly, results at sites with $PGA \geq 0.2g$ (Figure 3-9) show that the simplified procedure overestimates the full performance-based procedure by 3.69% and the pseudo-probabilistic underestimates by 10.3% on average. The simplified performance-based procedure also has a slightly higher R^2 value (0.9812) than the pseudo-probabilistic procedure (0.9631).

Overall, the simplified procedure produces a slightly better approximation of the full performance-based procedure. While a visual inspection of the comparison plots appear similar, the simplified procedure does indeed provide more consistent and accurate approximations of the full performance-based procedure than the pseudo-probabilistic approach on average.

3.7.2 Lateral Spread Comparison Results using Zhang et al. (2004) with Ku et al. (2012)

The comparison of predicted lateral spread displacements using Zhang et al. (2004) procedure with the Ku et al. (2012) triggering model are shown in Figure 3-10 and Figure 3-11, with Figure 3-10 presenting the results for sites with $PGA < 0.2g$ and Figure 3-11 presenting the results for sites with $PGA \geq 0.2g$.

For both the simplified performance-based procedure and the pseudo-probabilistic procedure, more scatter is observed for sites with $PGA < 0.2g$ (Figure 3-10). At sites with $PGA < 0.2g$ (Figure 3-10), slopes of the trend lines are 1.055 and 1.4925 for the simplified procedure and the pseudo-probabilistic procedure, respectively, suggesting that, on average, the simplified performance-based procedure is over-predicting the full performance-based procedure by 5.5% and the pseudo-probabilistic method is over-predicting by 49.25%. Considering the R^2 values, the simplified performance-based procedure produces a R^2 value around 0.94. Similarly, results at sites with $PGA \geq 0.2g$ (Figure 3-11) show that the simplified procedure overestimates the full performance-based procedure by 1.25% and the pseudo-probabilistic overestimates by 24.38%. At approximately 150 cm of lateral spread displacement, the pseudo-probabilistic procedure overestimates the full performance-based procedure while the simplified procedure underestimates the full performance-based procedure. The simplified performance-based procedure also has a slightly higher R^2 value (0.9628) than the pseudo-probabilistic procedure (0.9396).

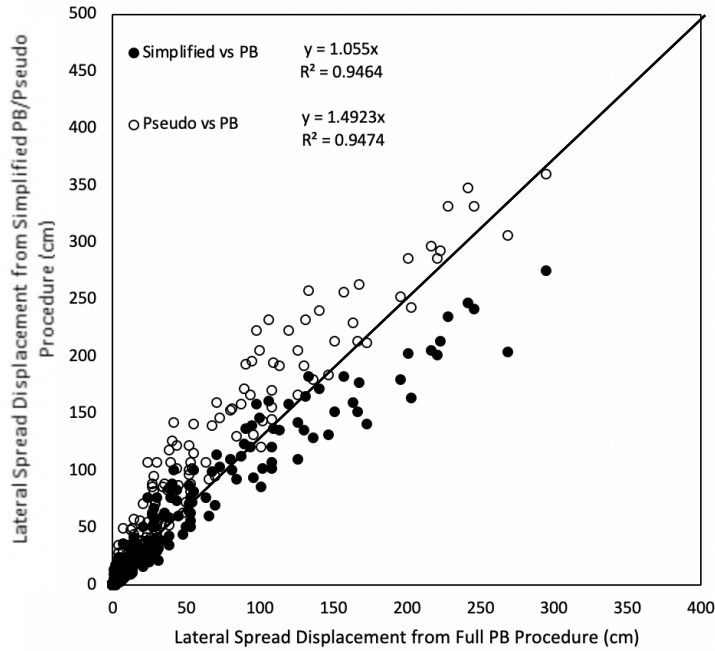


Figure 3-10. Lateral Spread Comparison Results using the Ku et al. (2012) Triggering Model for Sites with $PGA < 0.2g$ (for All Return Periods)

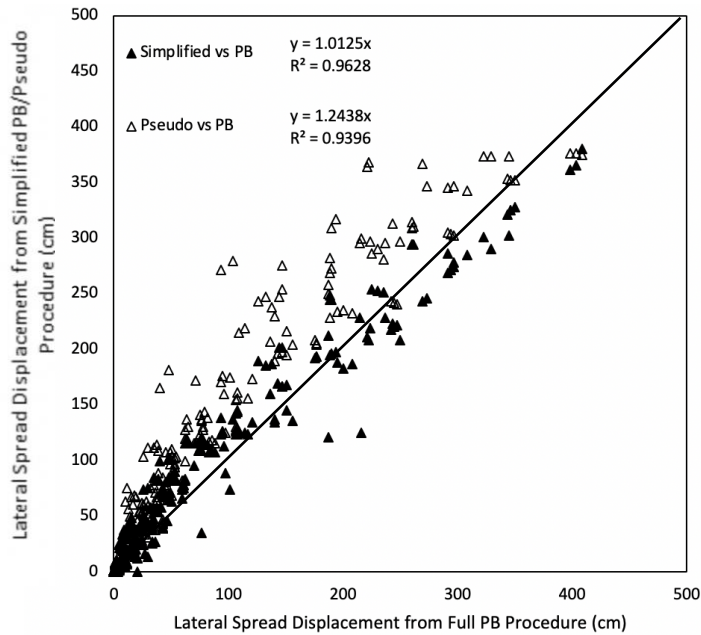


Figure 3-11. Lateral Spread Comparison Results using the Ku et al. (2012) Triggering Model for Sites with $PGA \geq 0.2g$ (for All Return Periods)

The results of the simplified and pseudo-probabilistic lateral spread procedures using Ku et al. (2012) are, fairly similar up to a displacement of 150 cm. However, based on the R^2 values and the trendlines, the simplified procedure produces an overall slightly better approximation of the full performance-based procedure.

3.8 Comparison with the Deterministic Procedure

This section will present the results of the deterministic comparison study for the Boulanger and Idriss (2014) and Ku et al. (2012) models. For each plot, computed results for the simplified performance-based procedure are plotted on the x-axis and the deterministic procedure results are plotted on the y-axis. This section will present the plots for liquefaction triggering, settlement, and lateral spread.

3.8.1 Locations and Profiles

Three locations were chosen across the United States: Butte, Salt Lake City, and San Francisco. For the deterministic procedure, ground motions are obtained through a Deterministic Seismic Hazard Analysis (DSHA). A DSHA involves deterministically assessing the seismic sources in the nearby region of the site of interest and identifying the source which produces the highest hazard in the area. The software EZ-FRISK was used to identify the top five seismic sources within 200 km for San Francisco, Butte, and Salt Lake City. The 2008 USGS Seismic Source Model within EZ-FRISK does not include some smaller faults in low seismic regions, such as Butte. Thus, the governing fault for Butte (Rocker Fault) was identified using the USGS quaternary fault database (USGS et al., 2006). In the case of Salt Lake City and San Francisco, EZ-FRISK provided values of M_w , PGA , and R for both the 50th (i.e. median) and 84th (i.e. median + σ) percentiles according using the New Generation Attenuation (NGA) models for the Western United States (Boore and Atkinson, 2008; Campbell and Bozorgnia, 2008; and Chiou and Youngs, 2008) and weighting schemes shown in Table 3-2. For Butte, the 50th and 84th percentile M_w values were estimated using a correlation with surface rupture length developed by Wells and Coppersmith (1994), and PGA was calculated using the same three (NGA) models based on measured dimensions and assumed characteristics of the Rocker Fault. Once the model inputs have been determined through the DSHA they are entered into the respective empirical liquefaction

hazard models. A summary of the input variables utilized in the deterministic analyses are provided in Table 3-3 . One single soil profile, shown in Figure 3-12, was used in this comparison.

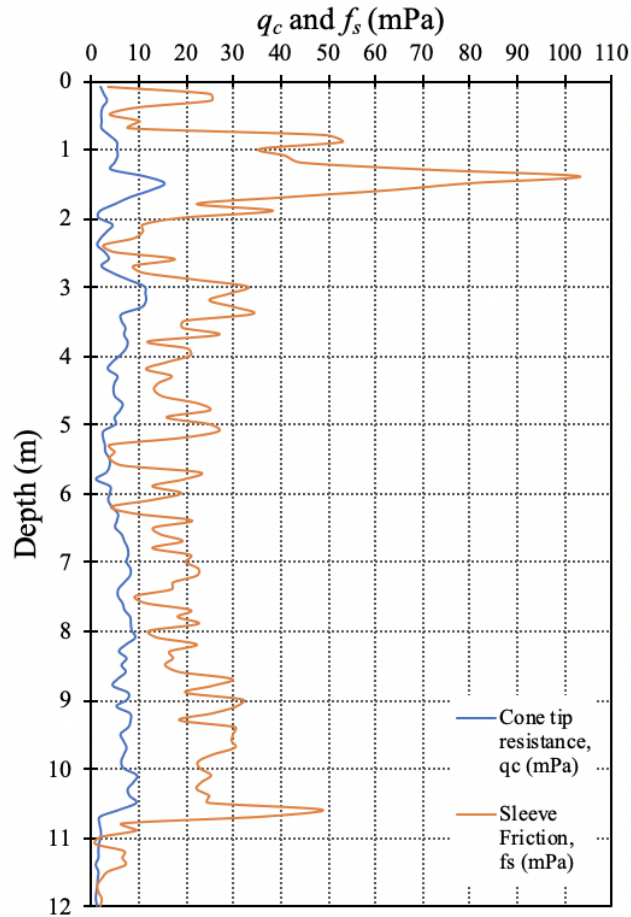


Figure 3-12. Soil Profile used for the deterministic comparison study.

Table 3-2. NGA model weights used in the deterministic procedure.

Attenuation Model	Weight
Boore & Atkinson (2008)	0.333
Campbell & Bozorgnia (2008)	0.333
Chiou & Youngs (2008)	0.333

Table 3-3. Input variables used in the deterministic models (a_{max} calculated using F_{pga} from AASHTO code).

Location	Latitude	Longitude	Distance [km]	Mean M_w	Median (50%)		Median + σ (84%)	
					PGA	a_{max}	PGA	a_{max}
Butte	46.003	-112.533	4.92	6.97	0.539	0.539	0.9202	0.9202
Salt Lake City	40.755	-111.898	1.02	7.0	0.5911	0.5911	1.005	1.005
San Francisco	37.775	-122.418	12.4	8.05	0.3175	0.3754	0.5426	0.5426

3.8.2 Liquefaction Triggering Comparison

The comparison results for the Robertson and Wride (2009) triggering model are presented in Figure 3-13, Figure 3-14, and Figure 3-15 for different representations of liquefaction triggering hazards: q_{req} , FS_L , and $CSR\%$, respectively. Each figure shows plots for the 475, 1039, and 2475-year return period. A comparison of the plots show that the deterministic analyses frequently over-predicts the simplified performance-based method for q_{req} and $CSR\%$ and under-predicts FS_L . However, in the case of San Francisco, the deterministic analyses often under-predicted the simplified performance-based method for q_{req} and $CSR\%$. The comparison plots also highlights the differences between the 50th and 84th percentile ground motion results. For example, in the case of San Francisco, the 84th percentile ground motions over-predicted values of q_{req} while the 50th percentile ground motions under-predicted q_{req} . However, in the case of Salt Lake City ($T_r = 1039$), both the 50th and 84th percentile ground motions over-predicted the simplified method. In addition, the 50th percentile ground motions more closely approximated the simplified performance-based method than the 84th percentile ground motions. In other cases, the 84th percentile ground motions produced closer approximations of the simplified method than the 50th percentile ground motions. These discrepancies and inconsistencies can be confusing for the engineer who has to decide which ground motions appropriately characterize the liquefaction hazard for the given site.

The comparison results for the Boulanger and Idriss (2014) triggering model are presented in Figure 3-16, Figure 3-17, and Figure 3-18 for q_{req} , FS_L , and $CSR\%$, respectively. Similar to the Robertson and Wride results, these plots also show that the deterministic analyses frequently over-predicted the simplified-based method for q_{req} and $CSR\%$ and under-predicted the FS_L . These plots also highlight the inconsistencies of the 50th and 84th percentile ground motions.

3.8.3 Robertson and Wide Comparison Results

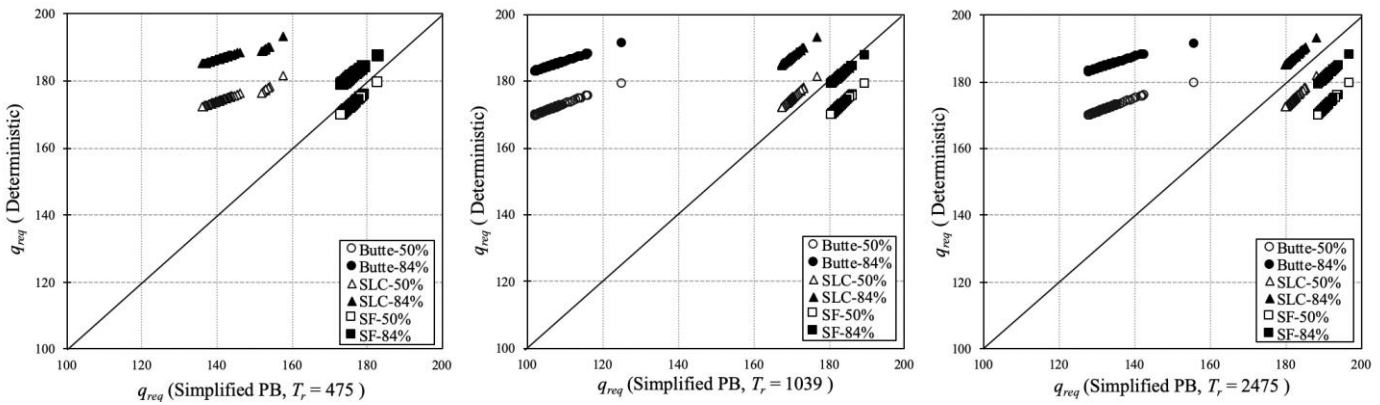


Figure 3-13. Comparison of deterministic and simplified performance-based values of q_{req} .

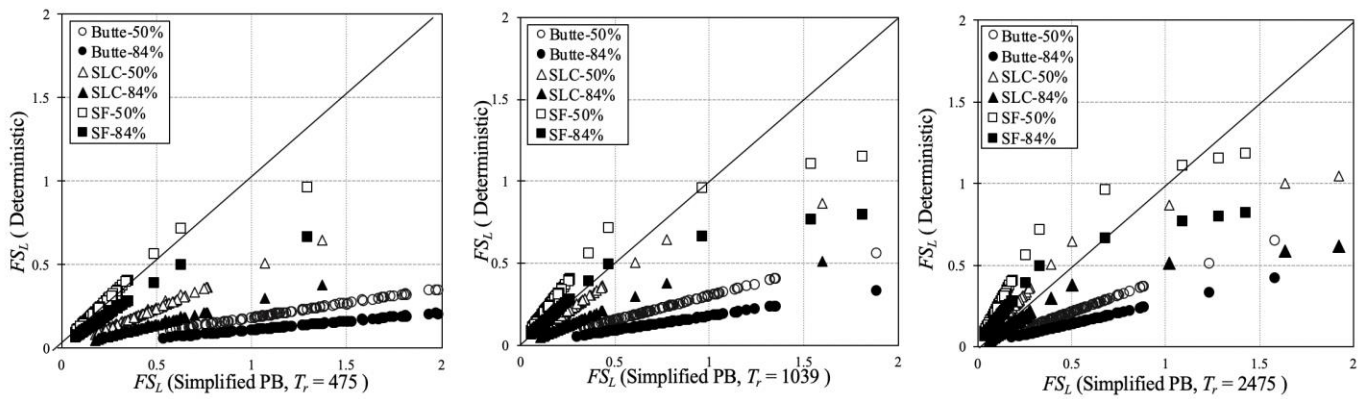


Figure 3-14. Comparison of deterministic and simplified performance-based values of FS_L .

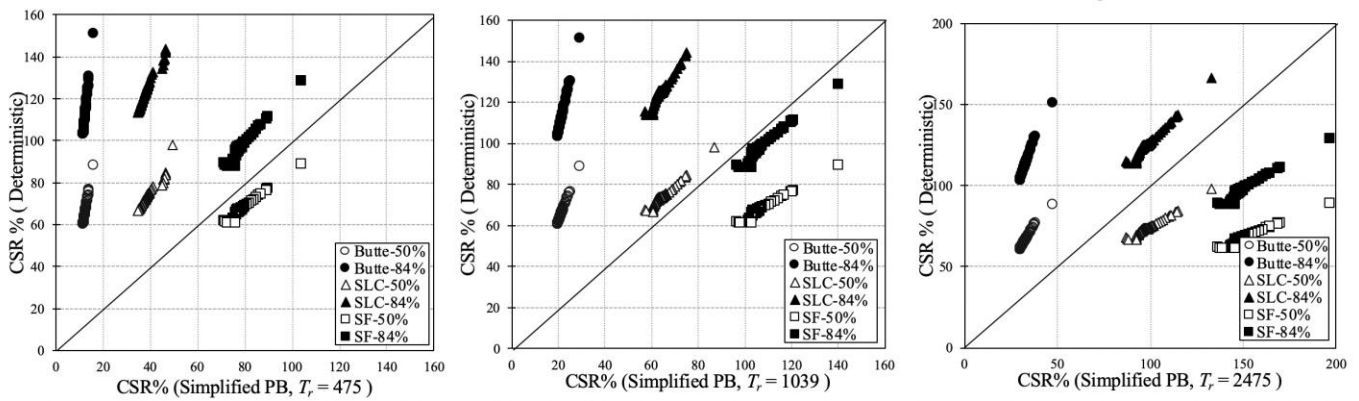


Figure 3-15. Comparison of deterministic and simplified performance-based values of $CSR\%$.

3.8.4 Boulanger and Idriss (2014) Comparison Results

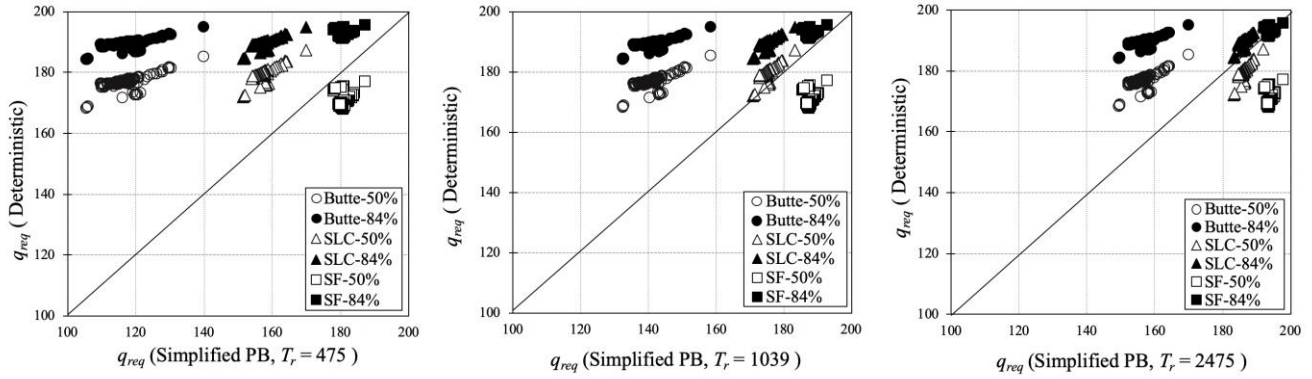


Figure 3-16. Comparison of deterministic and simplified performance-based values of q_{req} .

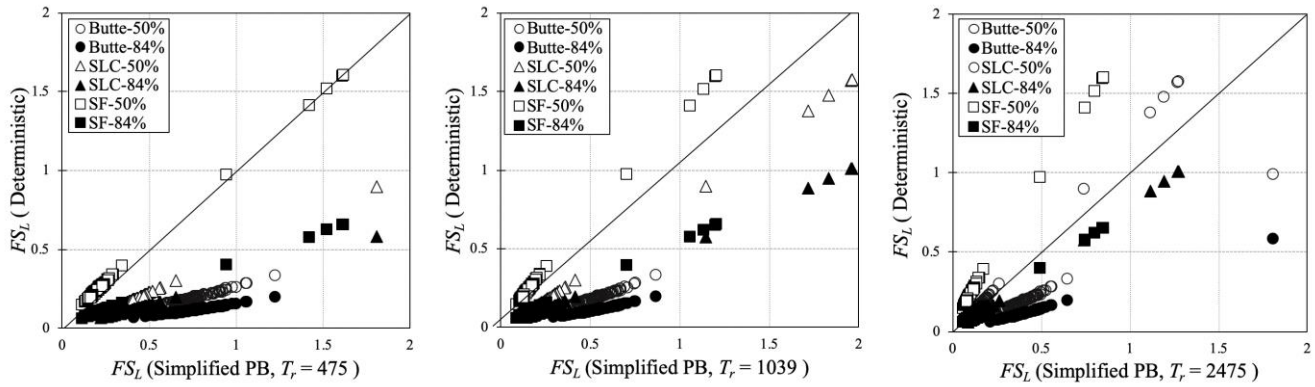


Figure 3-17. Comparison of deterministic and simplified performance-based values of FS_L .

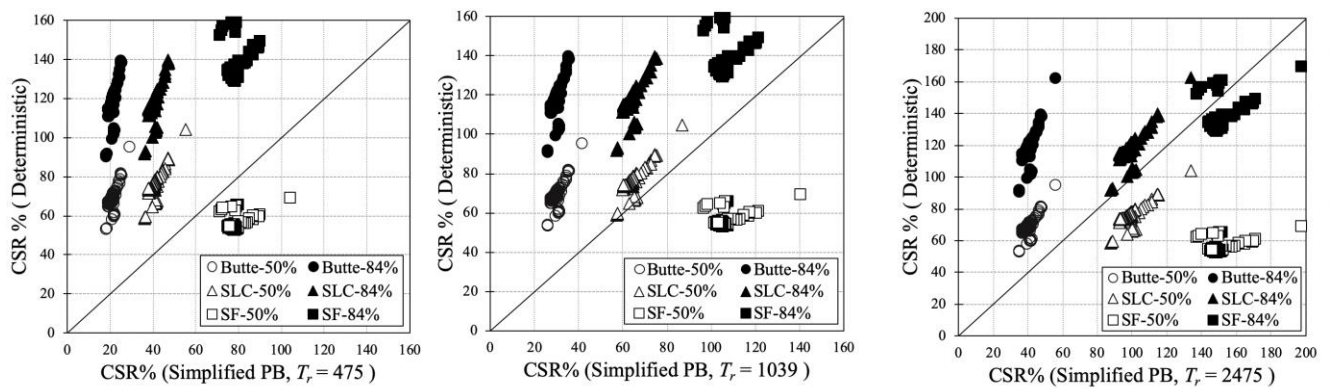


Figure 3-18. Comparison of deterministic and simplified performance-based values of $CSR\%$

3.8.5 Post-Liquefaction Settlement Comparison (Ishihara and Yoshimine (1992))

The comparison plots in this section show the results of the Ishihara and Yoshimine (1992) deterministic analyses using the Robertson and Wride (2009) (Figure 3-19) and Boulanger and Idriss (2014) (Figure 3-20) models. These comparison plots show that the deterministic analyses often over-predicted simplified performance-based vertical strains for cities of low to medium seismicity (Butte and Salt Lake City), and under-predicted vertical strains for cities of medium to high seismicity (San Francisco). In many cases, the 50th and 84th percentile ground motions produced similar results.

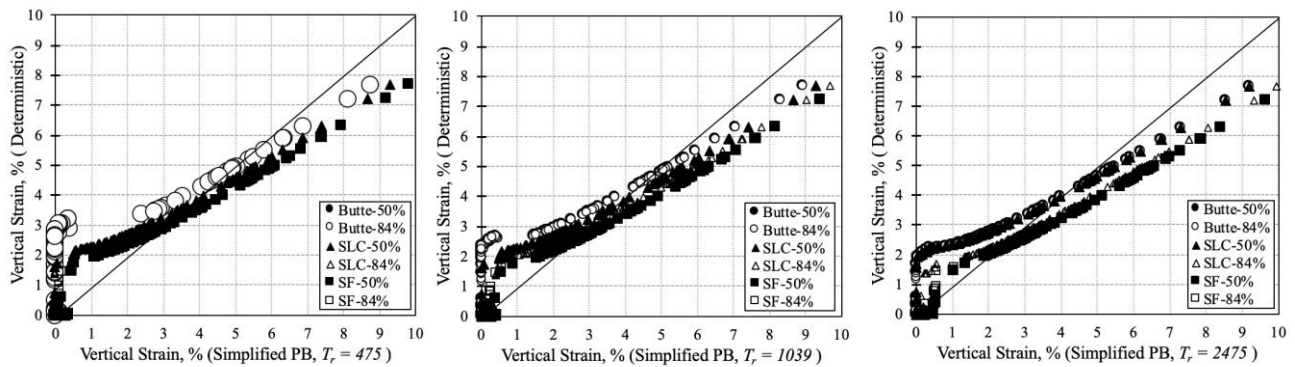


Figure 3-19. Comparison of deterministic and simplified performance-based vertical strains using the Robertson and Wride (2009) model.

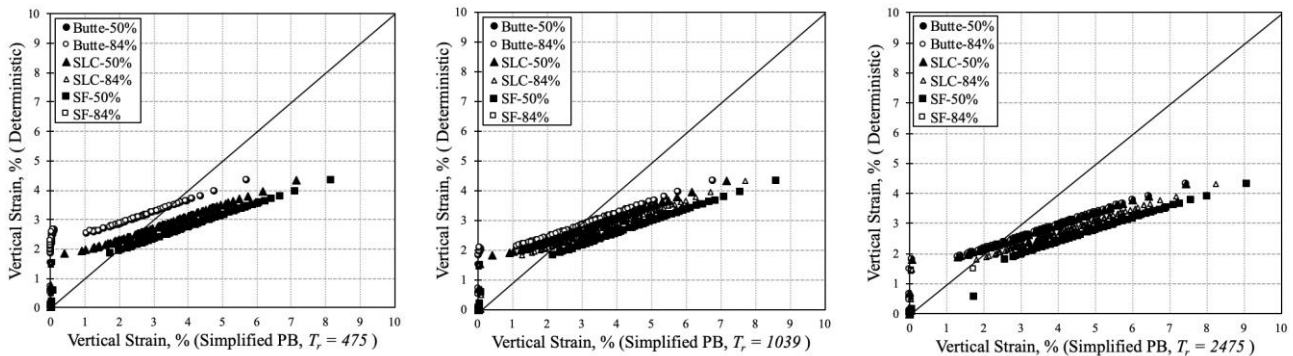


Figure 3-20. Comparison of deterministic and performance-based vertical strains using the Boulanger and Idriss (2014) model.

3.8.6 Lateral Spread Comparison Results (Zhang et al. (2004))

The comparison plots show the results of the Zhang et al. (2004) deterministic analyses using the Robertson and Wride (2009) (Figure 3-21) and Boulanger and Idriss (2014) (Figure 3-22) models. Based on these plots, the deterministic analyses greatly over-predicted the simplified performance-based method for low seismicity areas (Butte) for both models. When using the Robertson and Wride model, the deterministic analyses provided closer approximations of the simplified performance-based method for medium to high seismicity areas (Salt Lake City and San Francisco) at higher return periods. When using the Boulanger and Idriss model, the deterministic approach generally under-predicted the simplified method, with the exception of the 475-year return period. Similar to the settlement comparison plots, the 50th and 84th percentile ground motions also produced similar results.

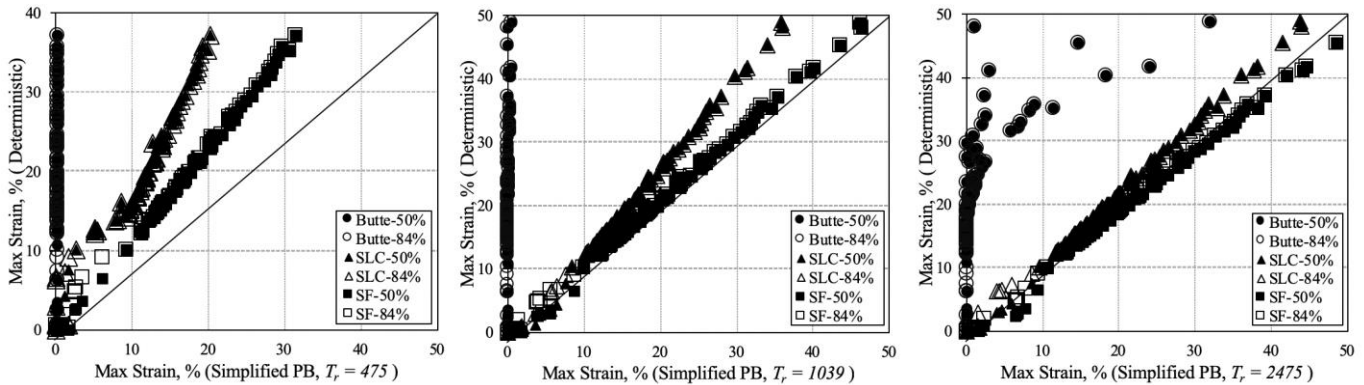


Figure 3-21. Comparison of deterministic and simplified performance-based maximum strains using the Robertson and Wride (2009) model.

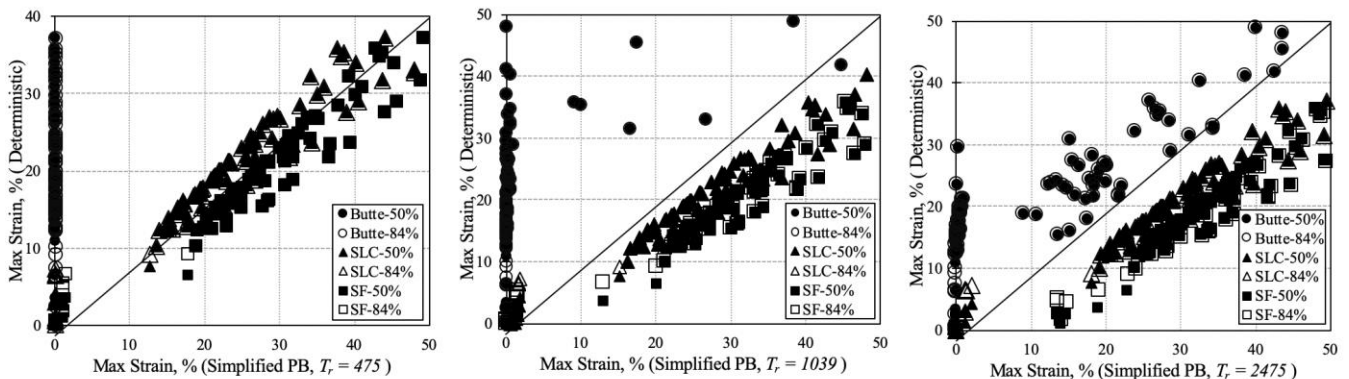


Figure 3-22. Comparison of deterministic and simplified performance-based maximum strains using the Boulanger and Idriss (2014) model.

3.9 Summary

This study analyzed several hazards: liquefaction triggering, post-liquefaction settlement, and lateral spread. The deterministic methods generally predicted significantly more earthquake induced hazard than probabilistic methods in Butte—an area of low seismicity. The deterministic results also generally showed more earthquake induced hazards than the probabilistic results at high return periods in Salt Lake City—an area of medium seismicity. In San Francisco—an area of high seismicity—the deterministic methods predicted slightly lower hazards than the probabilistic method, particularly at higher return periods. These results suggest that the deterministic results could be used as an upper-bound in areas of high seismicity, but in areas of low seismicity, the deterministic analysis could be optional. Engineers performing analyses in areas of medium to high seismicity could choose to use a deterministic analysis as a “reality check” against the simplified performance-based results. If both deterministic and performance-based methods are considered, the *lower of the deterministic and the probabilistic results* should govern the design.

This rule may seem counter-intuitive, but the idea is not completely foreign—when developing a spectral acceleration design envelope, seismic building code (e.g., IBC 2018) permits that the lower of the deterministic and probabilistic accelerations be used in design. Likewise, in a liquefaction hazard analysis, the lower value should govern. If the deterministic value is lower than the performance-based value, the combination of multiple seismic sources in the performance-based analysis may suggest greater liquefaction hazard than would be caused by a single earthquake event. Therefore, the deterministic analysis provides a type of “reality check” against the performance-based analysis, and the deterministic results should be accepted. If the performance-based value is lower than the deterministic value, the nearby governing fault may have a significantly low likelihood of rupturing within the design life of the structure. In this case, the deterministic results could be considered too extreme (especially for some projects which do not need to be designed to withstand such large events). Therefore, the performance-based results should be accepted as a representation of the more *likely* liquefaction hazard.

4.0 CONCLUSIONS

4.1 Summary

The purpose of the research performed for Tasks 8, 9, & 10 was to create the liquefaction parameter maps necessary for the simplified performance-based procedures and perform a comparison study. To accomplish this task, a grid study was performed to determine the appropriate spacing of points in order to create contours for each parameter: q_{req}^{ref} , CSR^{ref} , ε_v^{ref} (%) and γ_{max}^{ref} (%). These maps are included in the Appendix in PDF format. Overall, the simplified performance-based procedures better approximated the full performance-based method than conventional pseudo-probabilistic methods.

4.2 Limitations and Challenges

Users of the simplified performance-based methods should be aware that the simplified method is trying to estimate the results of a very complex procedure with a few correction equations; errors are inevitable. It is highly recommended that these methods be used by engineers who are capable of recognizing such errors. In addition, even though the cities and soil profiles that have been selected represent a diverse combination of seismicity and soil conditions, the correction equations may not perform as well for other locations and profiles that have not been tested.

REFERENCES

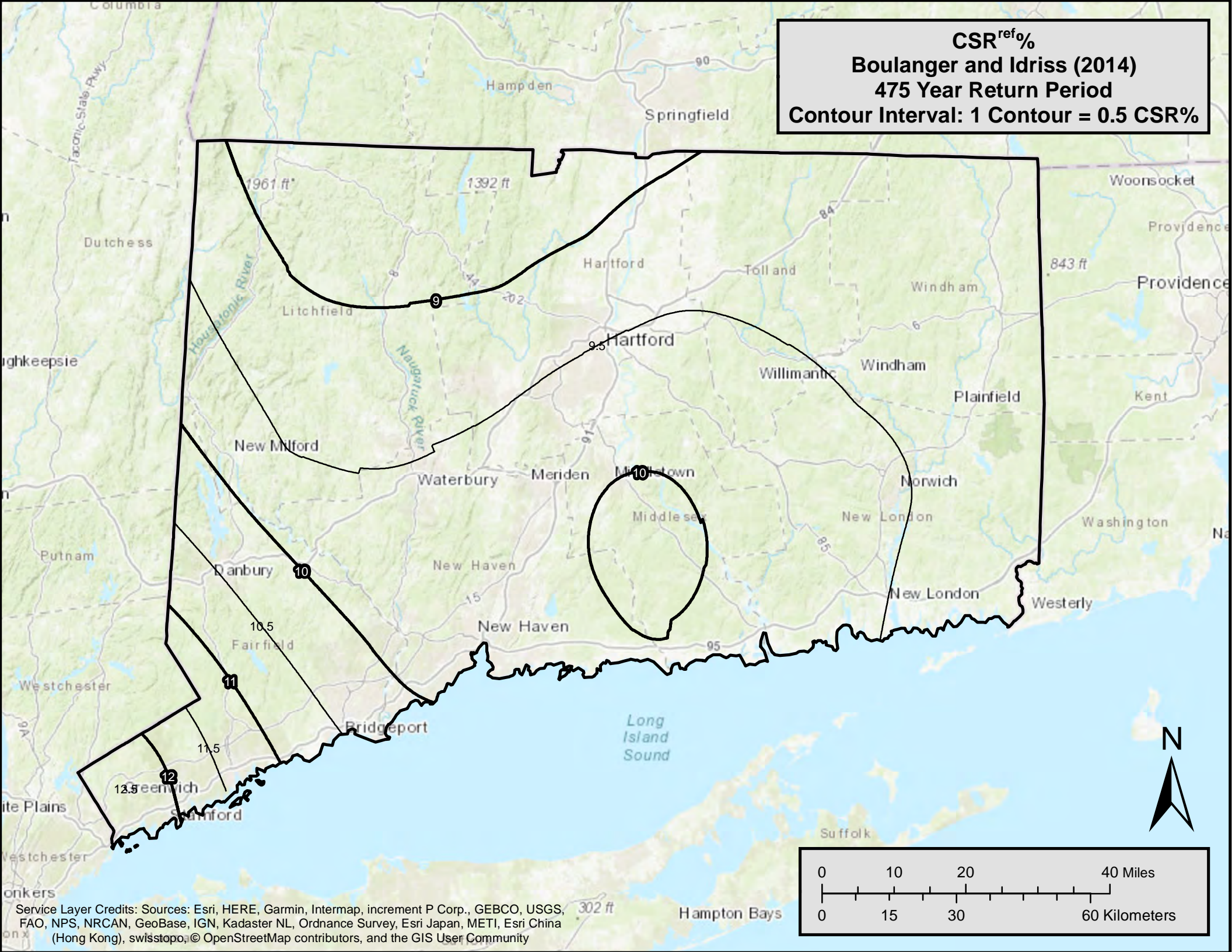
- Boulanger, R. W., and Idriss, I. M. (2014). CPT and SPT based liquefaction triggering procedures. *Rep. UCD/CGM-14/01*, Dept. of Civil and Environmental Engineering, Univ. of California–Davis, Davis, CA.
- Ekstrom, Levi Thomas (2015). “A Simplified Performance-based Procedure for the Prediction of Lateral Spread Displacements.” M.S. *Thesis, 2015, Brigham Young University, Provo, UT.*
- Error, Braden Michael (2017). “Development of a Simplified Performance-Based Procedure for the Assessment of Liquefaction-Induced Settlements Using Liquefaction Loading Maps.” M.S. *Thesis, 2015, Brigham Young University, Provo, UT.*
- Franke, K., Wright, A., and Ekstrom, L. (2014b). Comparative Study between Two Performance-Based Liquefaction Triggering Models for the Standard Penetration Test. *J. Geotech. Geoenviron. Eng.* , [10.1061/\(ASCE\)GT.1943-5606.0001094](https://doi.org/10.1061/(ASCE)GT.1943-5606.0001094) , 04014010.
- Ku, C.-S., Juang, C. H., Chang, C.-W., and Ching, J. (2012). “Probabilistic version of the Robertson and Wride method for liquefaction evaluation: development and application.” *Canadian Geotechnical Journal*, 49(1), 27-44.
- Mayfield, R. T., Kramer, S. L., and Huang, Y.-M. (2010). Simplified approximation procedure for performance-based evaluation of liquefaction potential. *J. Geotech. Geoenviron. Eng.*, [10.1061/\(ASCE\)GT.1943-5606.0000191](https://doi.org/10.1061/(ASCE)GT.1943-5606.0000191), 140–150.
- Ulmer, K. J. (2015). “Development of a Simplified Performance-Based Procedure for Assessment of Liquefaction Triggering Using Liquefaction Loading Maps.” M.S. *Thesis, 2015, Brigham Young University, Provo, UT.*
- USGS. (2014). USGS Unified Hazard Tool <https://earthquake.usgs.gov/hazards/interactive/> (October 25, 2018).
- Zhang, G., Robertson, P.K., and Brachman, R.W.I. (2004). Estimating liquefaction-induced lateral displacements using the Standard Penetration Test or Cone Penetration Test. *J. Geotech. Geoenviron. Eng.*, 130(8), 861-871.

A. APPENDIX

The liquefaction parameter maps are attached to the end of this report as a separate PDF file. The maps are organized by state in alphabetical order and for three return periods in three sections:

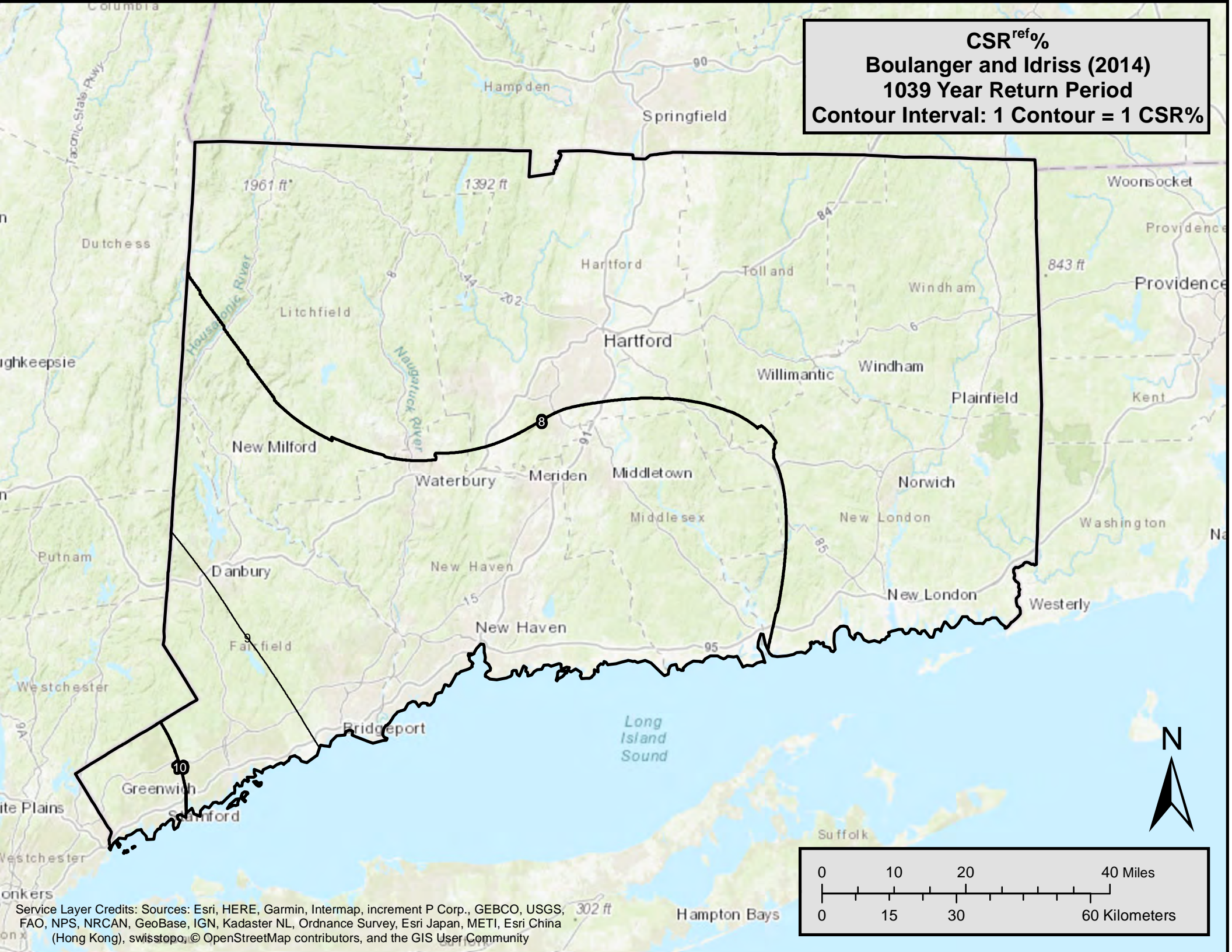
1. Liquefaction Triggering
 - a. Boulanger and Idriss (2014) , CSR^{ref} %
 - b. Ku et al. (2012), q_{req}^{ref}
2. Settlement
 - a. Boulanger and Idriss (2014), ε_v^{ref} (%)
 - b. Ku et al. (2012), ε_v^{ref} (%)
3. Lateral Spread
 - a. Boulanger and Idriss (2014), γ_{max}^{ref} (%)
 - b. Ku et al. (2012) , γ_{max}^{ref} (%)

CSR^{ref}%
Boulanger and Idriss (2014)
475 Year Return Period
Contour Interval: 1 Contour = 0.5 CSR%



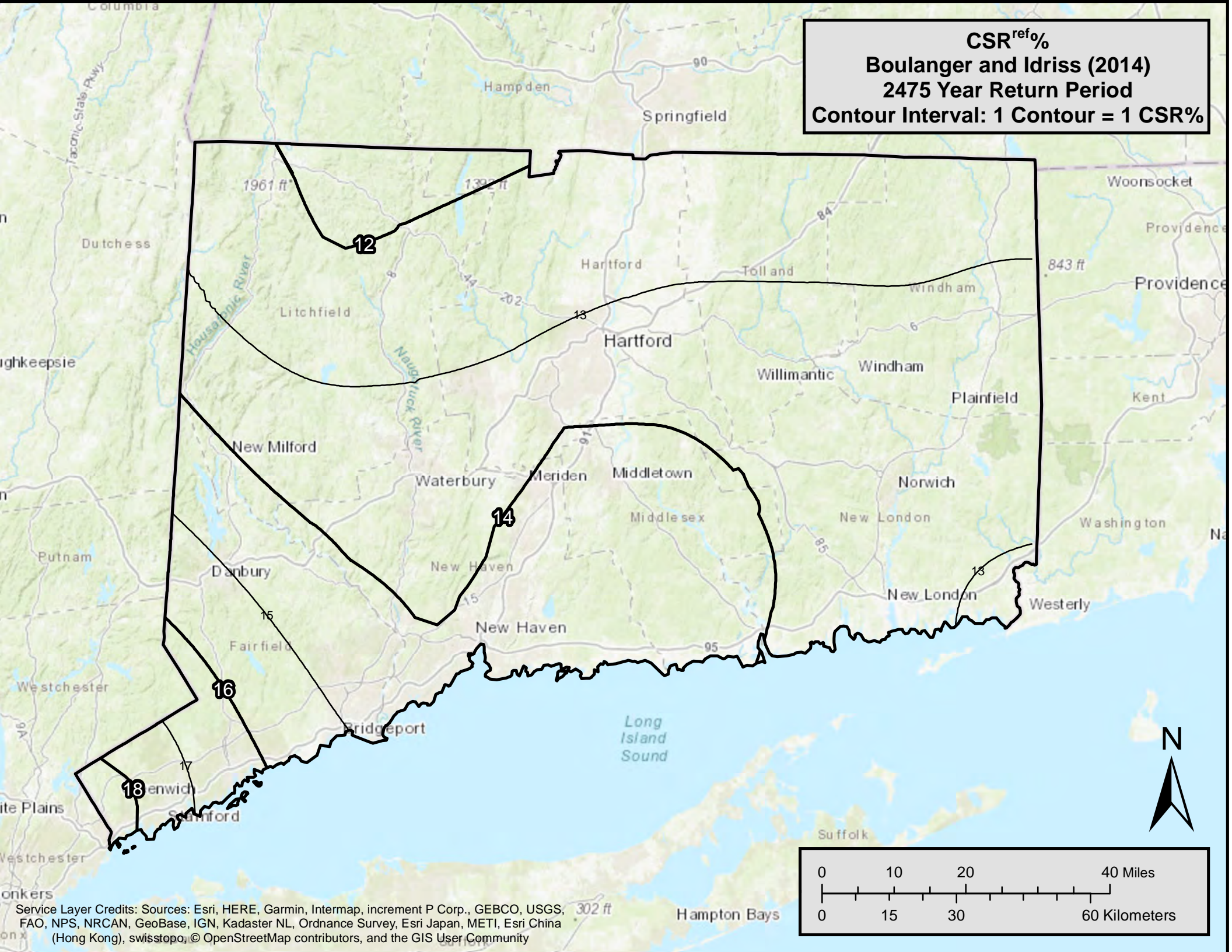
Service Layer Credits: Sources: Esri, HERE, Garmin, Intermap, increment P Corp., GEBCO, USGS, FAO, NPS, NRCAN, GeoBase, IGN, Kadaster NL, Ordnance Survey, Esri Japan, METI, Esri China (Hong Kong), swisstopo, © OpenStreetMap contributors, and the GIS User Community

CSR^{ref}%
Boulanger and Idriss (2014)
1039 Year Return Period
Contour Interval: 1 Contour = 1 CSR%



Service Layer Credits: Sources: Esri, HERE, Garmin, Intermap, increment P Corp., GEBCO, USGS, FAO, NPS, NRCAN, GeoBase, IGN, Kadaster NL, Ordnance Survey, Esri Japan, METI, Esri China (Hong Kong), swisstopo, © OpenStreetMap contributors, and the GIS User Community

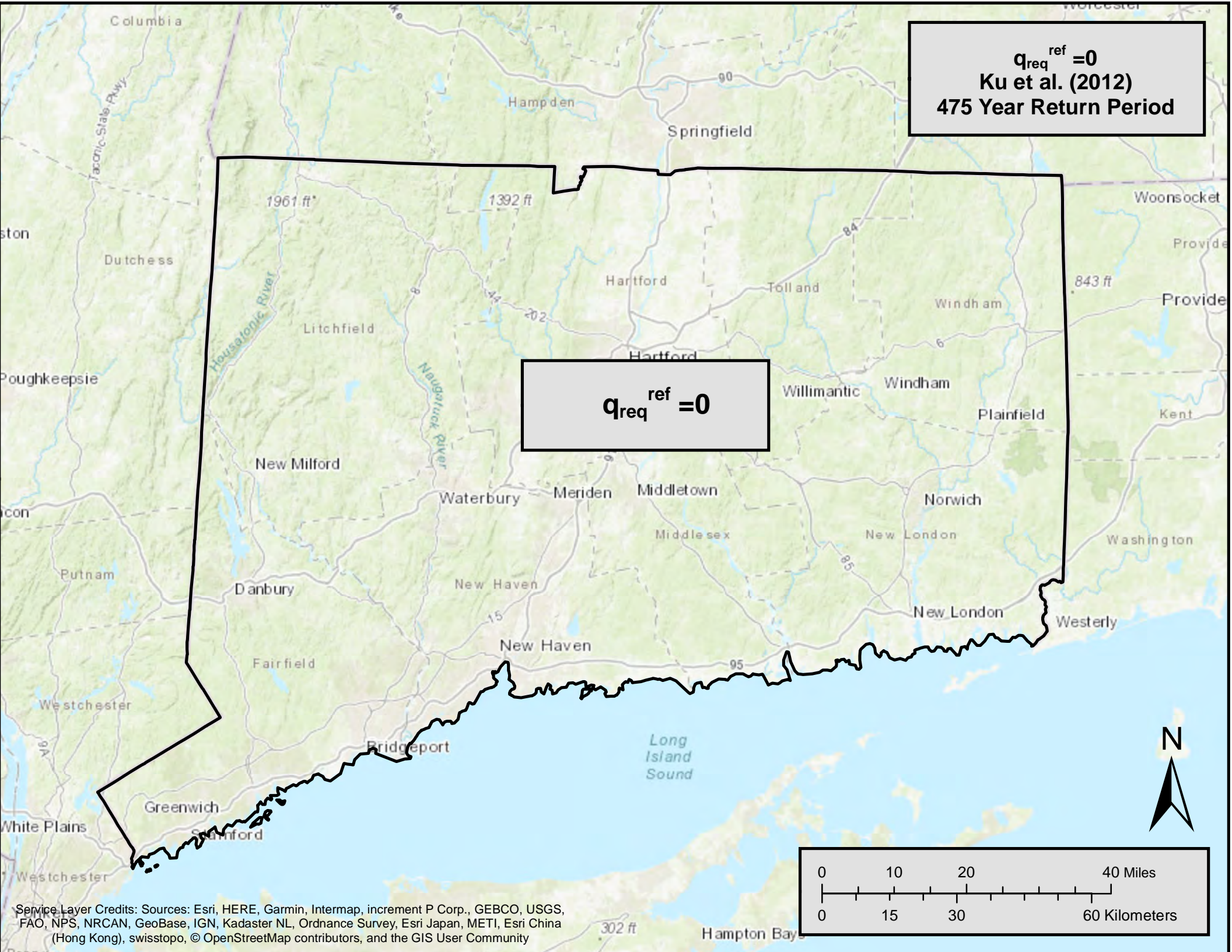
CSR^{ref}%
Boulanger and Idriss (2014)
2475 Year Return Period
Contour Interval: 1 Contour = 1 CSR%



Service Layer Credits: Sources: Esri, HERE, Garmin, Intermap, increment P Corp., GEBCO, USGS, FAO, NPS, NRCAN, GeoBase, IGN, Kadaster NL, Ordnance Survey, Esri Japan, METI, Esri China (Hong Kong), swisstopo, © OpenStreetMap contributors, and the GIS User Community

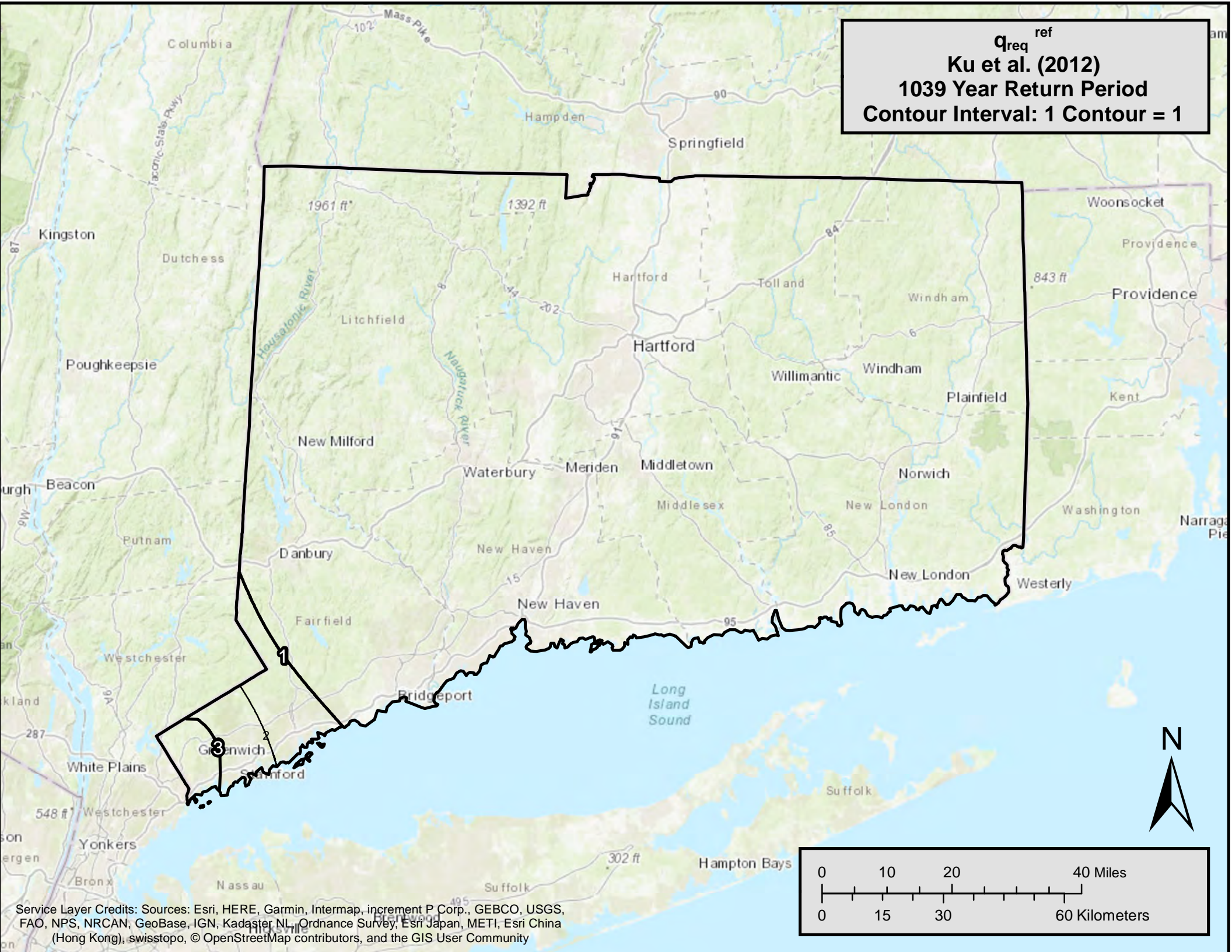
$q_{req}^{ref} = 0$
Ku et al. (2012)
475 Year Return Period

$q_{req}^{ref} = 0$



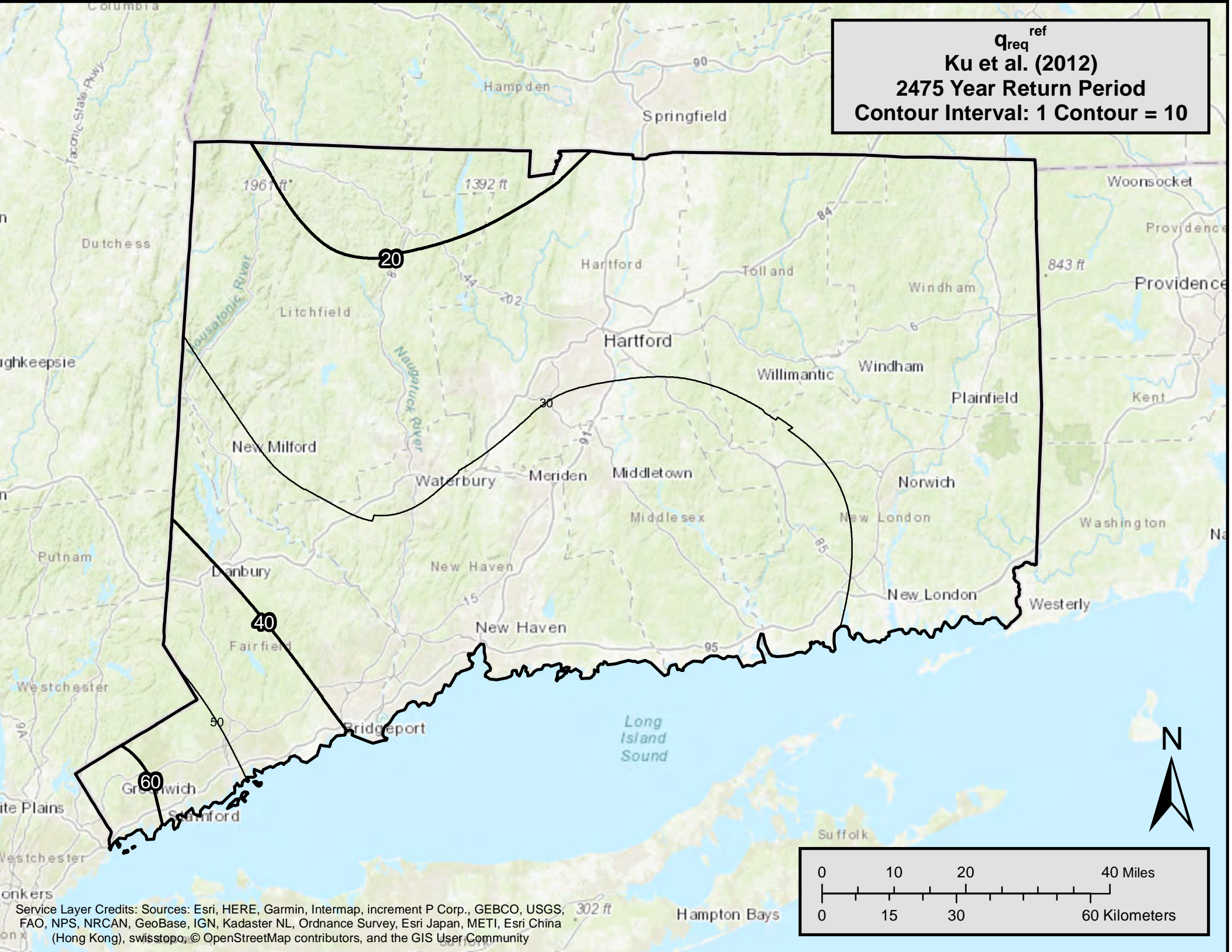
Service Layer Credits: Sources: Esri, HERE, Garmin, Intermap, increment P Corp., GEBCO, USGS, FAO, NPS, NRCAN, GeoBase, IGN, Kadaster NL, Ordnance Survey, Esri Japan, METI, Esri China (Hong Kong), swisstopo, © OpenStreetMap contributors, and the GIS User Community

Q_{req}^{ref}
Ku et al. (2012)
1039 Year Return Period
Contour Interval: 1 Contour = 1



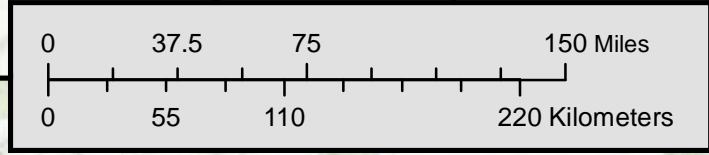
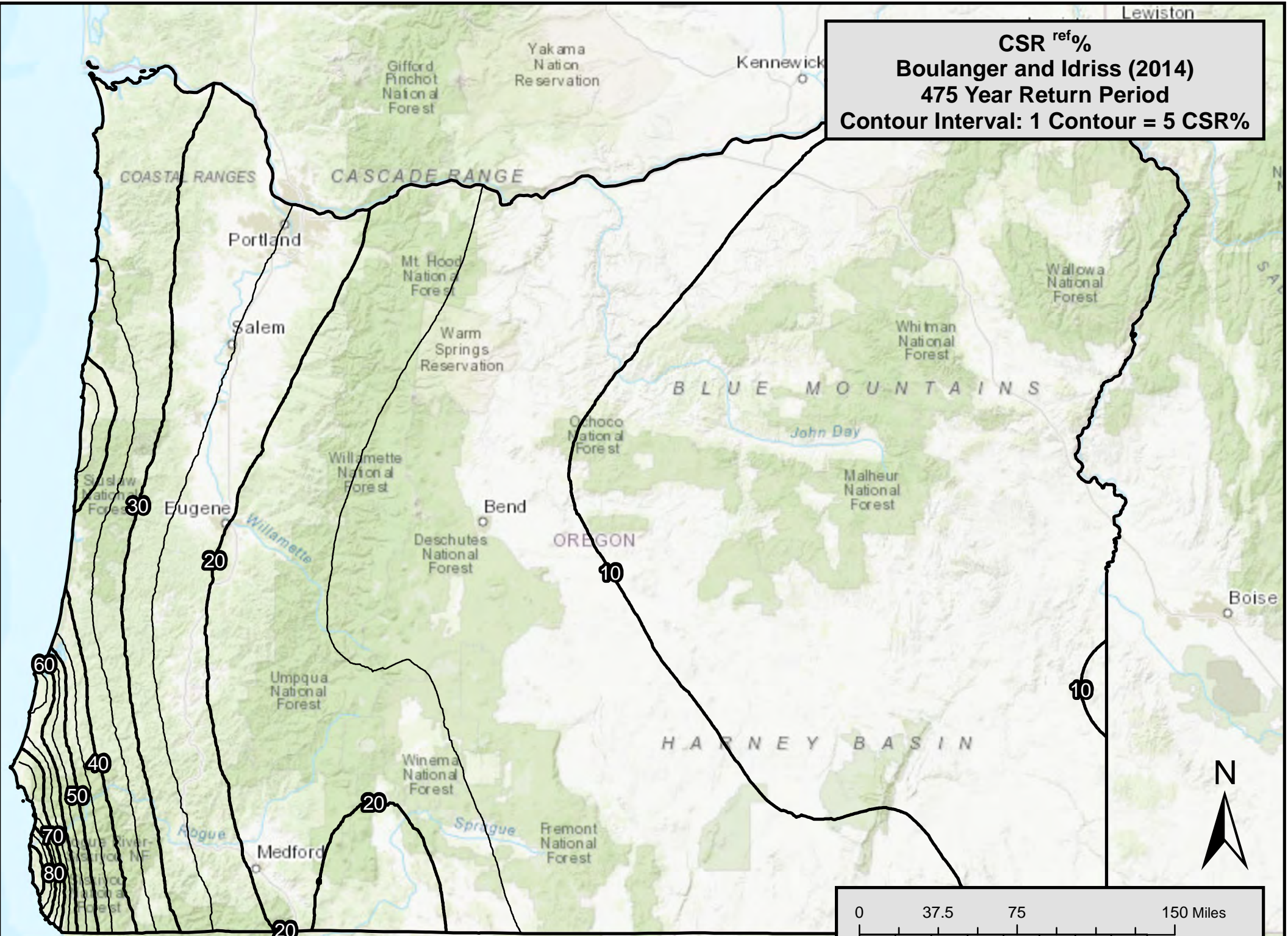
Service Layer Credits: Sources: Esri, HERE, Garmin, Intermap, increment P Corp., GEBCO, USGS, FAO, NPS, NRCAN, GeoBase, IGN, Kadaster NL, Ordnance Survey, Esri Japan, METI, Esri China (Hong Kong), swisstopo, © OpenStreetMap contributors, and the GIS User Community

Q_{req}^{ref}
Ku et al. (2012)
2475 Year Return Period
Contour Interval: 1 Contour = 10



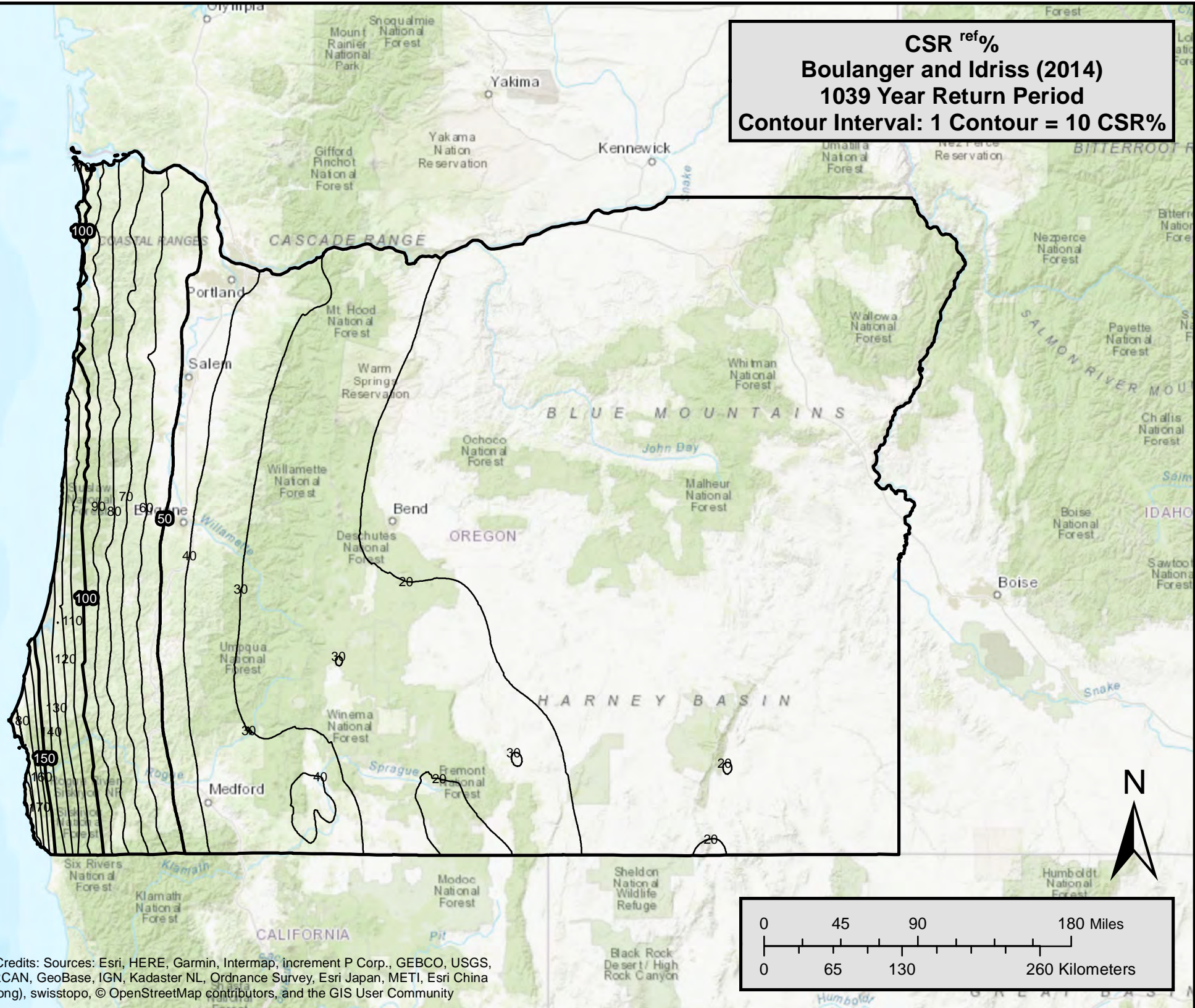
Service Layer Credits: Sources: Esri, HERE, Garmin, Intermap, increment P Corp., GEBCO, USGS, FAO, NPS, NRCAN, GeoBase, IGN, Kadaster NL, Ordnance Survey, Esri Japan, METI, Esri China (Hong Kong), swisstopo, © OpenStreetMap contributors, and the GIS User Community

CSR^{ref}%
Boulanger and Idriss (2014)
475 Year Return Period
Contour Interval: 1 Contour = 5 CSR%



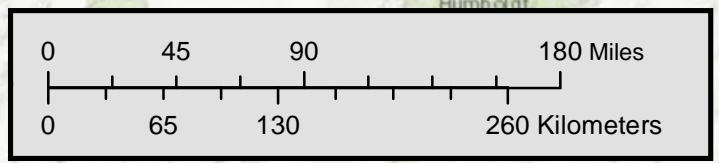
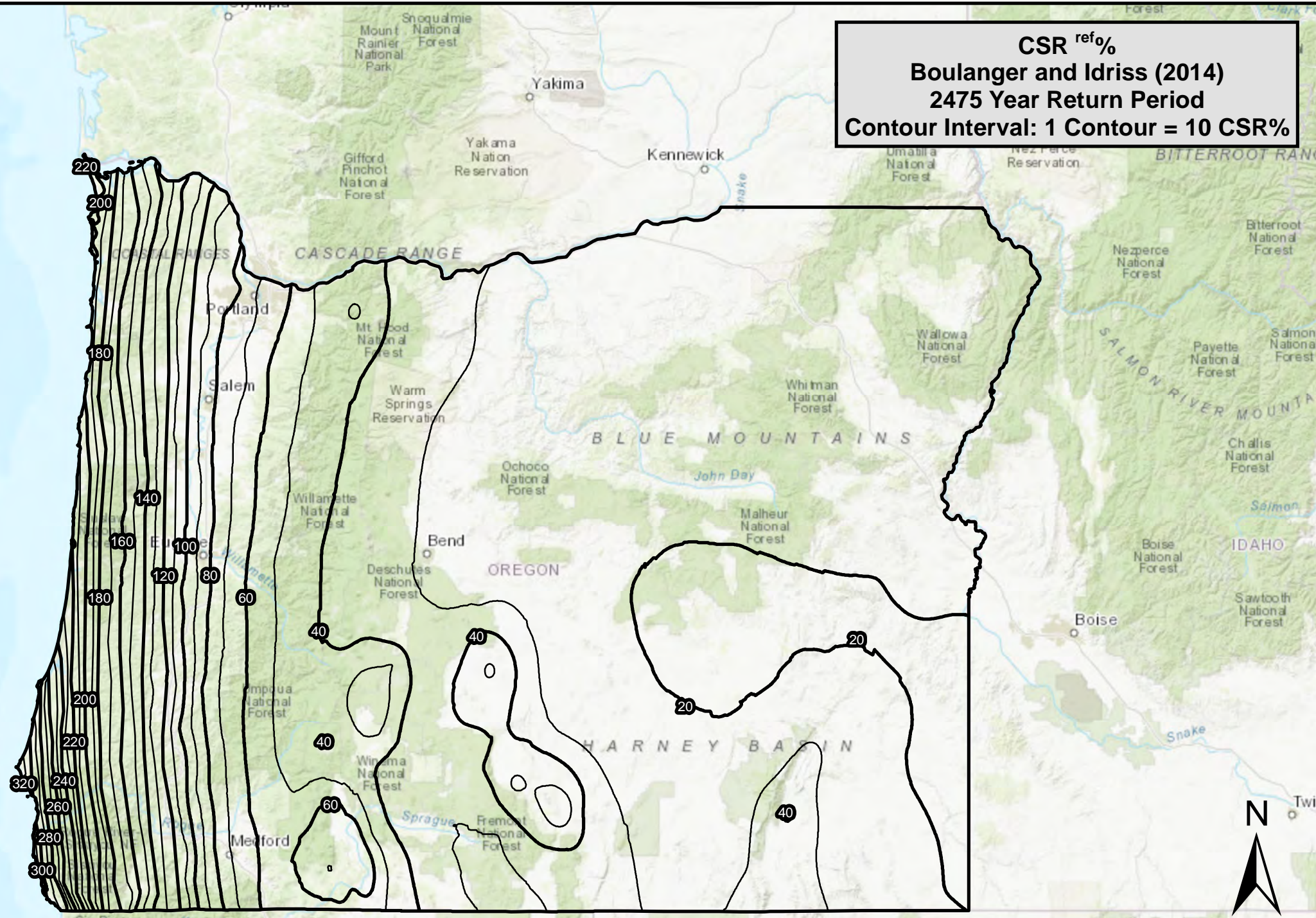
Service Layer Credits: Sources: Esri, HERE, Garmin, Intermap, increment P Corp., GEBCO, USGS, FAO, NPS, NRCAN, GeoBase, IGN, Kadaster NL, Ordnance Survey, Esri Japan, METI, Esri China (Hong Kong), swisstopo, © OpenStreetMap contributors, and the GIS User Community

CSR^{ref}%
Boulanger and Idriss (2014)
1039 Year Return Period
Contour Interval: 1 Contour = 10 CSR%



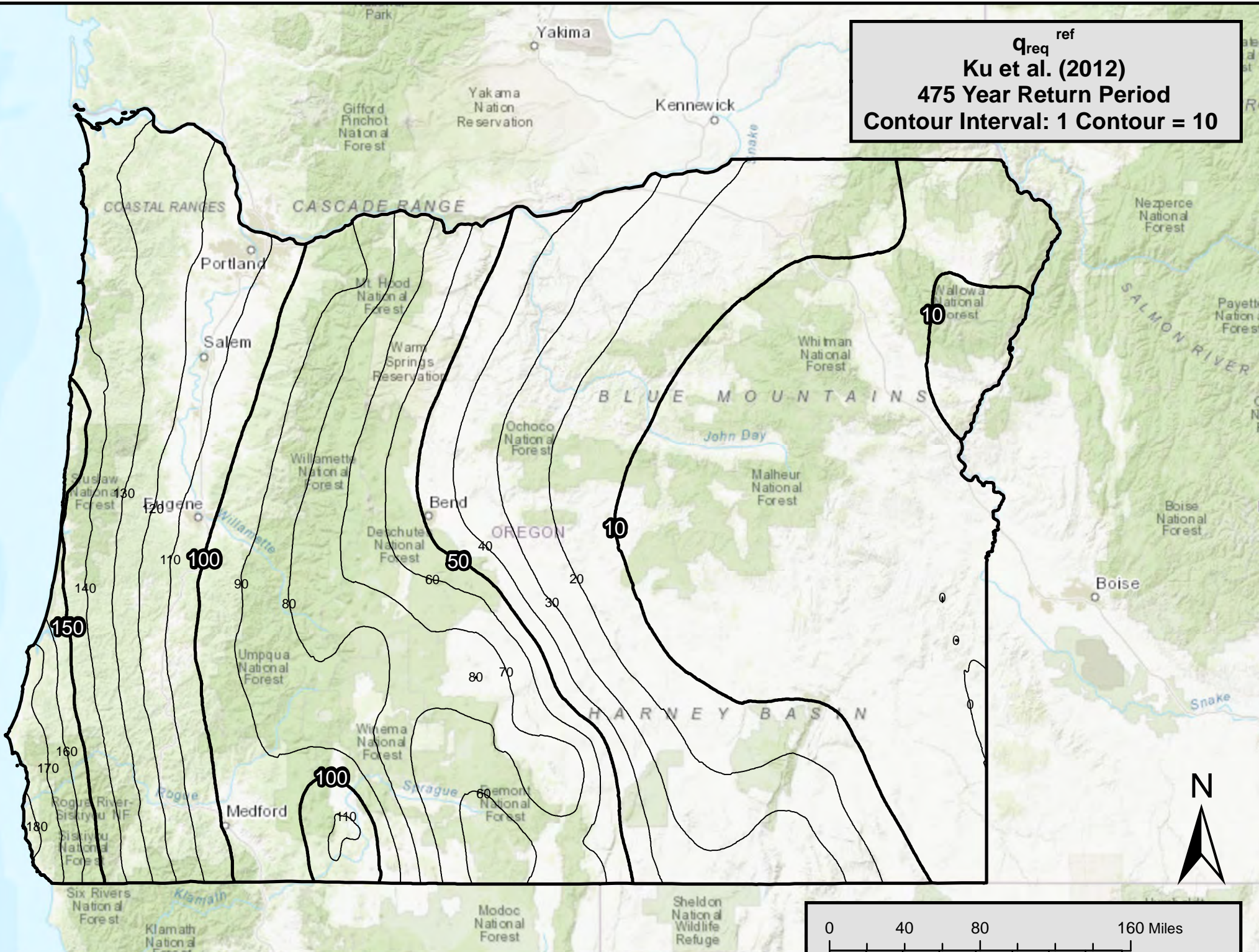
Service Layer Credits: Sources: Esri, HERE, Garmin, Intermap, increment P Corp., GEBCO, USGS, FAO, NPS, NRCAN, GeoBase, IGN, Kadaster NL, Ordnance Survey, Esri Japan, METI, Esri China (Hong Kong), swisstopo, © OpenStreetMap contributors, and the GIS User Community

CSR^{ref}%
Boulanger and Idriss (2014)
2475 Year Return Period
Contour Interval: 1 Contour = 10 CSR%



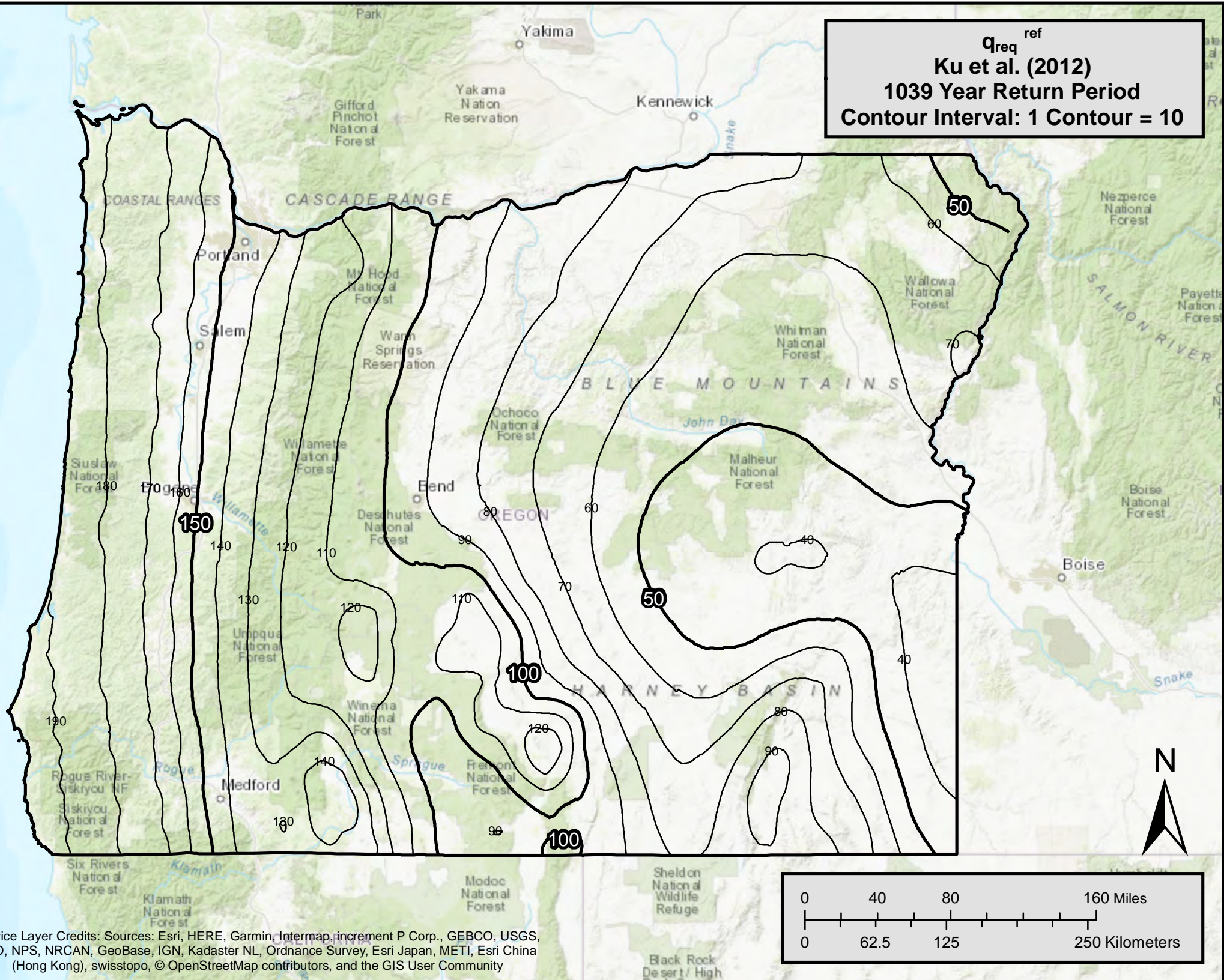
Service Layer Credits: Sources: Esri, HERE, Garmin, Intermap, increment P Corp., GEBCO, USGS, FAO, NPS, NRCAN, GeoBase, IGN, Kadaster NL, Ordnance Survey, Esri Japan, METI, Esri China (Hong Kong), swisstopo, © OpenStreetMap contributors, and the GIS User Community

Q_{req}^{ref}
Ku et al. (2012)
475 Year Return Period
Contour Interval: 1 Contour = 10



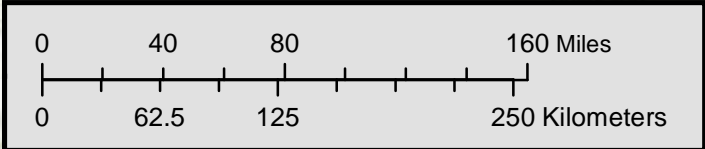
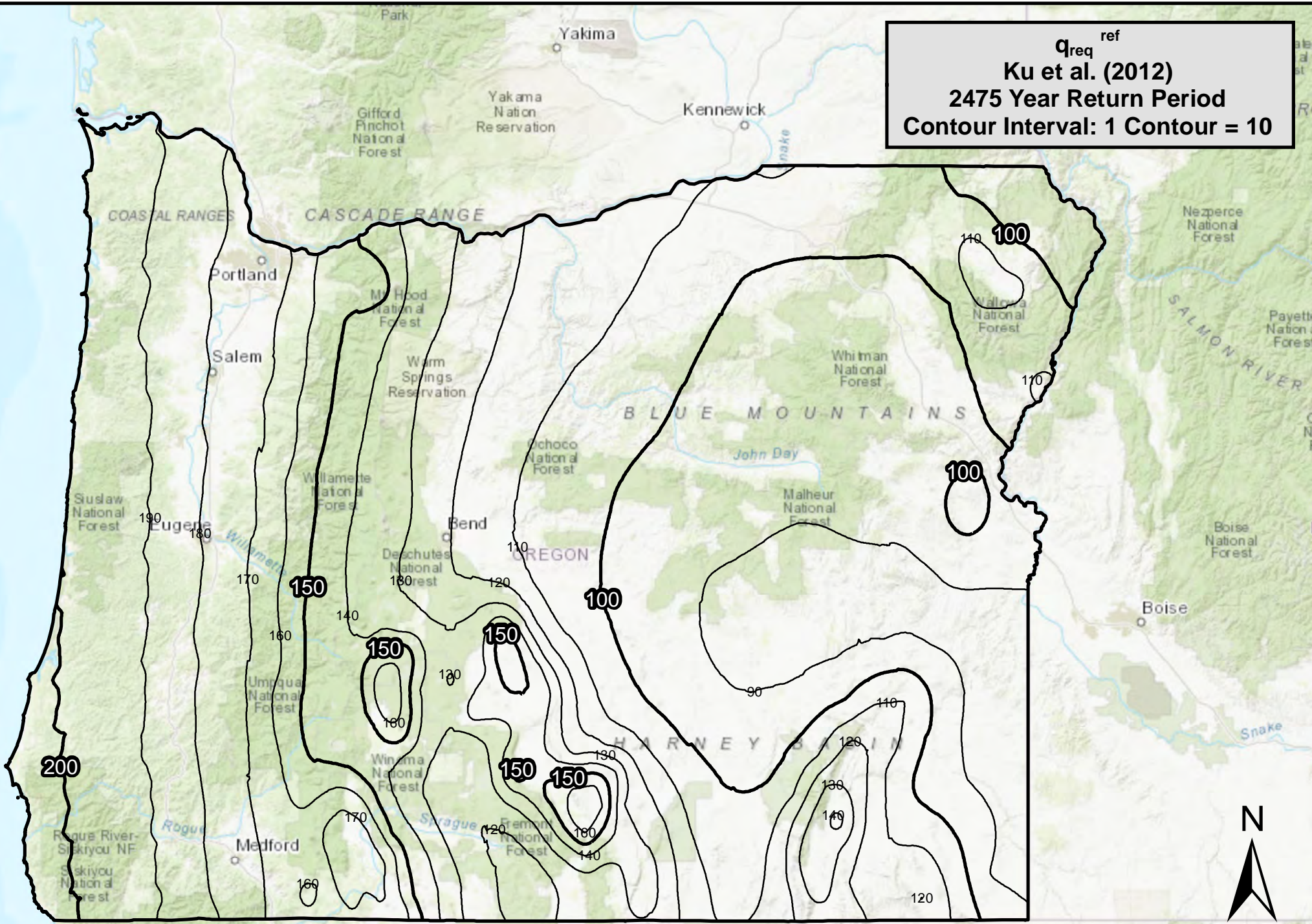
Service Layer Credits: Sources: Esri, HERE, Garmin, Intermap, increment P Corp., GEBCO, USGS, FAO, NPS, NRCAN, GeoBase, IGN, Kadaster NL, Ordnance Survey, Esri Japan, METI, Esri China (Hong Kong), swisstopo, © OpenStreetMap contributors, and the GIS User Community

Q_{req}^{ref}
Ku et al. (2012)
1039 Year Return Period
Contour Interval: 1 Contour = 10



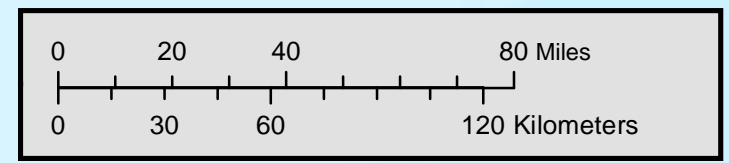
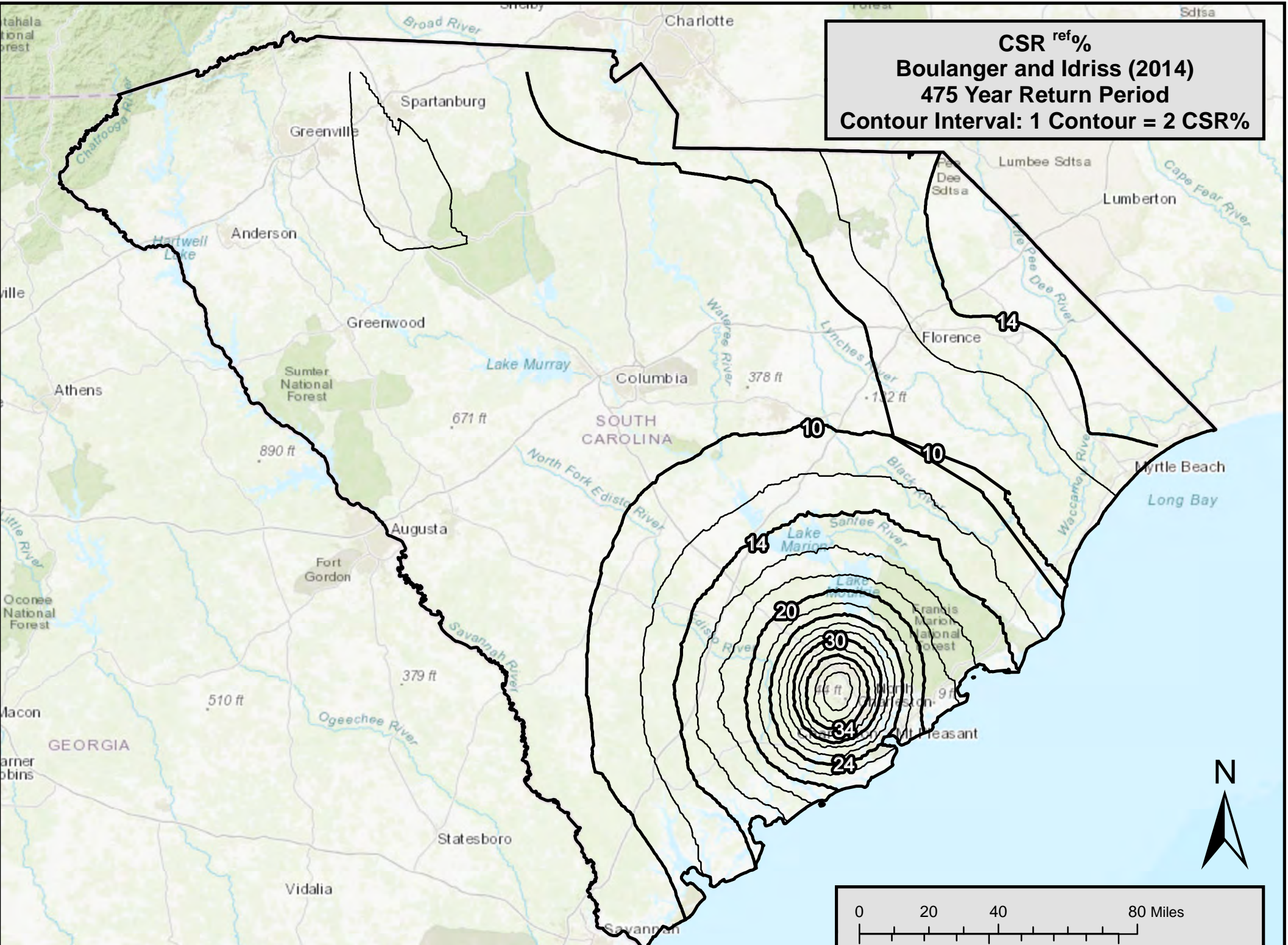
Service Layer Credits: Sources: Esri, HERE, Garmin, Intermap, increment P Corp., GEBCO, USGS, FAO, NPS, NRCAN, GeoBase, IGN, Kadaster NL, Ordnance Survey, Esri Japan, METI, Esri China (Hong Kong), swisstopo, © OpenStreetMap contributors, and the GIS User Community

Q_{req}^{ref}
Ku et al. (2012)
2475 Year Return Period
Contour Interval: 1 Contour = 10



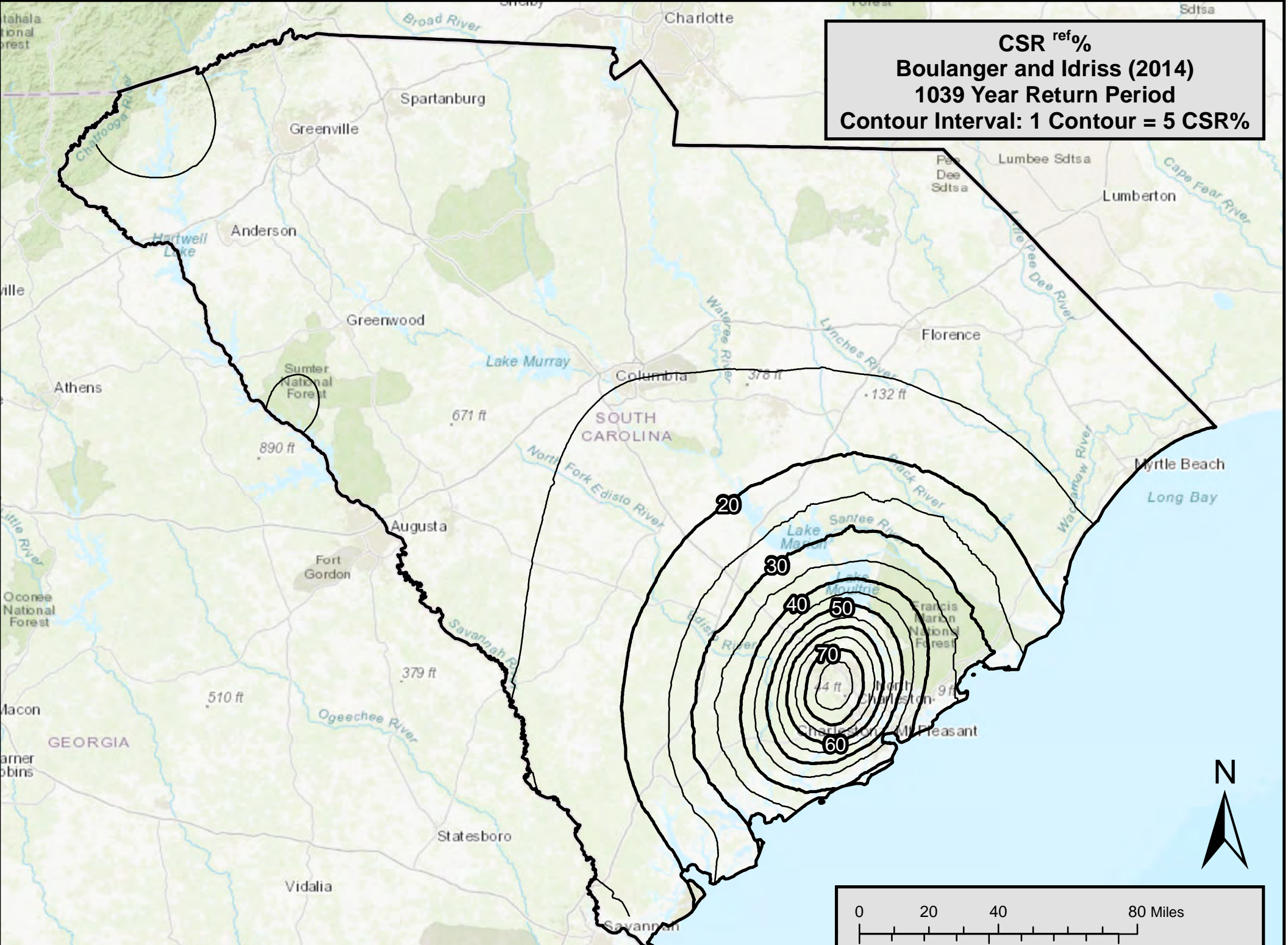
Service Layer Credits: Sources: Esri, HERE, Garmin, Intermap, increment P Corp., GEBCO, USGS, FAO, NPS, NRCAN, GeoBase, IGN, Kadaster NL, Ordnance Survey, Esri Japan, METI, Esri China (Hong Kong), swisstopo, © OpenStreetMap contributors, and the GIS User Community

CSR^{ref}%
Boulanger and Idriss (2014)
475 Year Return Period
Contour Interval: 1 Contour = 2 CSR%



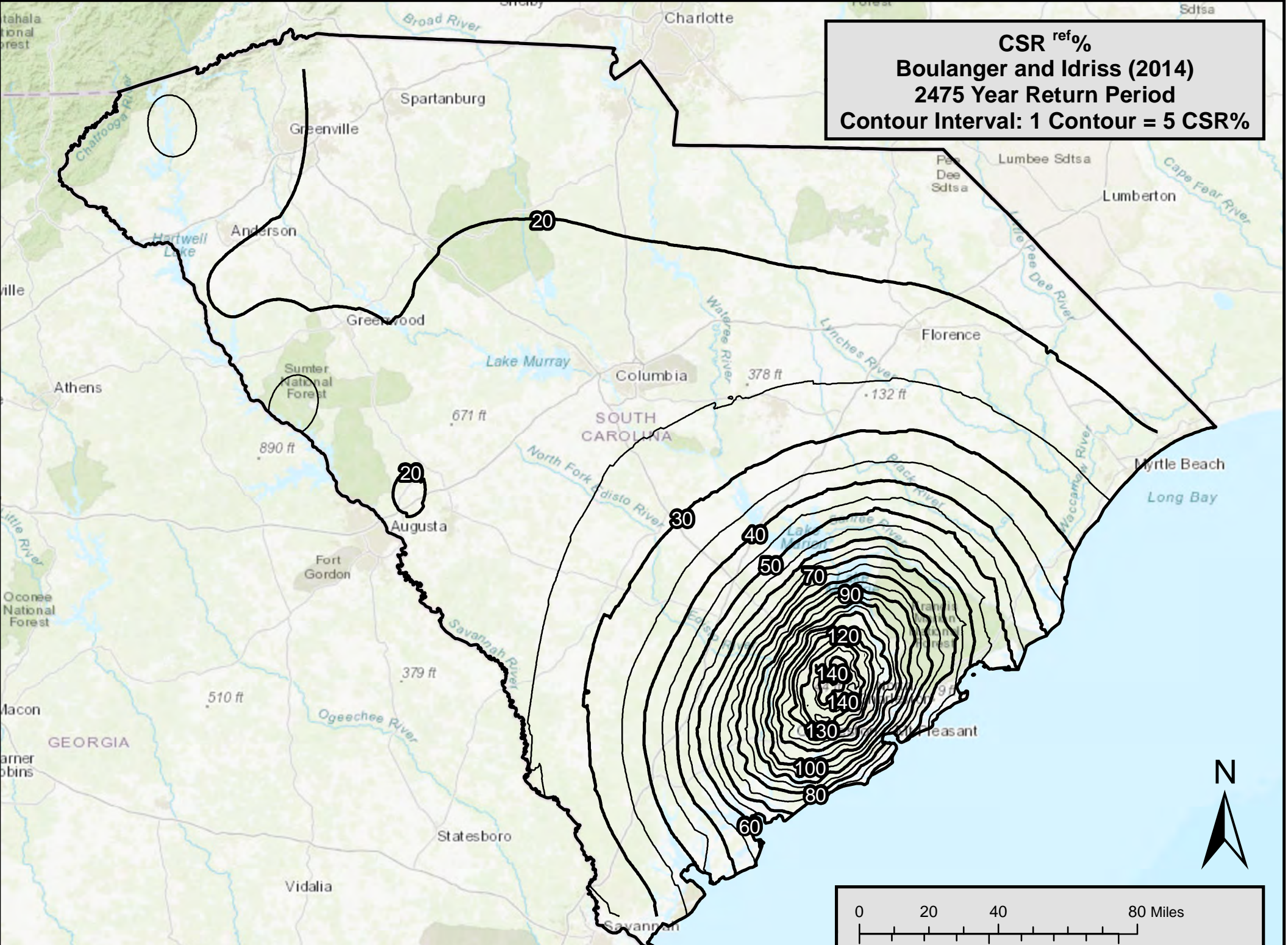
Service Layer Credits: Sources: Esri, HERE, Garmin, Intermap, increment P Corp., GEBCO, USGS, FAO, NPS, NRCAN, GeoBase, IGN, Kadaster NL, Ordnance Survey, Esri Japan, METI, Esri China (Hong Kong), swisstopo, © OpenStreetMap contributors, and the GIS User Community

CSR^{ref}%
Boulanger and Idriss (2014)
1039 Year Return Period
Contour Interval: 1 Contour = 5 CSR%



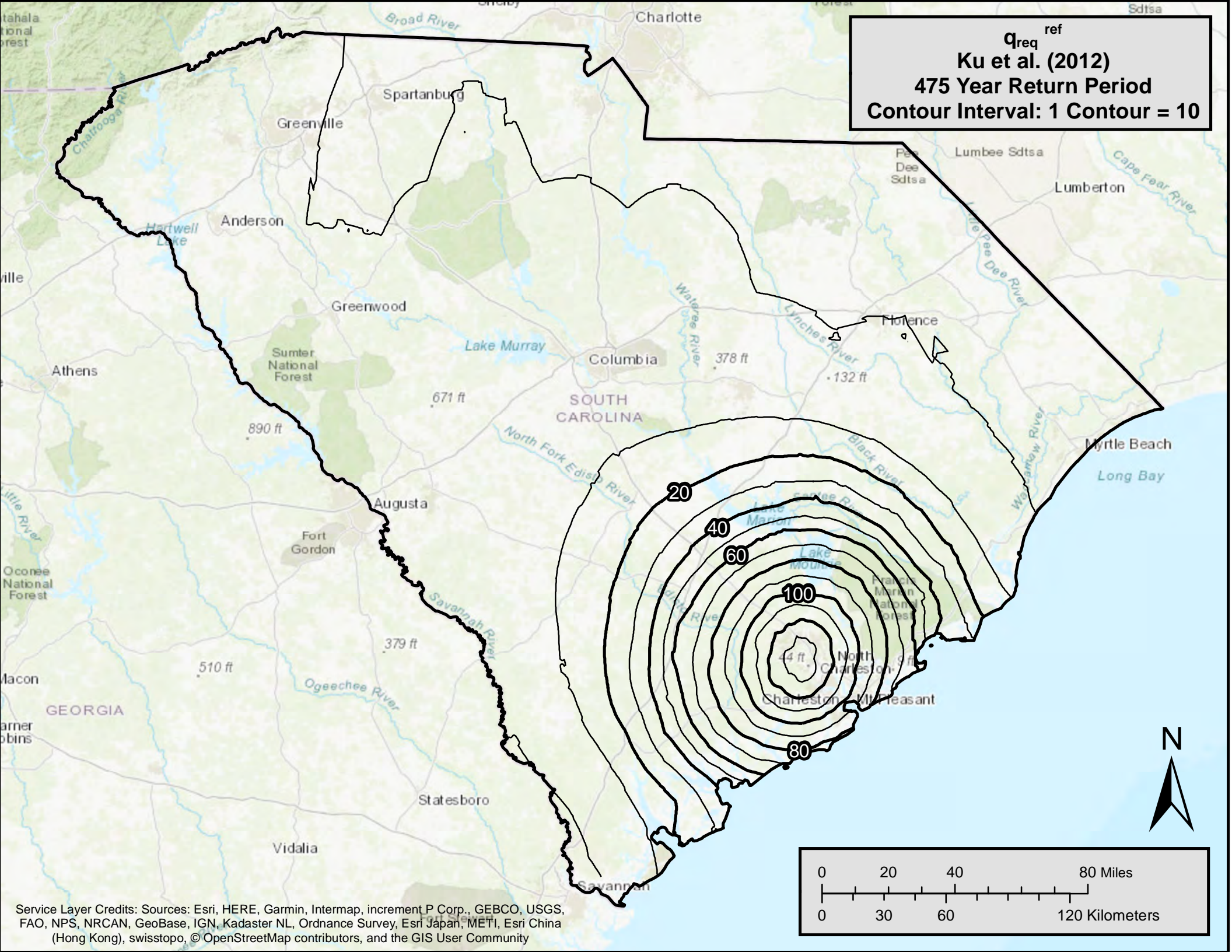
Service Layer Credits: Sources: Esri, HERE, Garmin, Intermap, increment P Corp., GEBCO, USGS, FAO, NPS, NRCAN, GeoBase, IGN, Kadaster NL, Ordnance Survey, Esri Japan, METI, Esri China (Hong Kong), swisstopo, © OpenStreetMap contributors, and the GIS User Community

CSR^{ref}%
Boulanger and Idriss (2014)
2475 Year Return Period
Contour Interval: 1 Contour = 5 CSR%



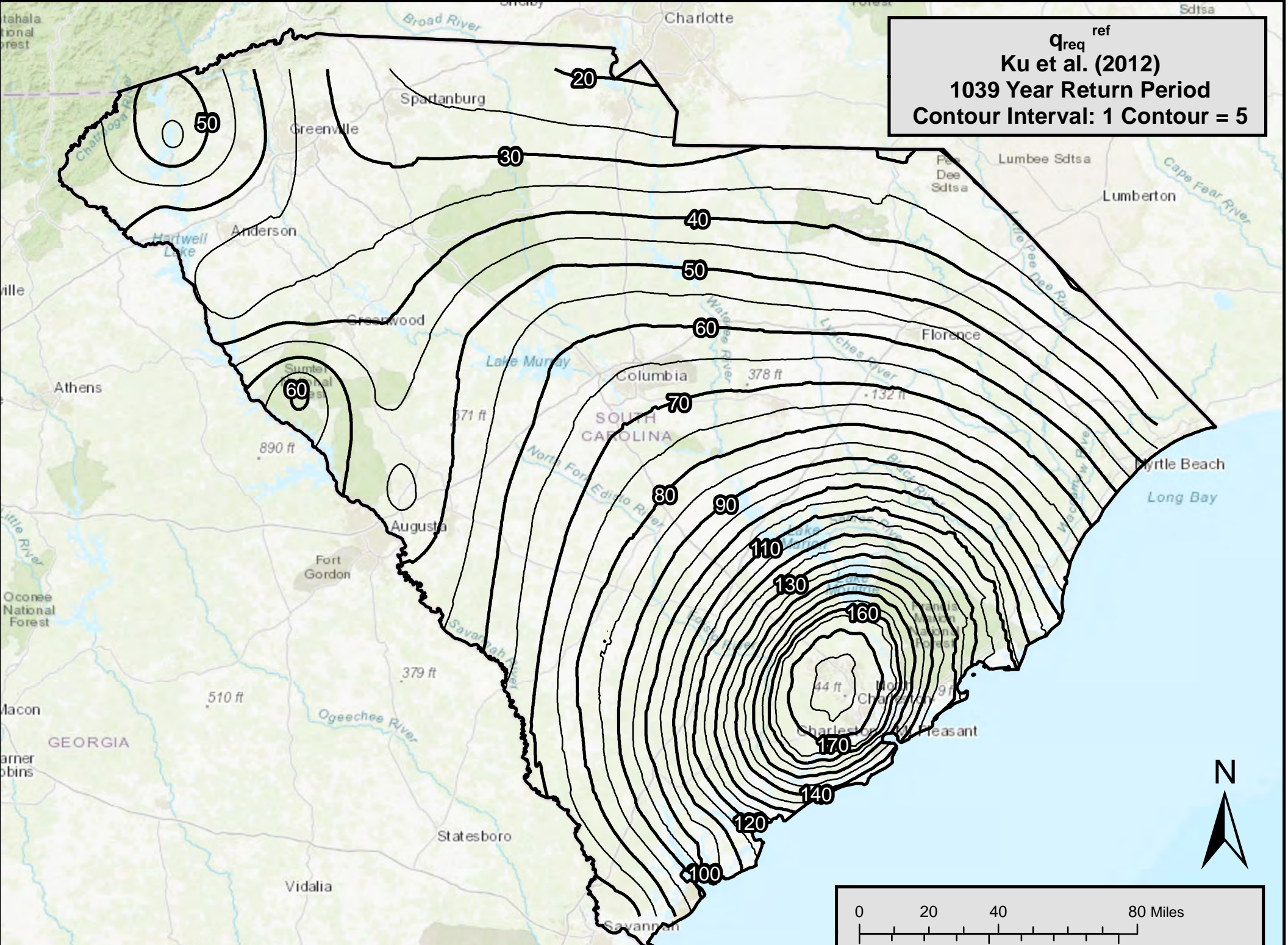
Service Layer Credits: Sources: Esri, HERE, Garmin, Intermap, increment P Corp., GEBCO, USGS, FAO, NPS, NRCAN, GeoBase, IGN, Kadaster NL, Ordnance Survey, Esri Japan, METI, Esri China (Hong Kong), swisstopo, © OpenStreetMap contributors, and the GIS User Community

Q_{req}^{ref}
Ku et al. (2012)
475 Year Return Period
Contour Interval: 1 Contour = 10



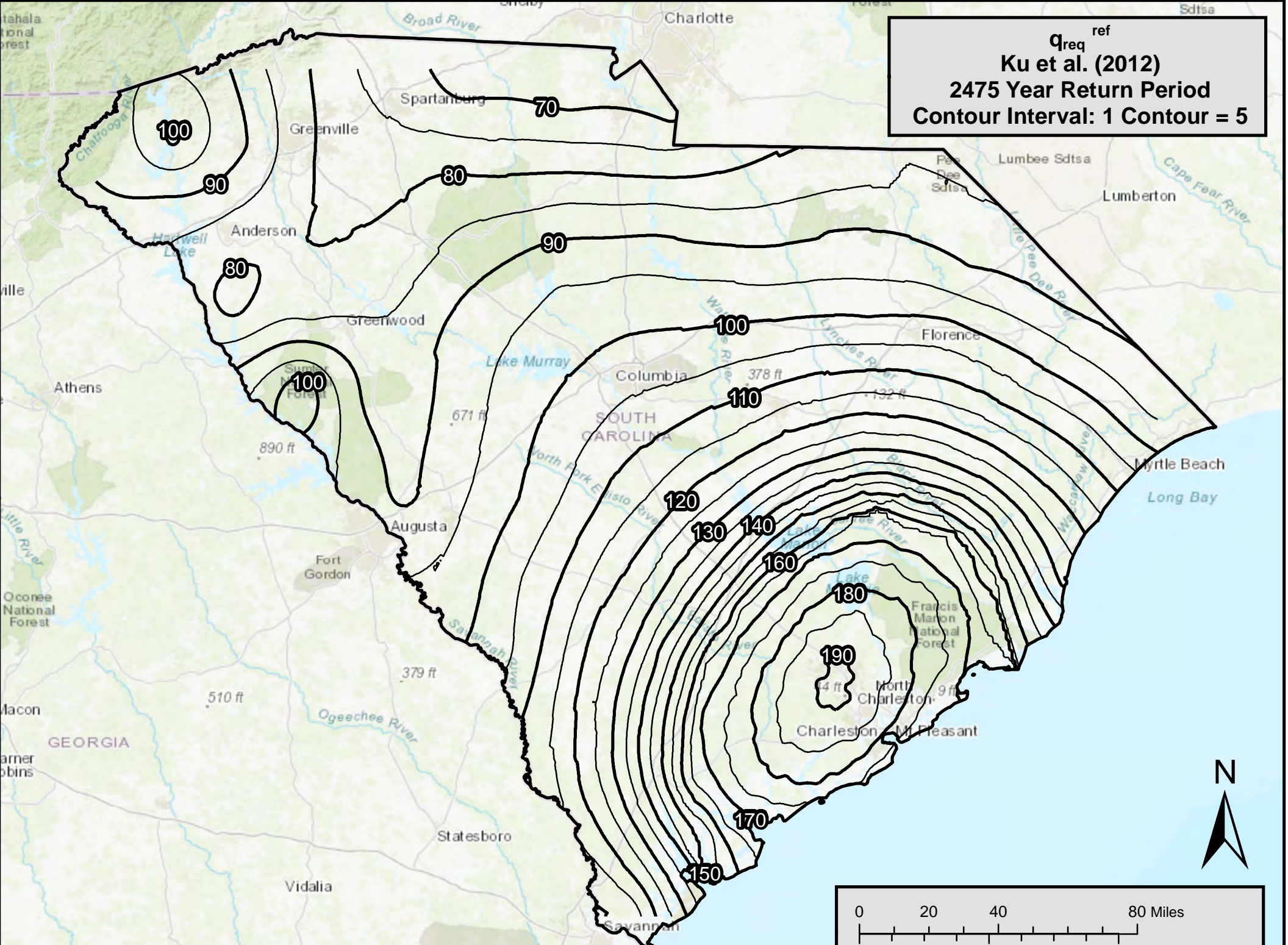
Service Layer Credits: Sources: Esri, HERE, Garmin, Intermap, increment P Corp., GEBCO, USGS, FAO, NPS, NRCAN, GeoBase, IGN, Kadaster NL, Ordnance Survey, Esri Japan, METI, Esri China (Hong Kong), swisstopo, © OpenStreetMap contributors, and the GIS User Community

Q_{req}^{ref}
Ku et al. (2012)
1039 Year Return Period
Contour Interval: 1 Contour = 5



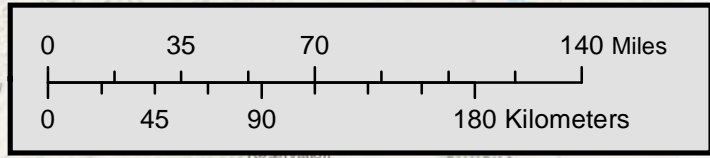
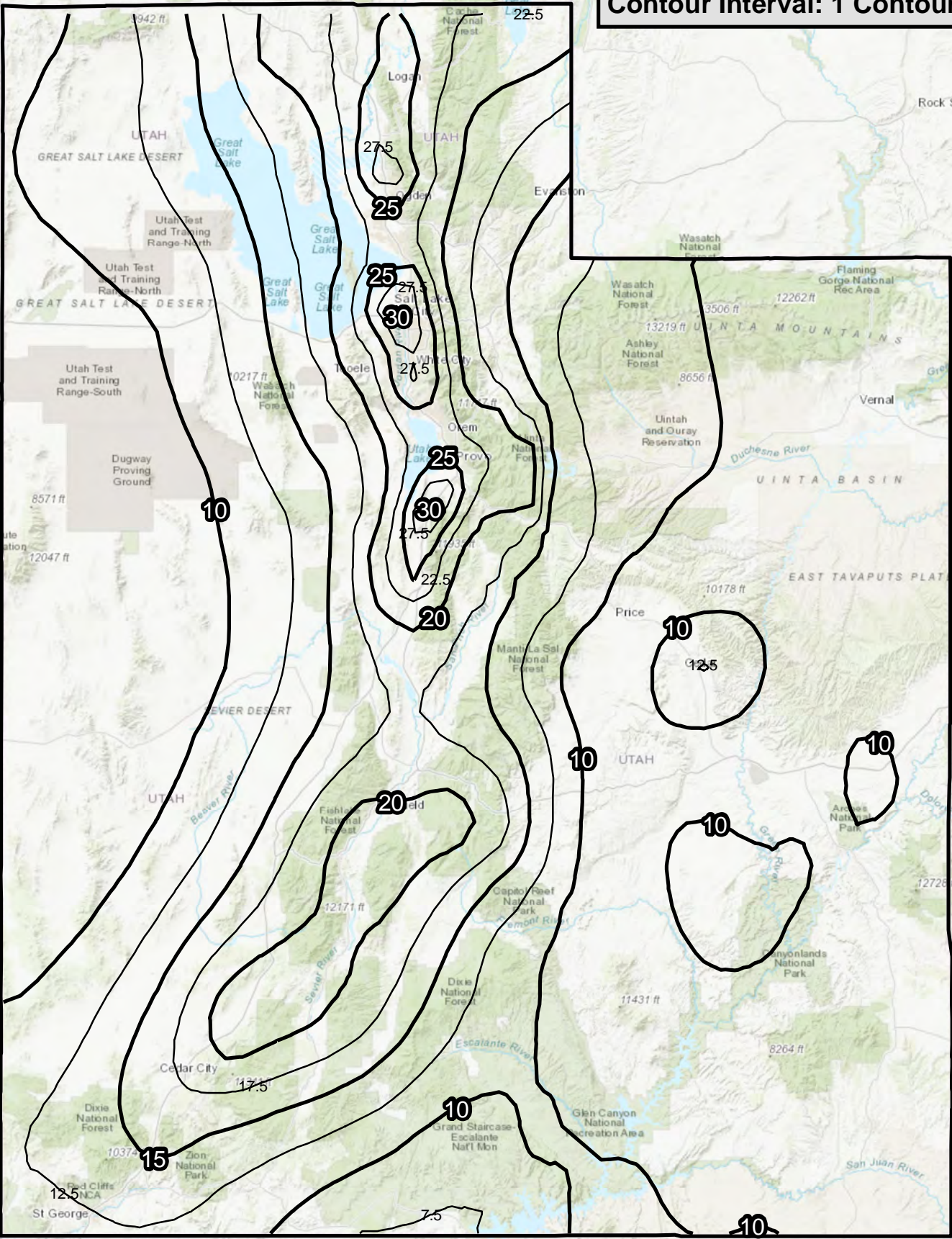
Service Layer Credits: Sources: Esri, HERE, Garmin, Intermap, increment P Corp., GEBCO, USGS, FAO, NPS, NRCAN, GeoBase, IGN, Kadaster NL, Ordnance Survey, Esri Japan, METI, Esri China (Hong Kong), swisstopo, © OpenStreetMap contributors, and the GIS User Community

Q_{req}^{ref}
Ku et al. (2012)
2475 Year Return Period
Contour Interval: 1 Contour = 5



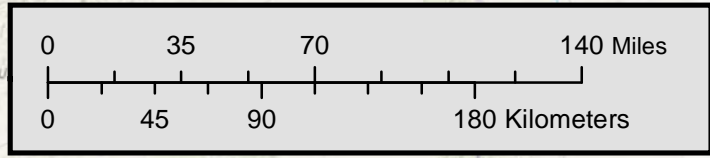
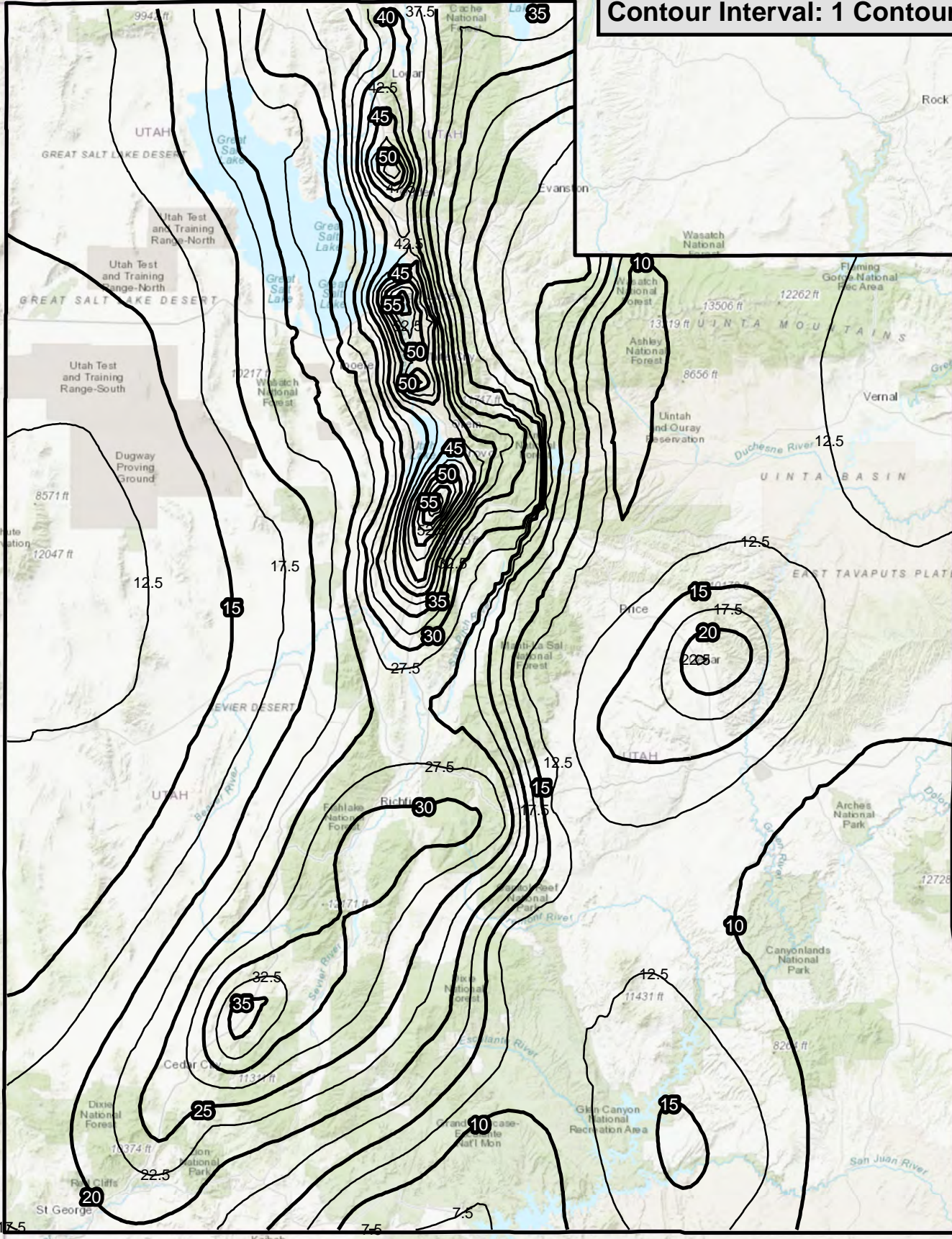
Service Layer Credits: Sources: Esri, HERE, Garmin, Intermap, increment P Corp., GEBCO, USGS, FAO, NPS, NRCAN, GeoBase, IGN, Kadaster NL, Ordnance Survey, Esri Japan, METI, Esri China (Hong Kong), swisstopo, © OpenStreetMap contributors, and the GIS User Community

CSR_{ref}%
Boulanger and Idriss (2014)
475 Year Return Period
Contour Interval: 1 Contour = 2.5 CSR%



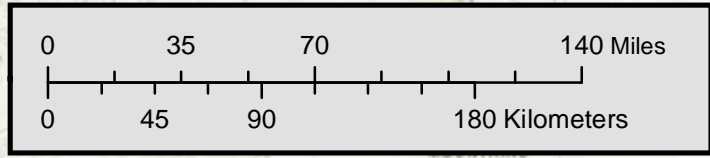
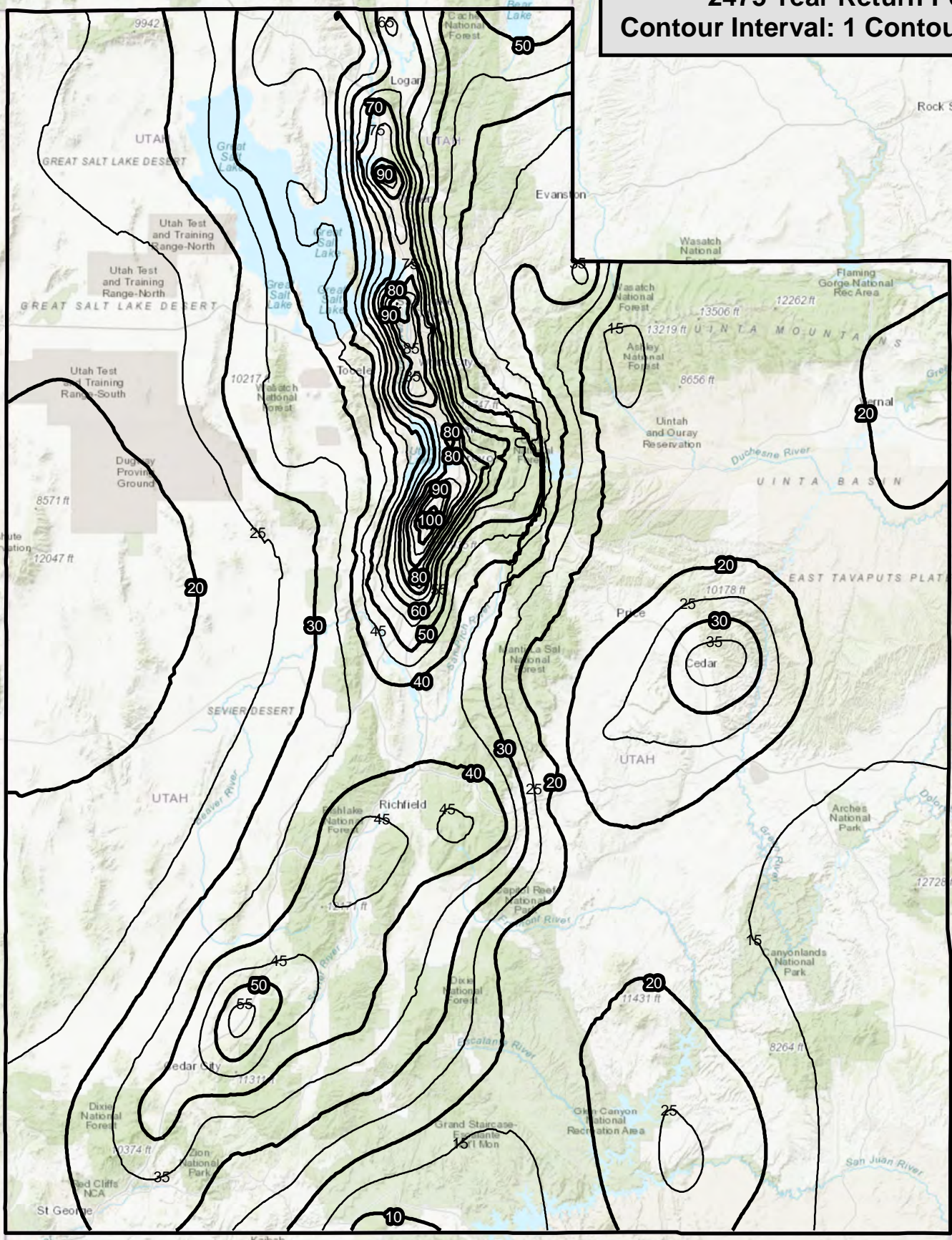
Service Layer Credits: Sources: Esri, HERE, Garmin, Intermap, increment P Corp., GEBCO, USGS, FAO, NPS, NRCAN, GeoBase, IGN, Kadaster NL, Ordnance Survey, Esri Japan, METI, Esri China (Hong Kong), swisstopo, © OpenStreetMap contributors, and the GIS User Community

CSR^{ref}%
Boulanger and Idriss (2014)
1039 Year Return Period
Contour Interval: 1 Contour = 2.5 CSR%



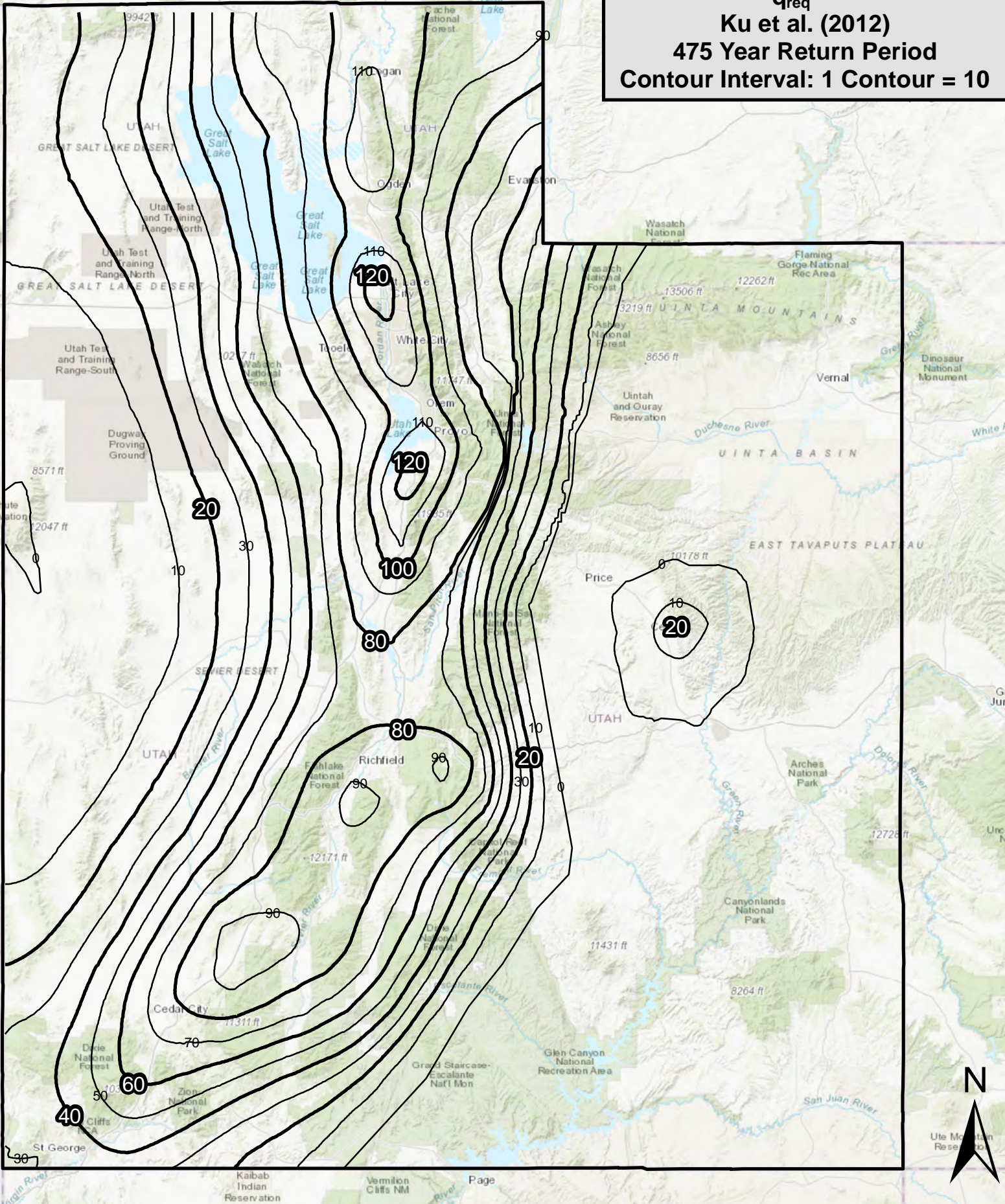
Service Layer Credits: Sources: Esri, HERE, Garmin, Intermap, increment P Corp., GEBCO, USGS, FAO, NPS, NRCAN, GeoBase, IGN, Kadaster NL, Ordnance Survey, Esri Japan, METI, Esri China (Hong Kong), swisstopo, © OpenStreetMap contributors, and the GIS User Community

CSR^{ref}%
Boulanger and Idriss (2014)
2475 Year Return Period
Contour Interval: 1 Contour = 5 CSR%

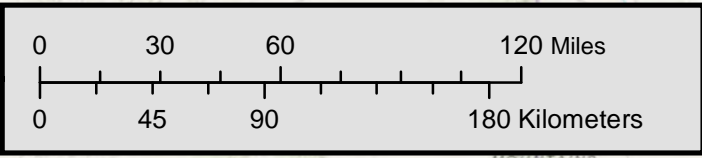


Service Layer Credits: Sources: Esri, HERE, Garmin, Intermap, increment P Corp., GEBCO, USGS, FAO, NPS, NRCAN, GeoBase, IGN, Kadaster NL, Ordnance Survey, Esri Japan, METI, Esri China (Hong Kong), swisstopo, © OpenStreetMap contributors, and the GIS User Community

Q_{req}^{ref}
Ku et al. (2012)
475 Year Return Period
Contour Interval: 1 Contour = 10



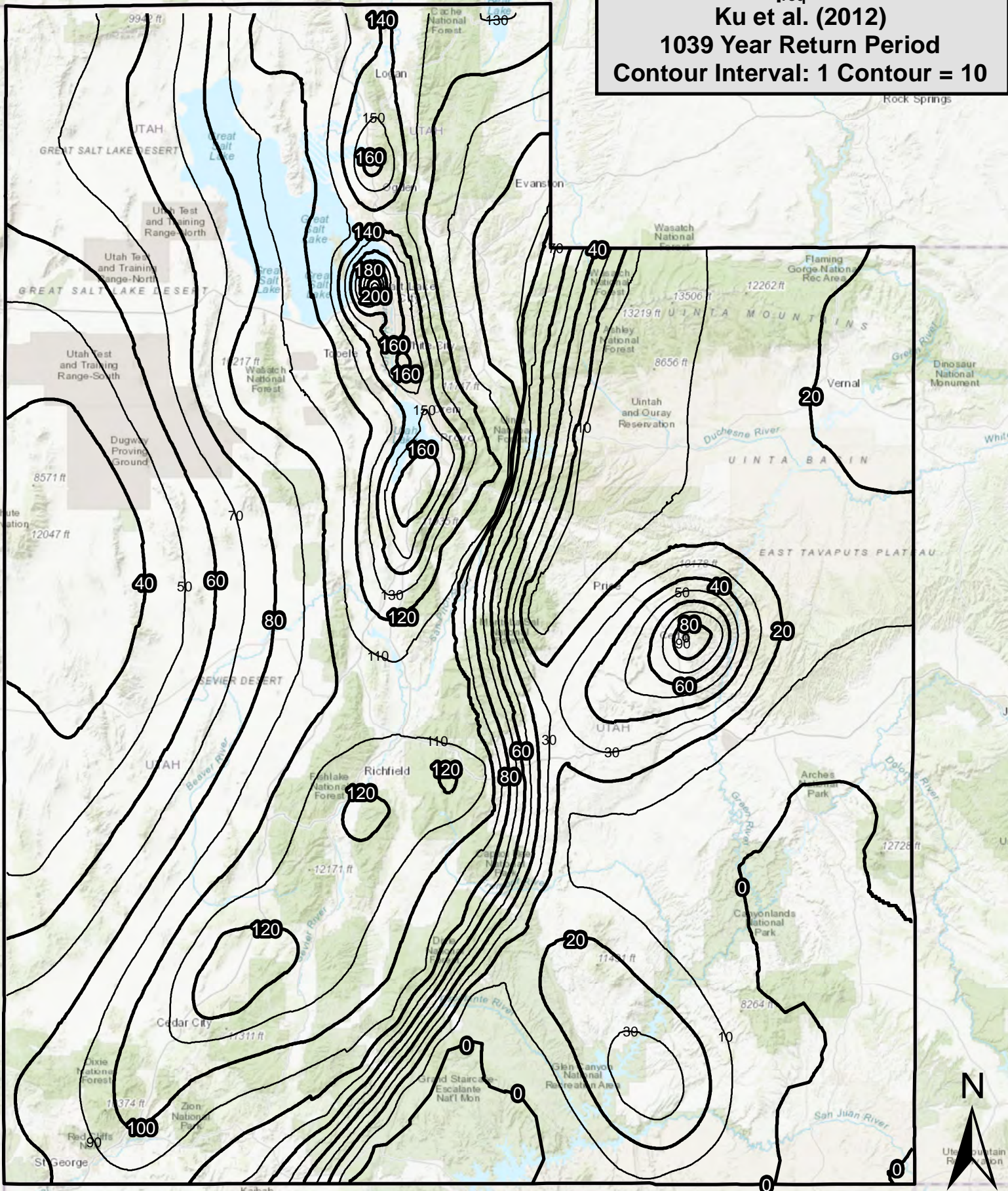
Service Layer Credits: Sources: Esri, HERE, Garmin, Intermap, increment P Corp., GEBCO, USGS, FAO, NPS, NRCAN, GeoBase, IGN, Kadaster NL, Ordnance Survey, Esri Japan, METI, Esri China (Hong Kong), swisstopo, © OpenStreetMap contributors, and the GIS User Community



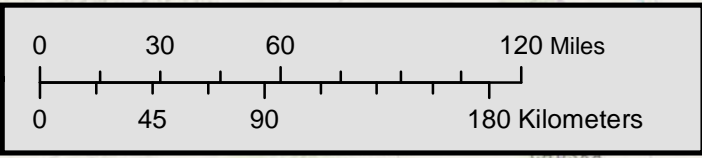
8061 ft

10300 ft

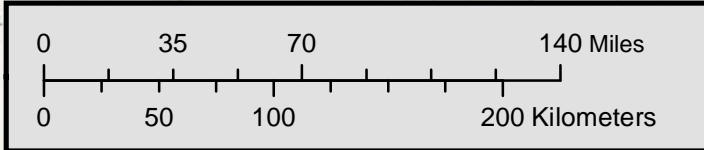
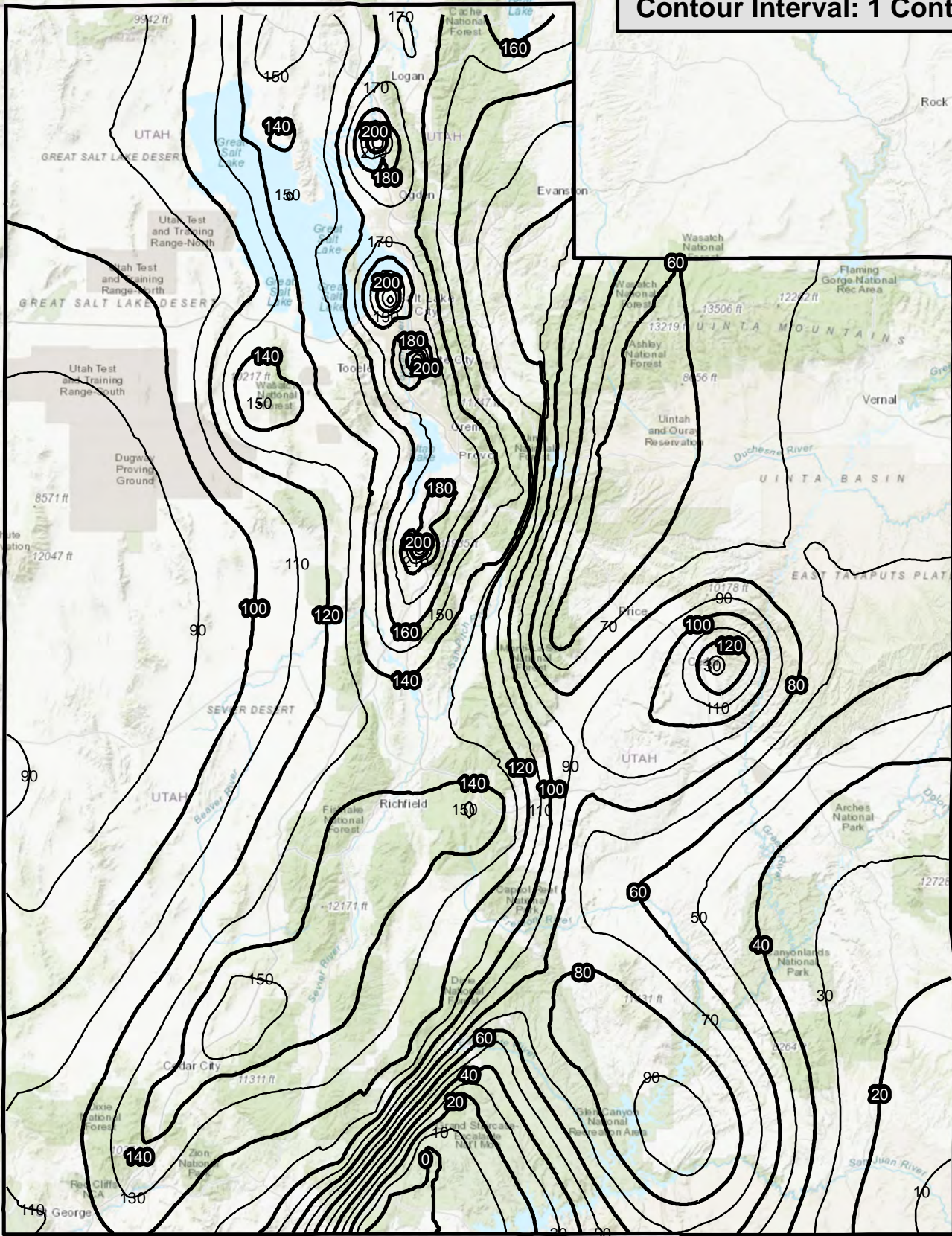
Q_{req}^{ref}
Ku et al. (2012)
1039 Year Return Period
Contour Interval: 1 Contour = 10



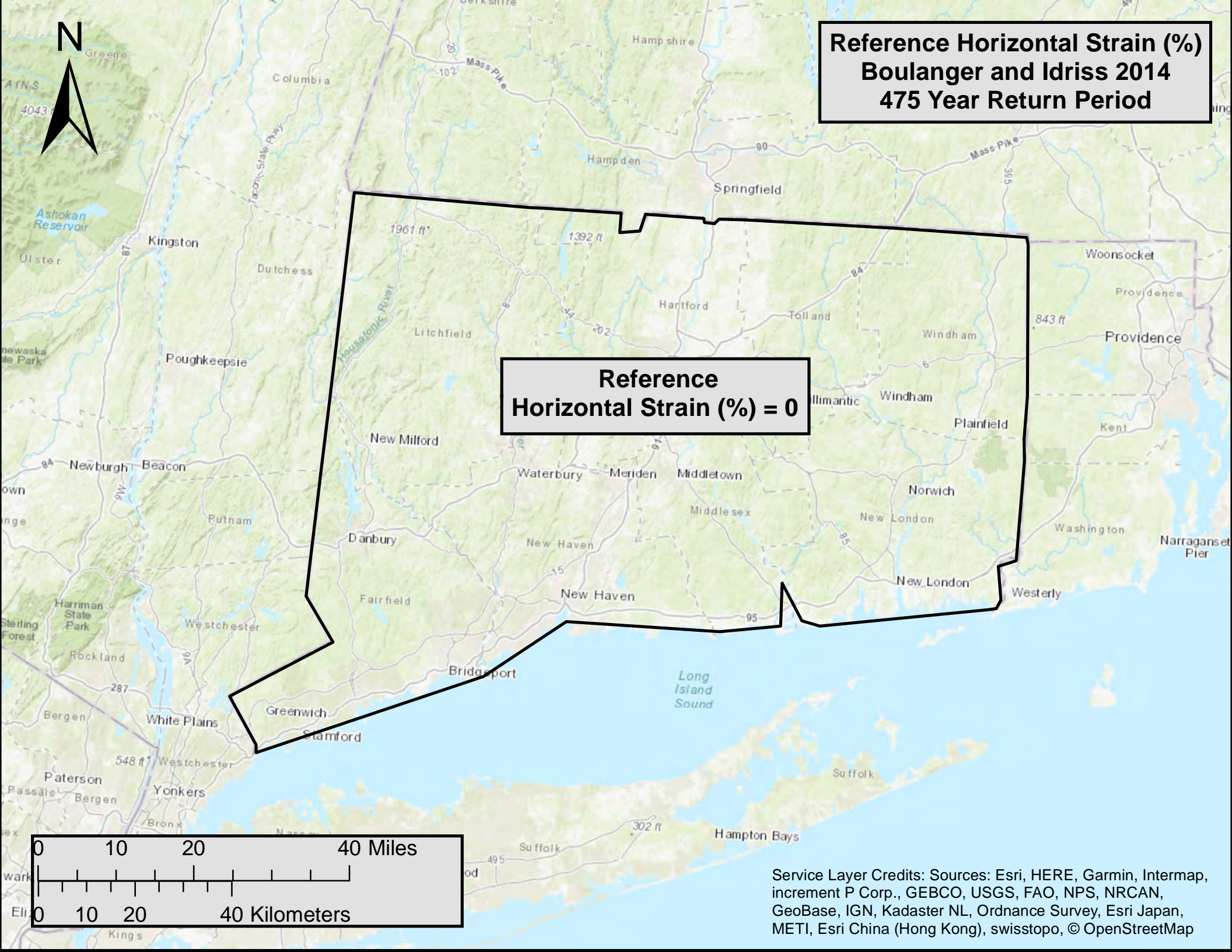
Service Layer Credits: Sources: Esri, HERE, Garmin, Intermap, increment P Corp., GEBCO, USGS, FAO, NPS, NRCAN, GeoBase, IGN, Kadaster NL, Ordnance Survey, Esri Japan, METI, Esri China (Hong Kong), swisstopo, © OpenStreetMap contributors, and the GIS User Community



Q_{req}^{ref}
Ku et al. (2012)
2475 Year Return Period
Contour Interval: 1 Contour = 10

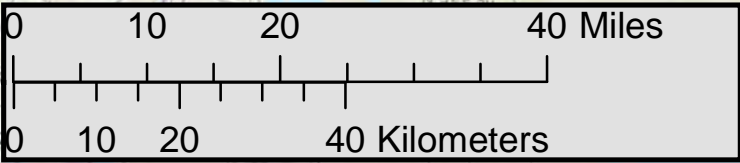


Service Layer Credits: Sources: Esri, HERE, Garmin, Intermap, increment P Corp., GEBCO, USGS, FAO, NPS, NRCAN, GeoBase, IGN, Kadaster NL, Ordnance Survey, Esri Japan, METI, Esri China (Hong Kong), swisstopo, © OpenStreetMap contributors, and the GIS User Community



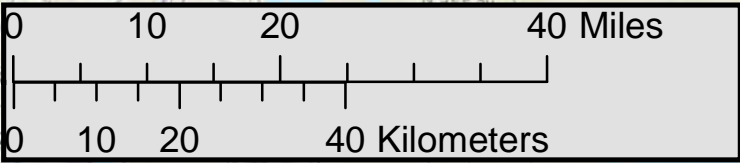
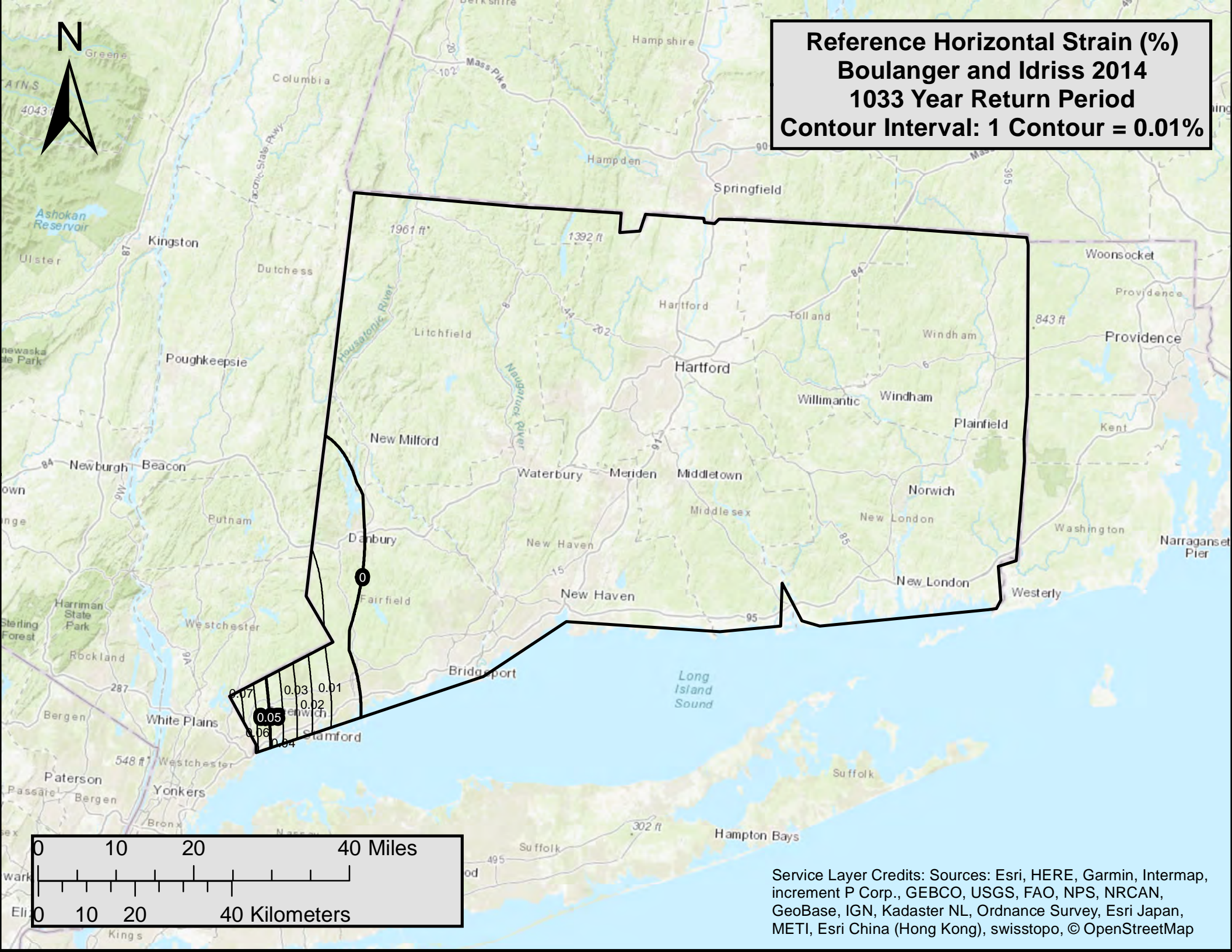
**Reference Horizontal Strain (%)
Boulanger and Idriss 2014
475 Year Return Period**

**Reference
Horizontal Strain (%) = 0**



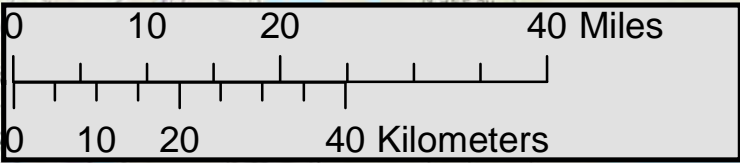
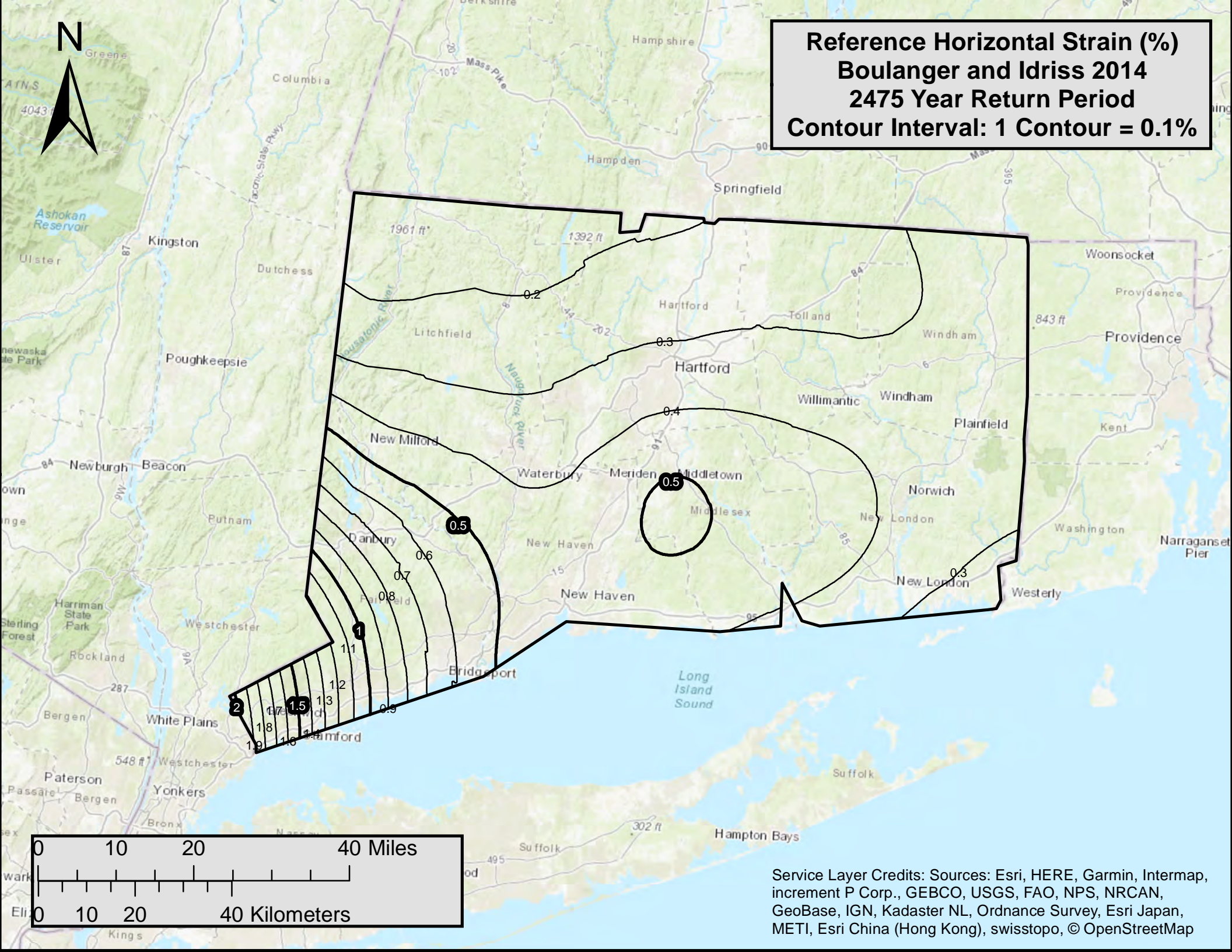
Service Layer Credits: Sources: Esri, HERE, Garmin, Intermap, increment P Corp., GEBCO, USGS, FAO, NPS, NRCAN, GeoBase, IGN, Kadaster NL, Ordnance Survey, Esri Japan, METI, Esri China (Hong Kong), swisstopo, © OpenStreetMap

Reference Horizontal Strain (%)
Boulanger and Idriss 2014
1033 Year Return Period
Contour Interval: 1 Contour = 0.01%

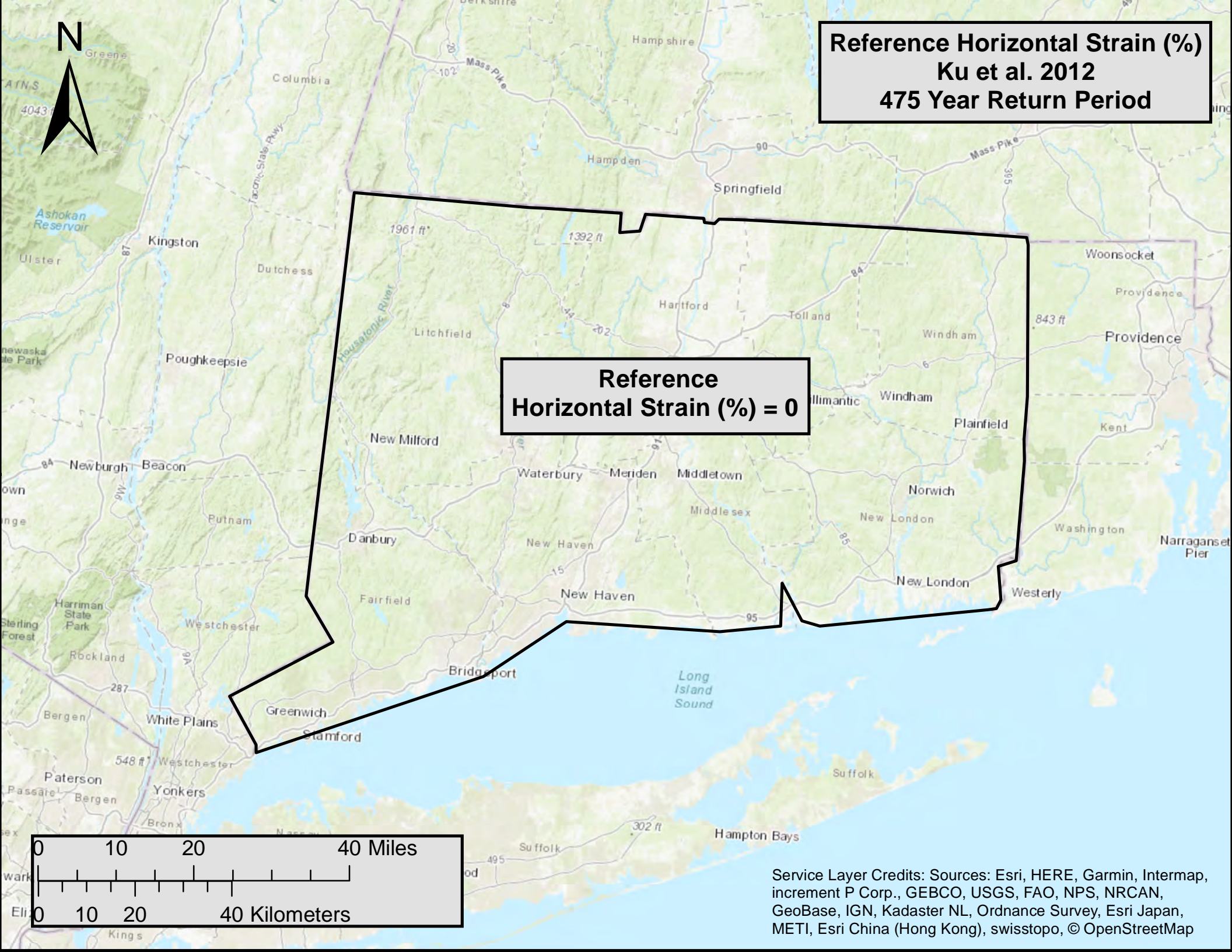


Service Layer Credits: Sources: Esri, HERE, Garmin, Intermap, increment P Corp., GEBCO, USGS, FAO, NPS, NRCAN, GeoBase, IGN, Kadaster NL, Ordnance Survey, Esri Japan, METI, Esri China (Hong Kong), swisstopo, © OpenStreetMap

Reference Horizontal Strain (%)
Boulanger and Idriss 2014
2475 Year Return Period
Contour Interval: 1 Contour = 0.1%

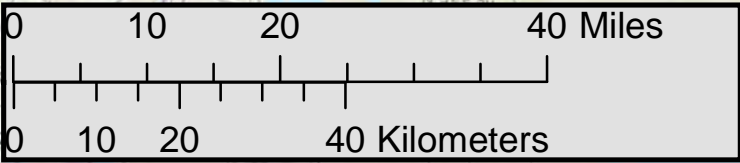


Service Layer Credits: Sources: Esri, HERE, Garmin, Intermap, increment P Corp., GEBCO, USGS, FAO, NPS, NRCAN, GeoBase, IGN, Kadaster NL, Ordnance Survey, Esri Japan, METI, Esri China (Hong Kong), swisstopo, © OpenStreetMap

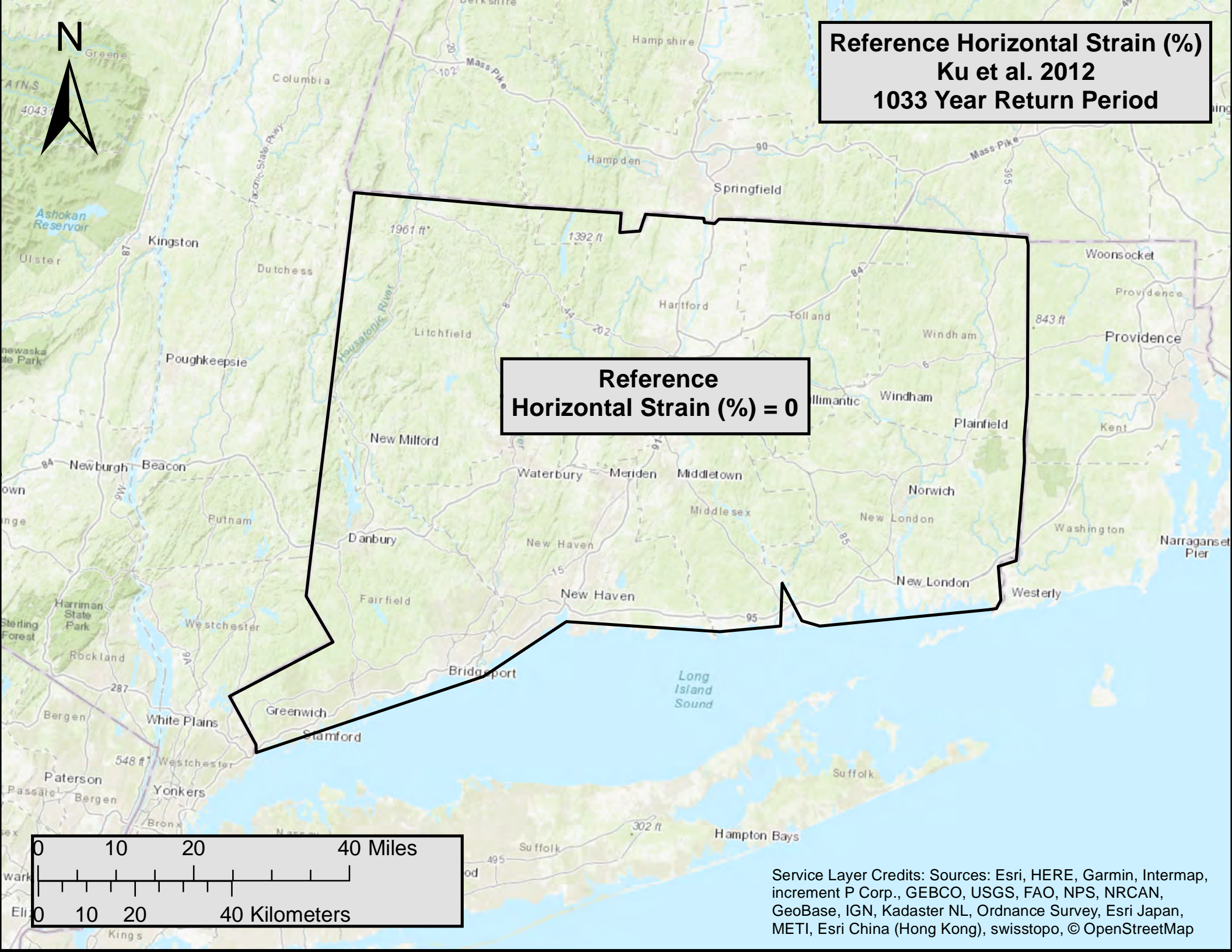


Reference Horizontal Strain (%)
Ku et al. 2012
475 Year Return Period

Reference
Horizontal Strain (%) = 0

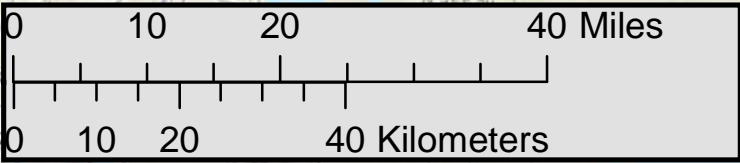


Service Layer Credits: Sources: Esri, HERE, Garmin, Intermap, increment P Corp., GEBCO, USGS, FAO, NPS, NRCAN, GeoBase, IGN, Kadaster NL, Ordnance Survey, Esri Japan, METI, Esri China (Hong Kong), swisstopo, © OpenStreetMap



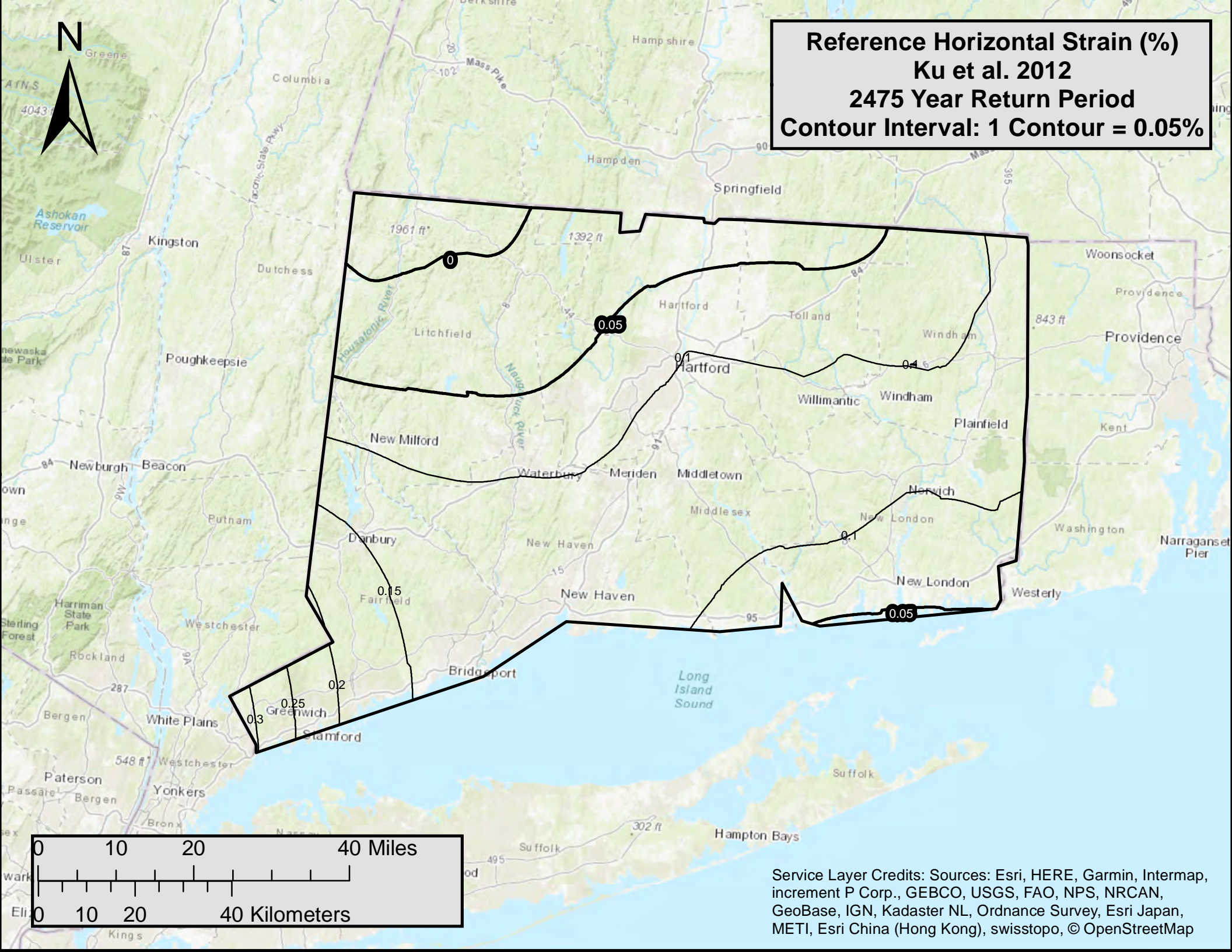
Reference Horizontal Strain (%)
Ku et al. 2012
1033 Year Return Period

Reference
Horizontal Strain (%) = 0



Service Layer Credits: Sources: Esri, HERE, Garmin, Intermap, increment P Corp., GEBCO, USGS, FAO, NPS, NRCAN, GeoBase, IGN, Kadaster NL, Ordnance Survey, Esri Japan, METI, Esri China (Hong Kong), swisstopo, © OpenStreetMap

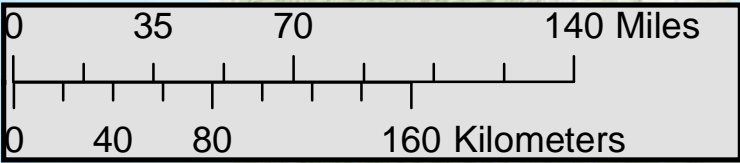
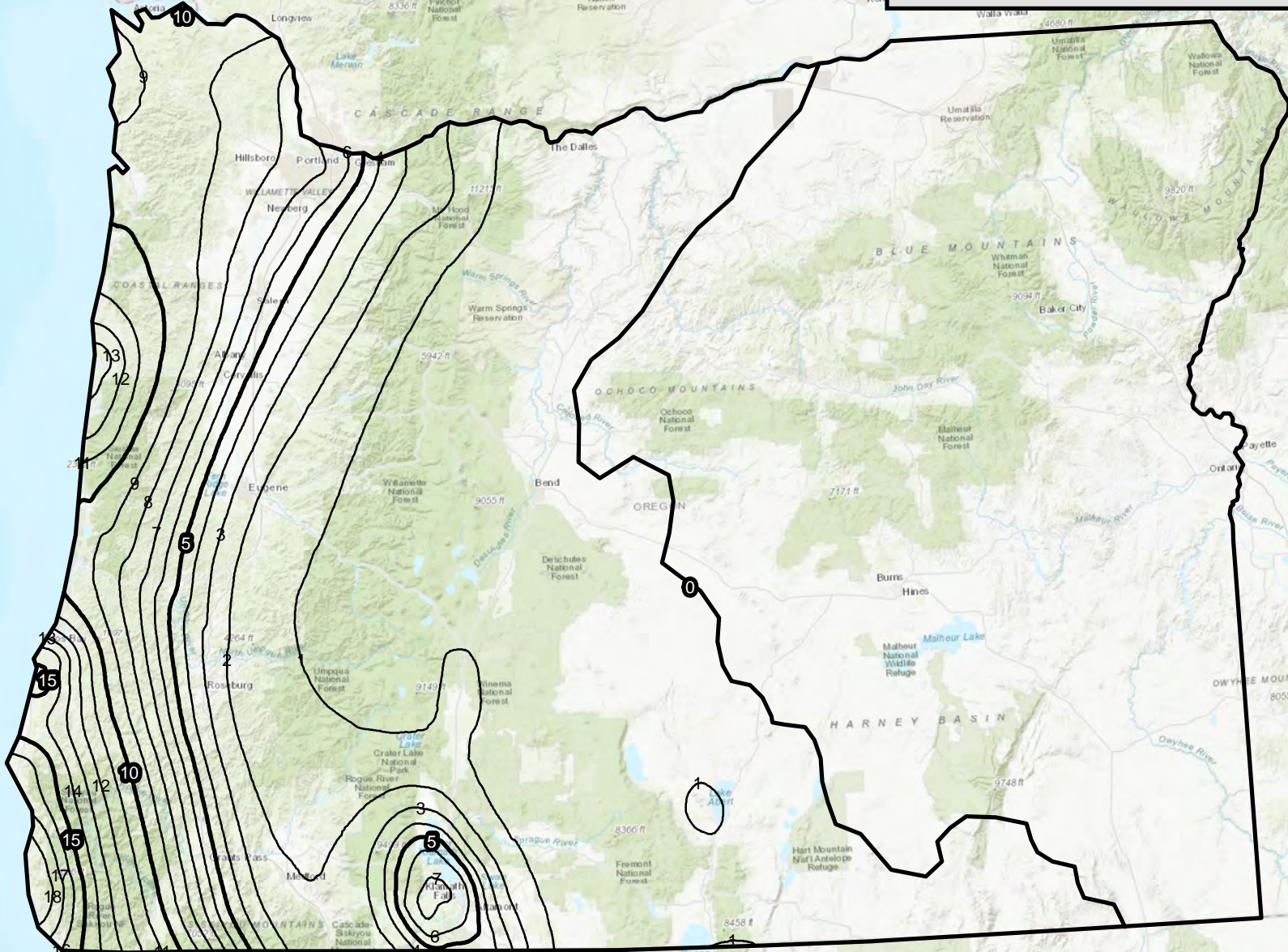
Reference Horizontal Strain (%)
Ku et al. 2012
2475 Year Return Period
Contour Interval: 1 Contour = 0.05%



Service Layer Credits: Sources: Esri, HERE, Garmin, Intermap, increment P Corp., GEBCO, USGS, FAO, NPS, NRCAN, GeoBase, IGN, Kadaster NL, Ordnance Survey, Esri Japan, METI, Esri China (Hong Kong), swisstopo, © OpenStreetMap



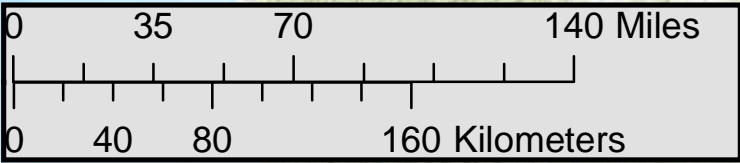
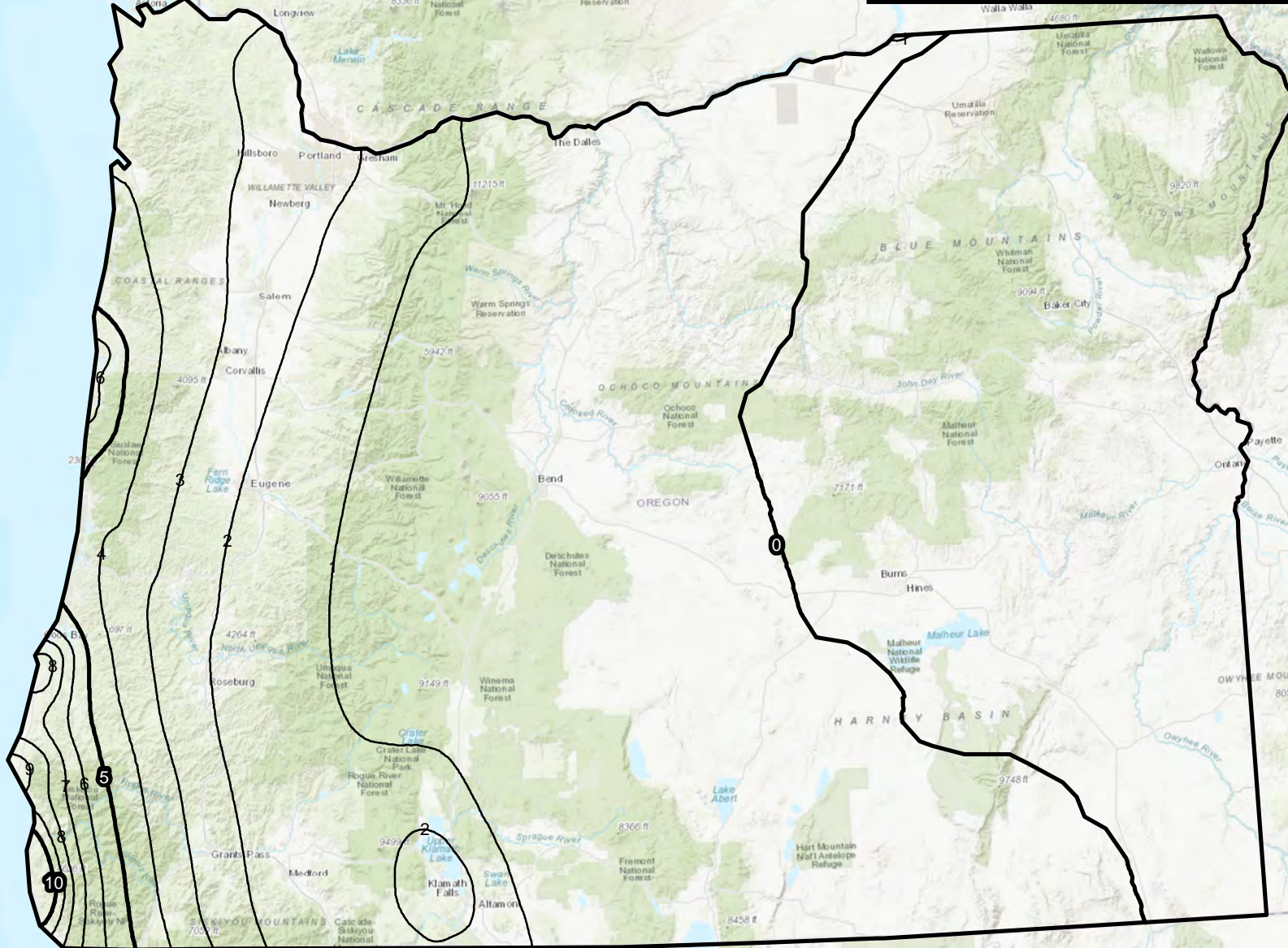
**Reference Horizontal Strain
Boulanger and Idriss 2014
475 Year Return Period
Contour Interval: 1 Contour = 1 (%)**



Service Layer Credits: Sources: Esri, HERE, Garmin, Intermap, increment P Corp., GEBCO, USGS, FAO, NPS, NRCAN, GeoBase, IGN, Kadaster NL, Ordnance Survey, Esri Japan, METI, Esri China (Hong Kong), swisstopo, © OpenStreetMap



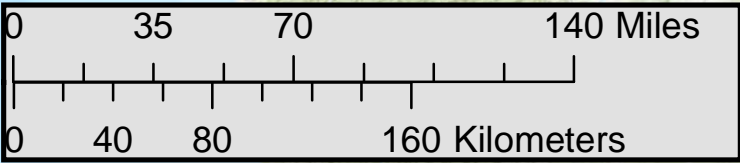
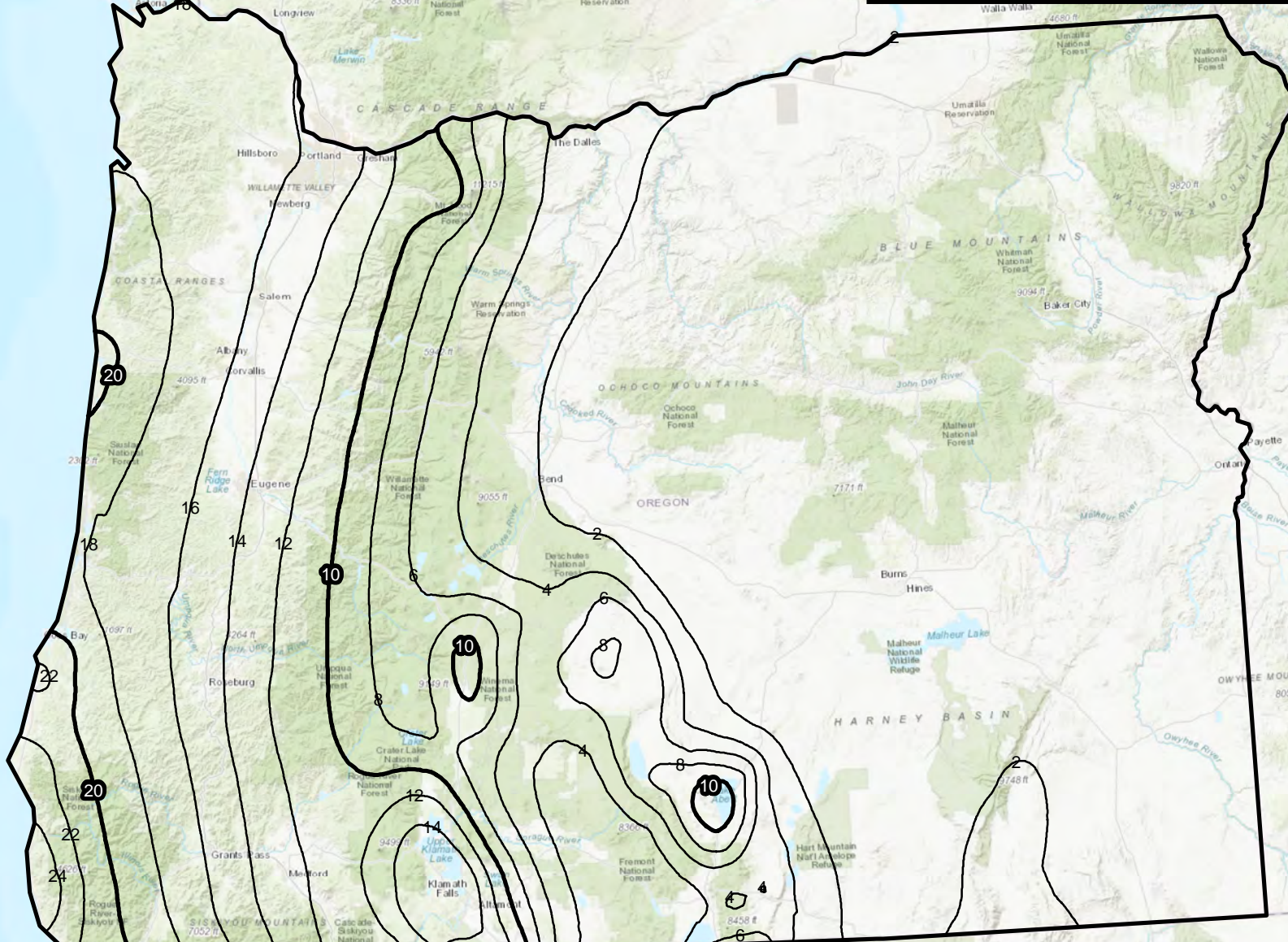
Reference Horizontal Strain
Ku et al. 2012
475 Year Return Period
Contour Interval: 1 Contour = 1 (%)



Service Layer Credits: Sources: Esri, HERE, Garmin, Intermap, increment P Corp., GEBCO, USGS, FAO, NPS, NRCAN, GeoBase, IGN, Kadaster NL, Ordnance Survey, Esri Japan, METI, Esri China (Hong Kong), swisstopo, © OpenStreetMap



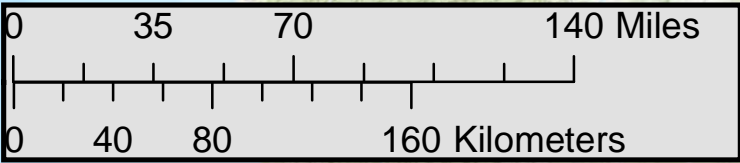
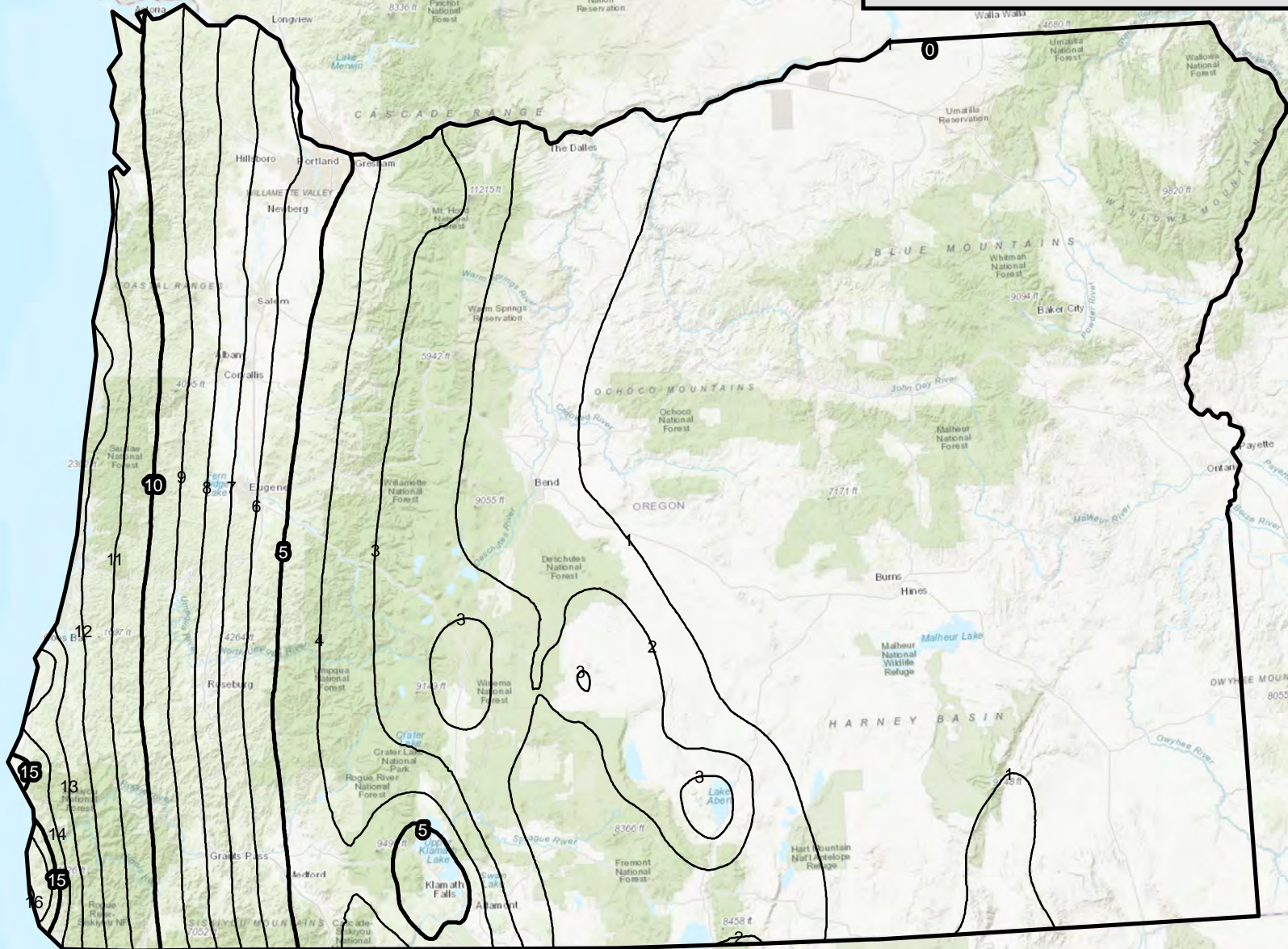
**Reference Horizontal Strain
Boulanger and Idriss 2014
1033 Year Return Period
Contour Interval: 1 Contour = 2 (%)**



Service Layer Credits: Sources: Esri, HERE, Garmin, Intermap, increment P Corp., GEBCO, USGS, FAO, NPS, NRCAN, GeoBase, IGN, Kadaster NL, Ordnance Survey, Esri Japan, METI, Esri China (Hong Kong), swisstopo, © OpenStreetMap



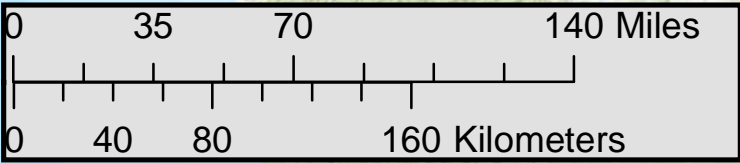
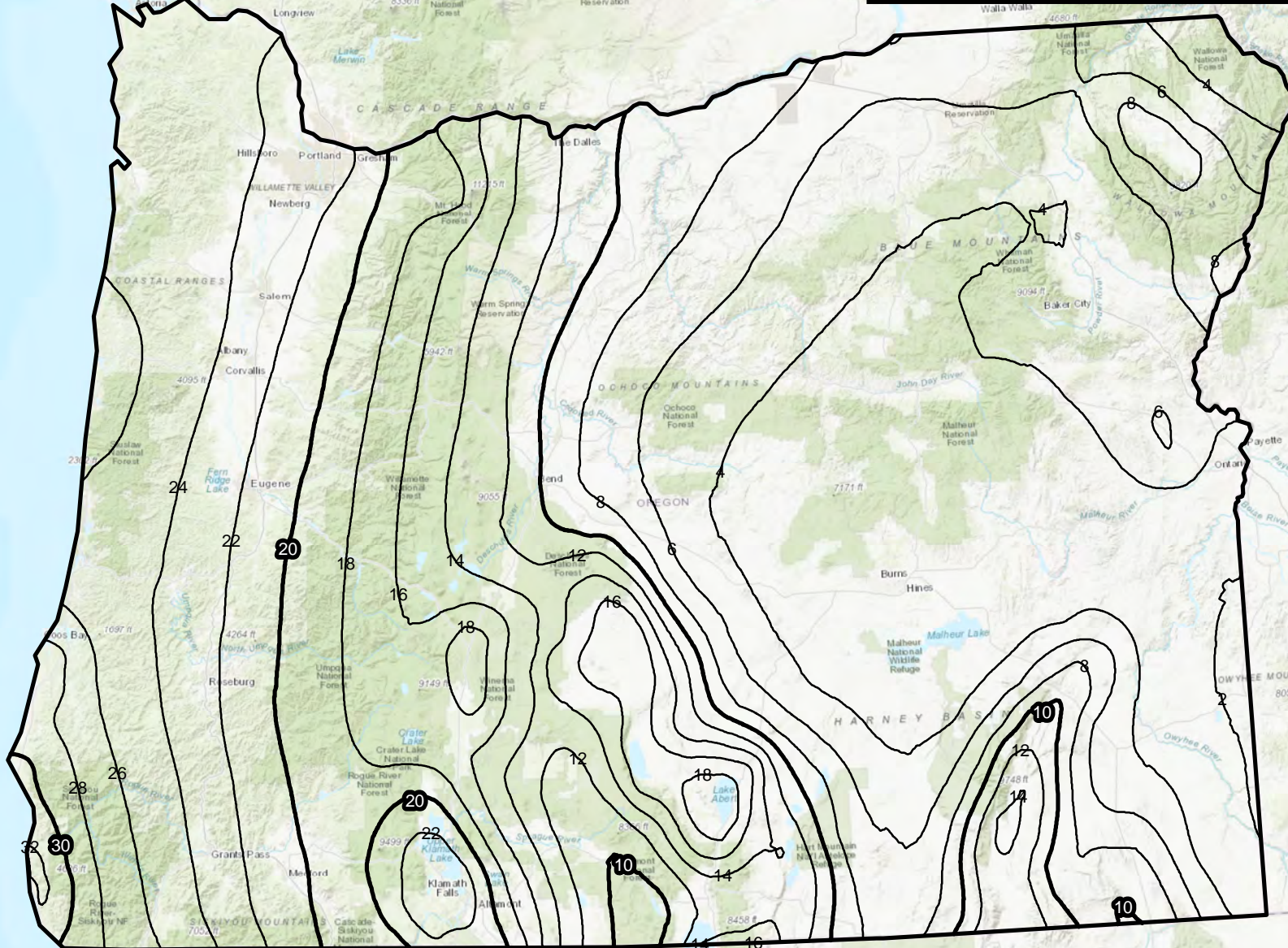
Reference Horizontal Strain
Ku et al. 2012
1033 Year Return Period
Contour Interval: 1 Contour = 1 (%)



Service Layer Credits: Sources: Esri, HERE, Garmin, Intermap, increment P Corp., GEBCO, USGS, FAO, NPS, NRCAN, GeoBase, IGN, Kadaster NL, Ordnance Survey, Esri Japan, METI, Esri China (Hong Kong), swisstopo, © OpenStreetMap



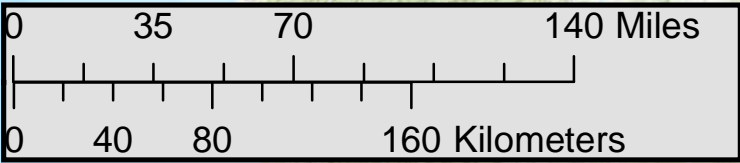
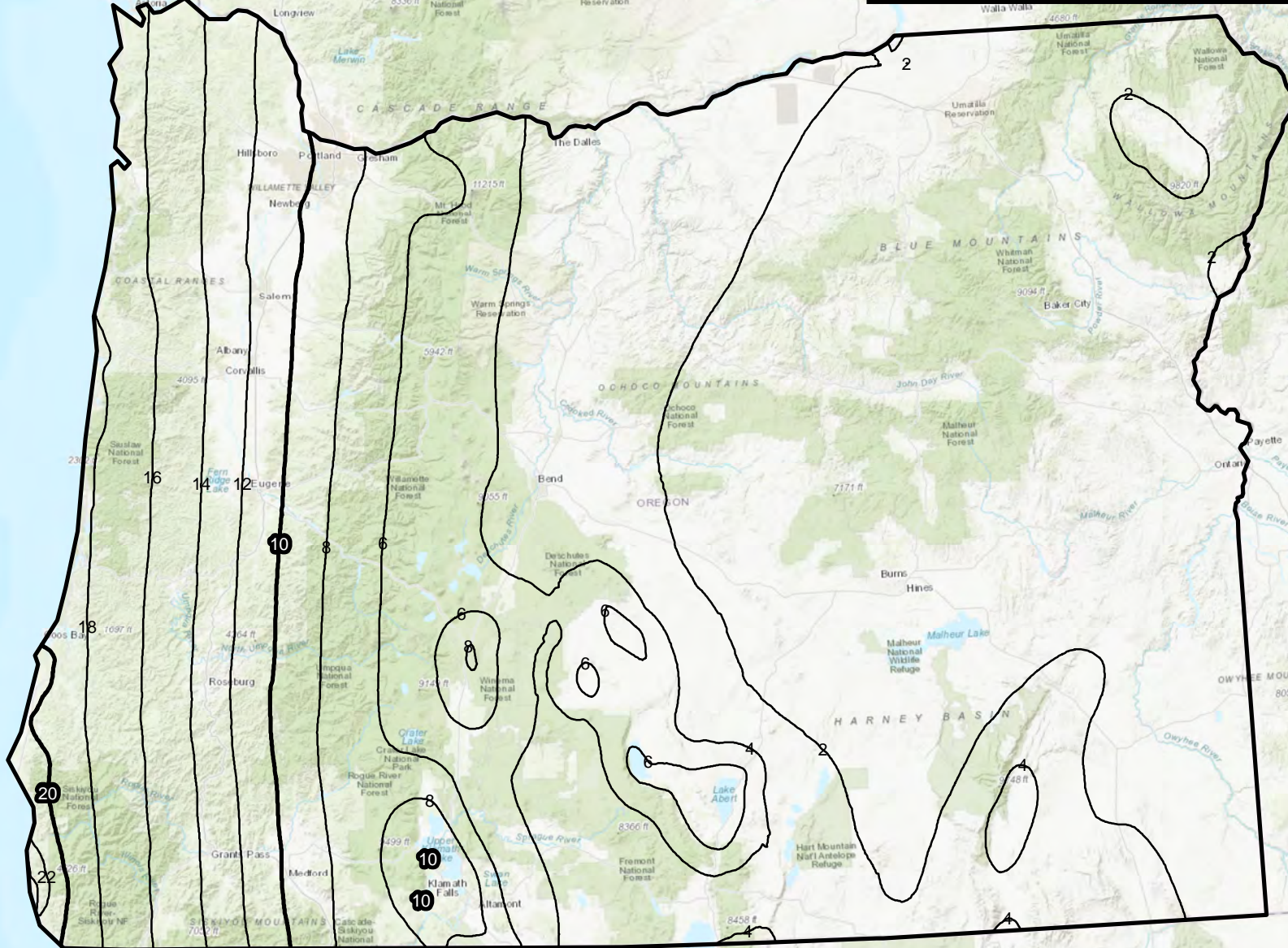
**Reference Horizontal Strain
Boulanger and Idriss 2014
2475 Year Return Period
Contour Interval: 1 Contour = 2 (%)**



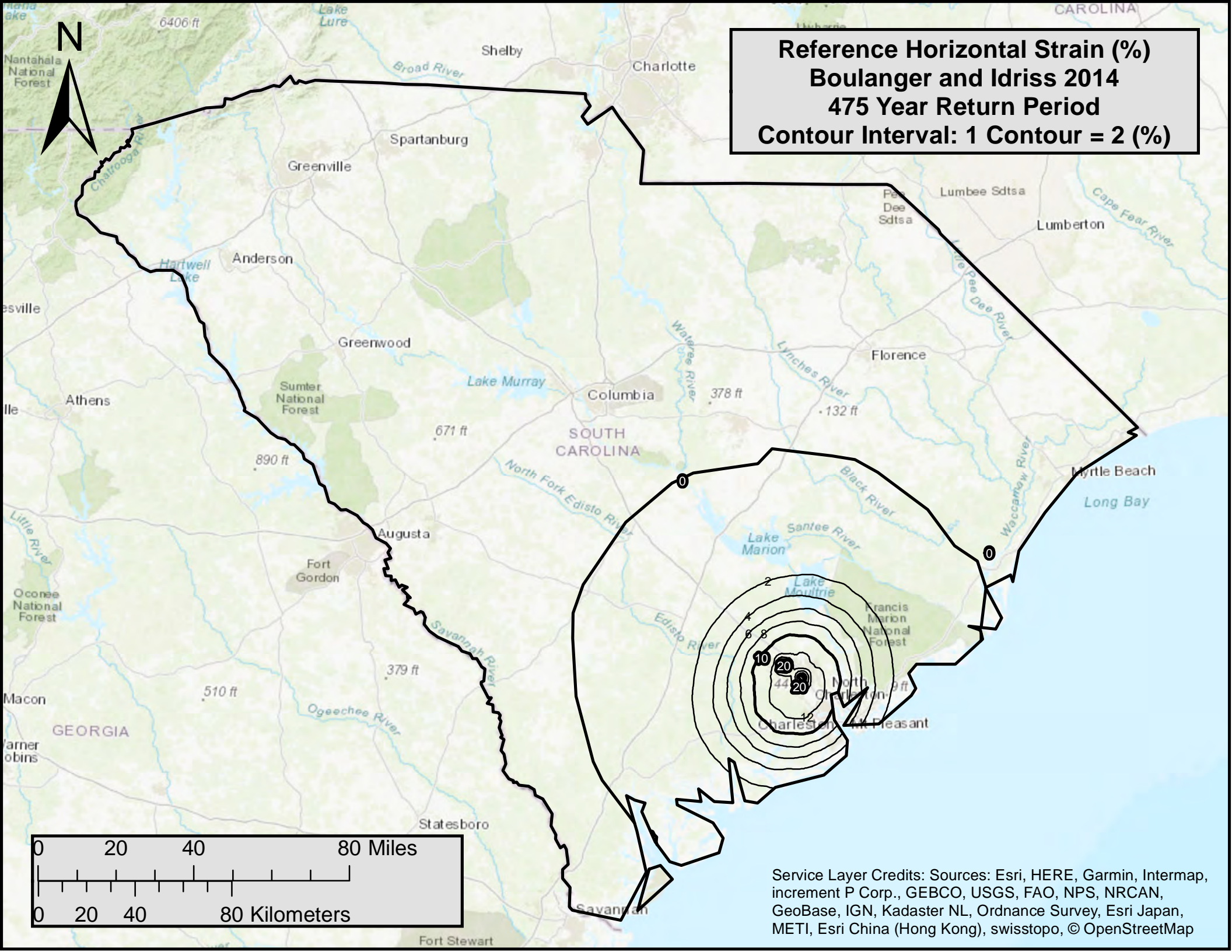
Service Layer Credits: Sources: Esri, HERE, Garmin, Intermap, increment P Corp., GEBCO, USGS, FAO, NPS, NRCAN, GeoBase, IGN, Kadaster NL, Ordnance Survey, Esri Japan, METI, Esri China (Hong Kong), swisstopo, © OpenStreetMap

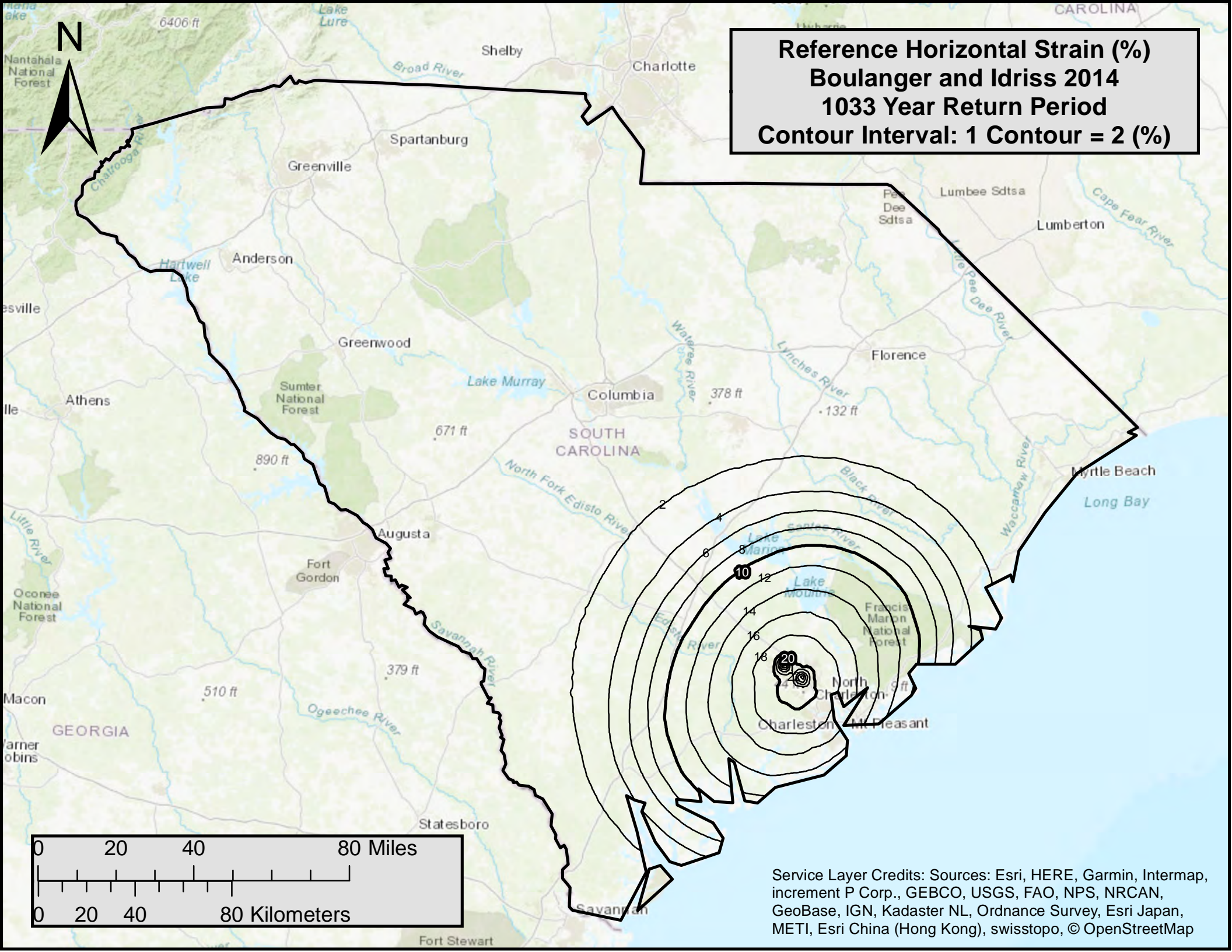


Reference Horizontal Strain
Ku et al. 2012
2475 Year Return Period
Contour Interval: 1 Contour = 2 (%)

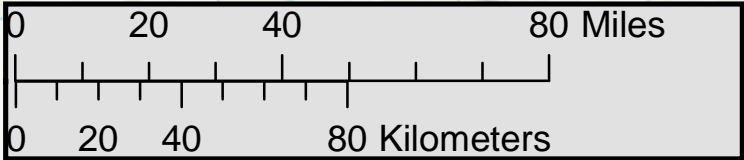


Service Layer Credits: Sources: Esri, HERE, Garmin, Intermap, increment P Corp., GEBCO, USGS, FAO, NPS, NRCAN, GeoBase, IGN, Kadaster NL, Ordnance Survey, Esri Japan, METI, Esri China (Hong Kong), swisstopo, © OpenStreetMap

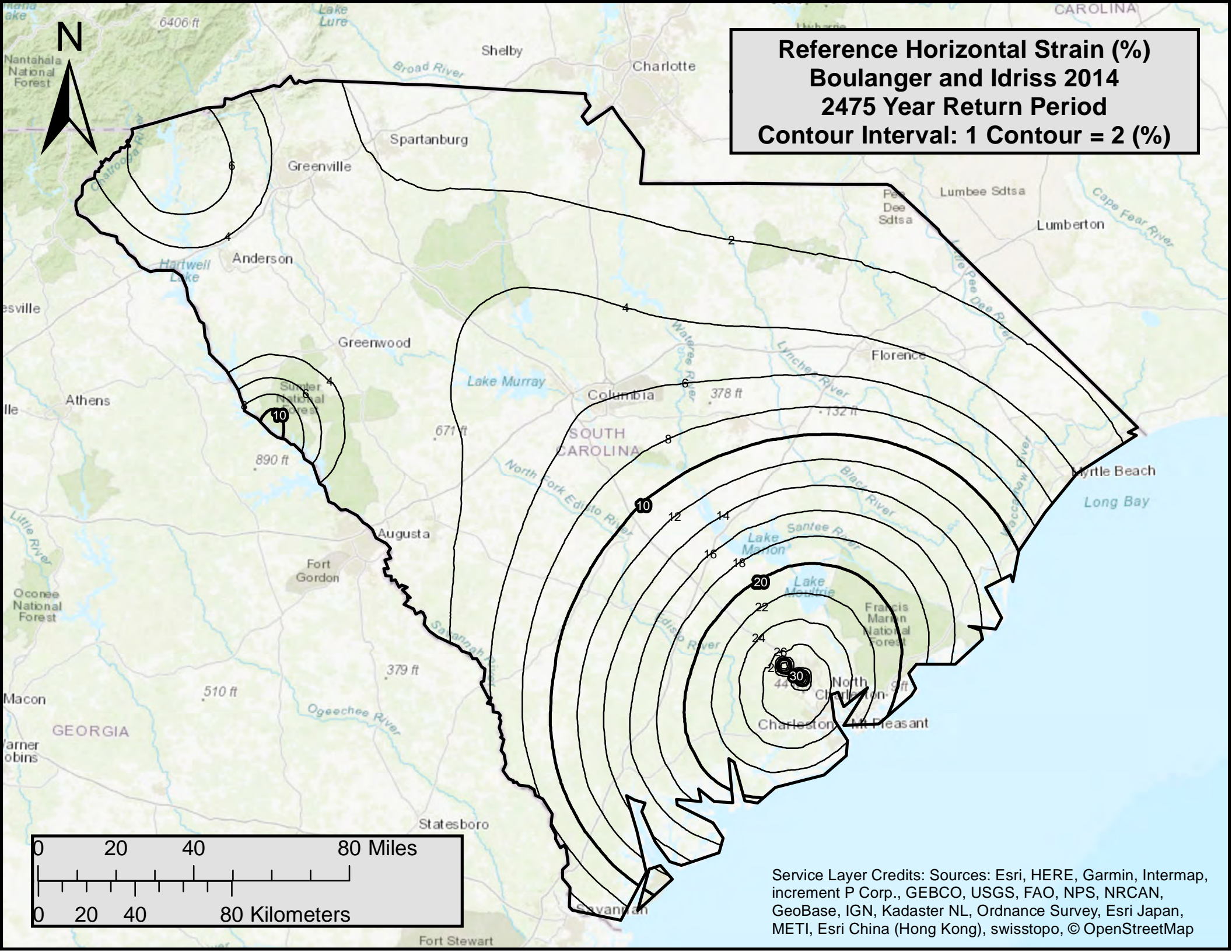


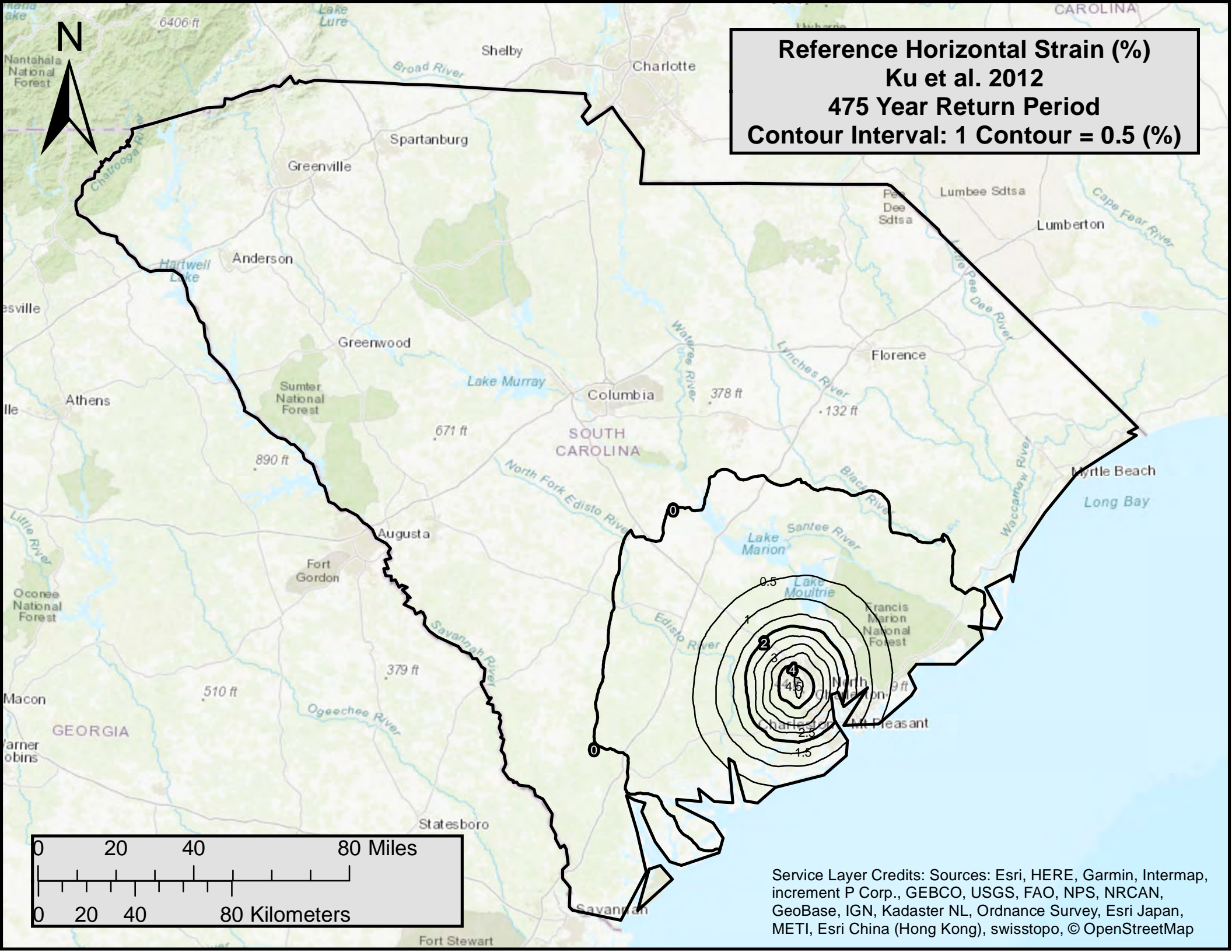


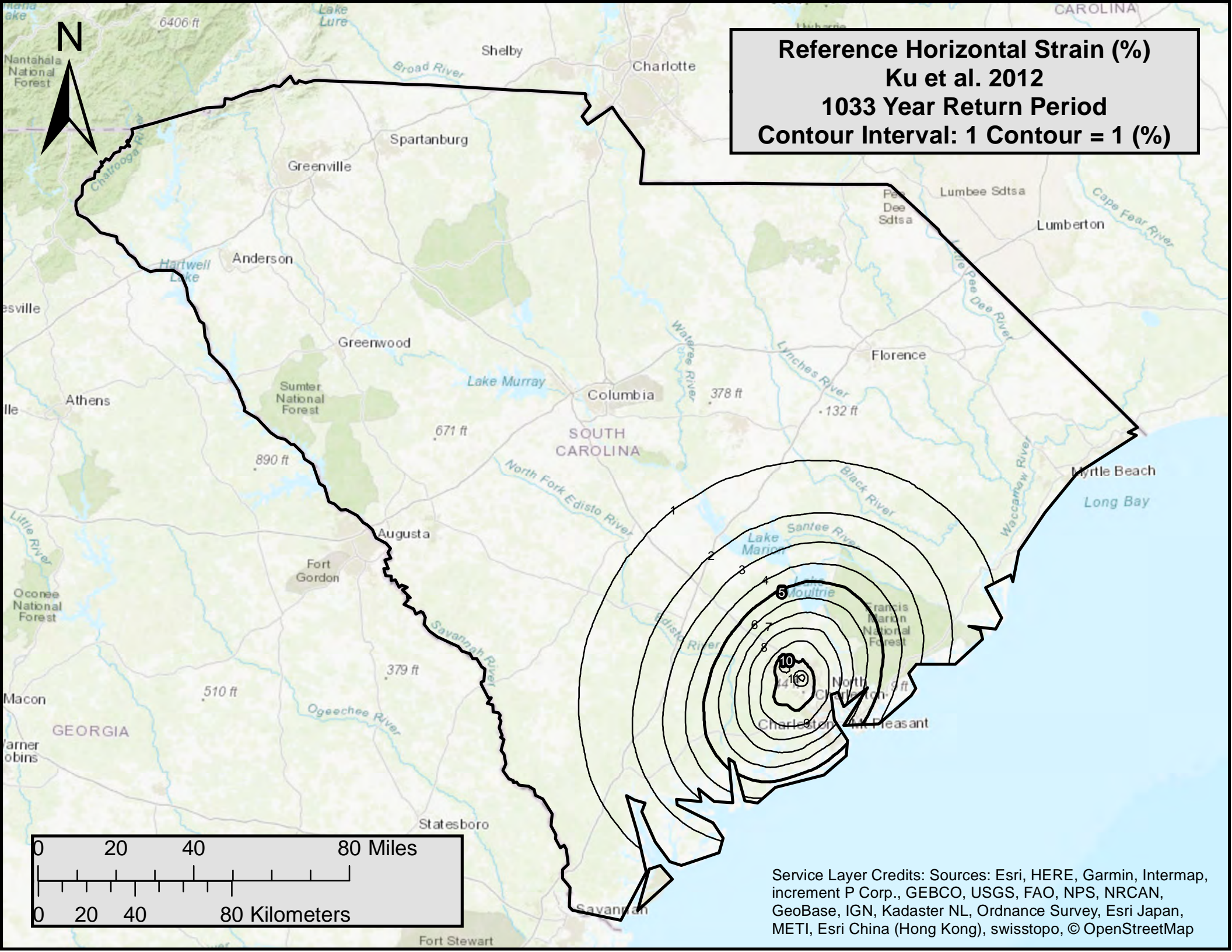
Reference Horizontal Strain (%)
Boulanger and Idriss 2014
1033 Year Return Period
Contour Interval: 1 Contour = 2 (%)



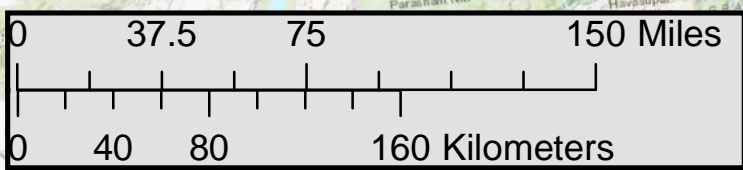
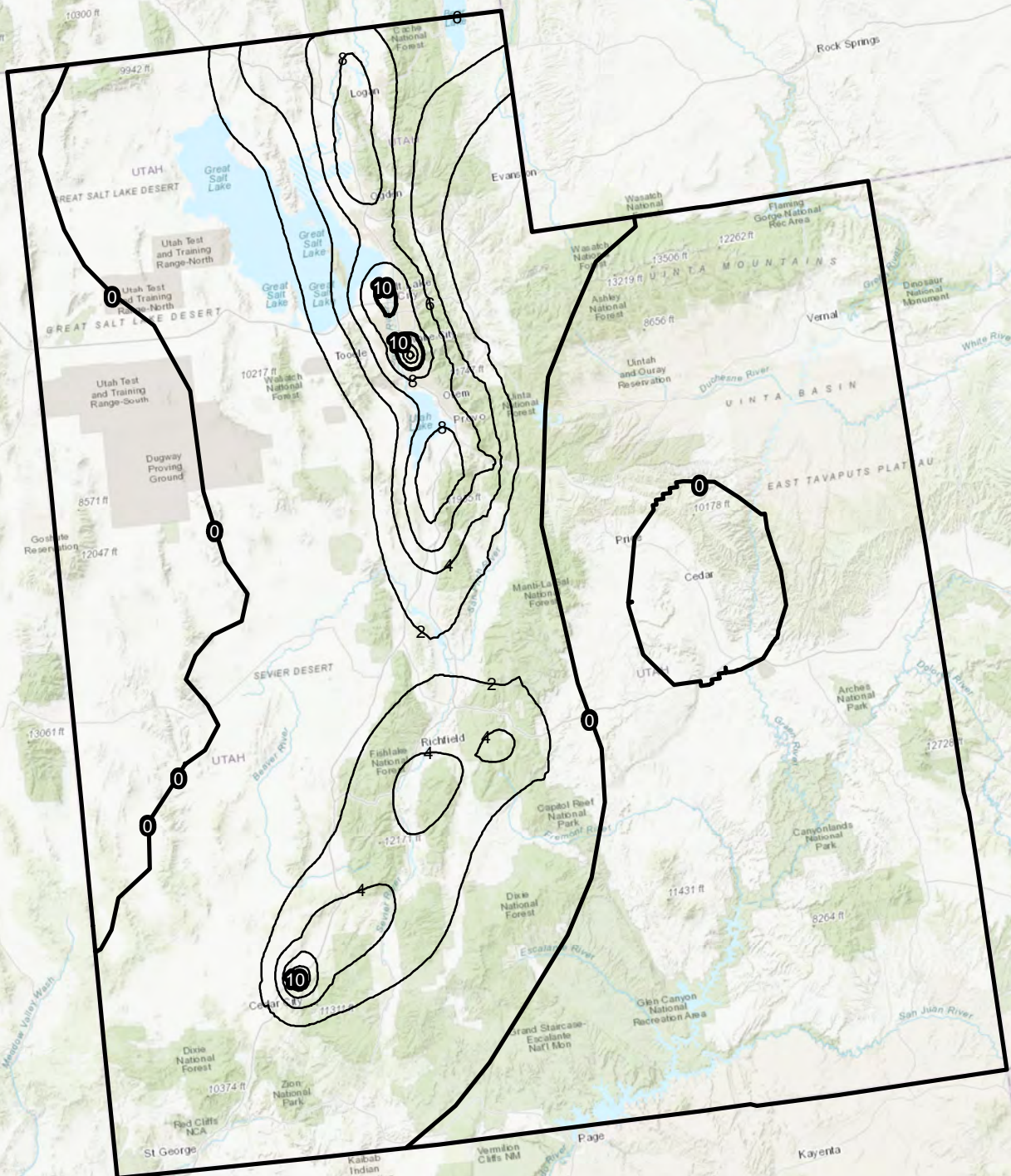
Service Layer Credits: Sources: Esri, HERE, Garmin, Intermap, increment P Corp., GEBCO, USGS, FAO, NPS, NRCAN, GeoBase, IGN, Kadaster NL, Ordnance Survey, Esri Japan, METI, Esri China (Hong Kong), swisstopo, © OpenStreetMap





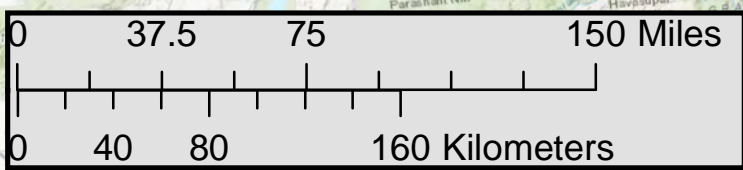
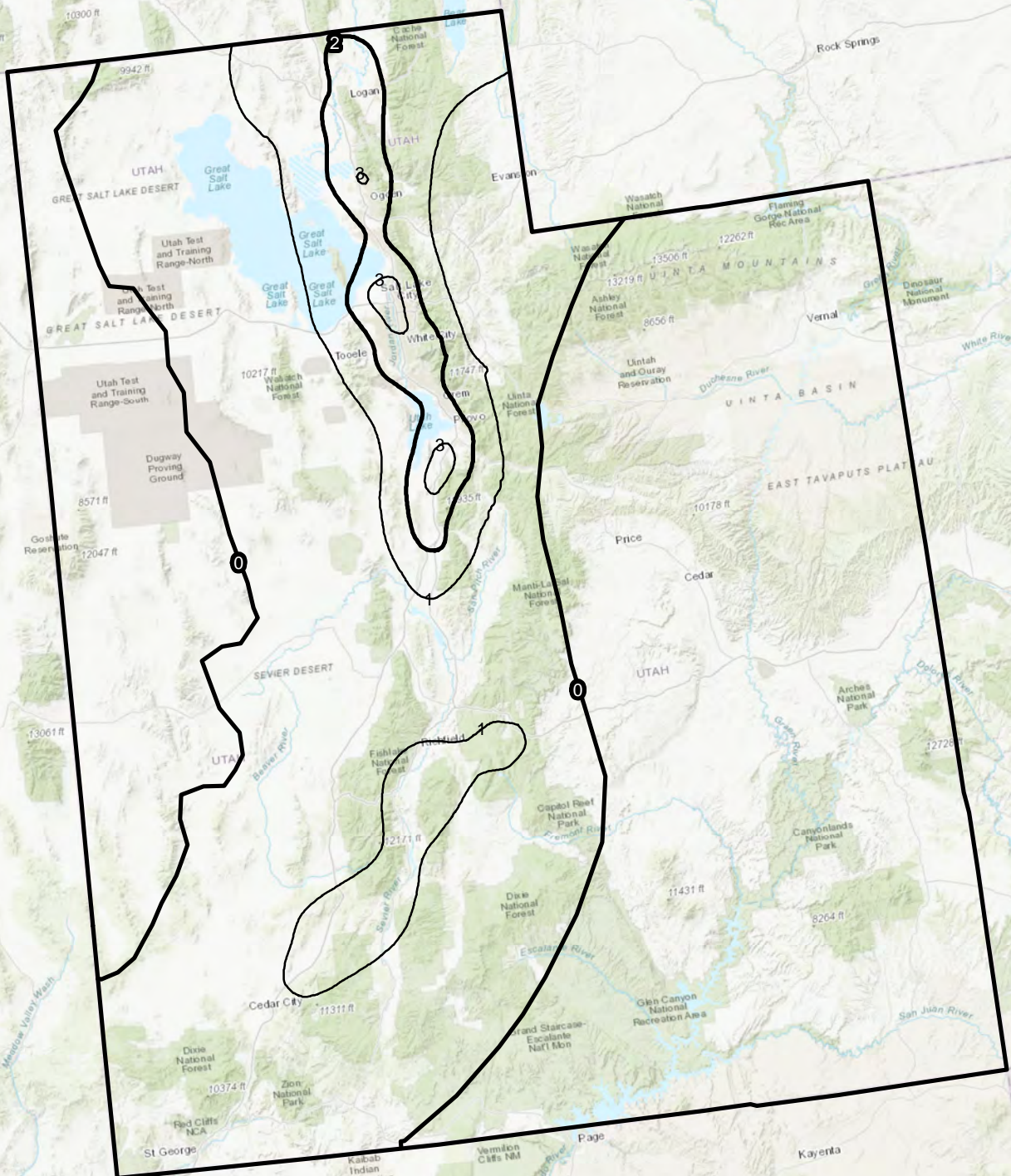


**Reference Horizontal Strain
Boulanger and Idriss 2014
475 Year Return Period
Contour Interval: 1 Contour = 2 (%)**



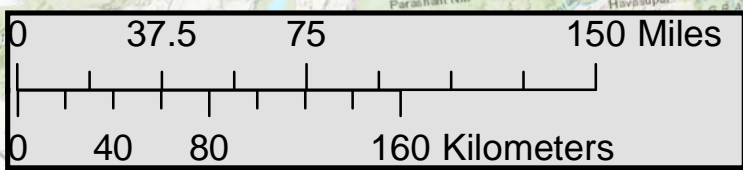
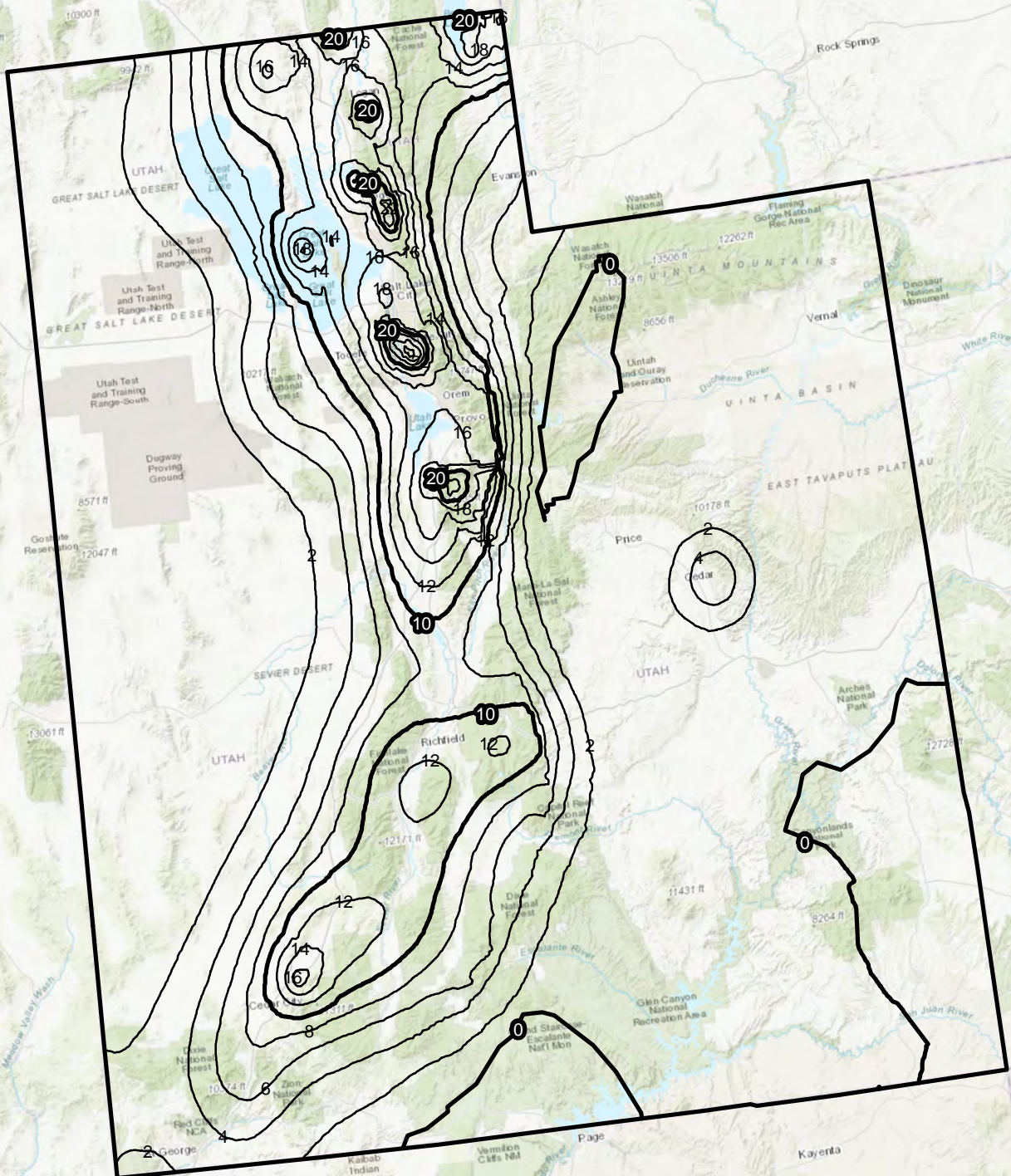
Service Layer Credits: Sources: Esri, HERE, Garmin, Intermap, increment P Corp., GEBCO, USGS, FAO, NPS, NRCAN, GeoBase, IGN, Kadaster NL, Ordnance Survey, Esri Japan, METI, Esri China (Hong Kong), swisstopo, © OpenStreetMap

**Reference Horizontal Strain
Ku et al. 2012
475 Year Return Period
Contour Interval: 1 Contour = 1 (%)**



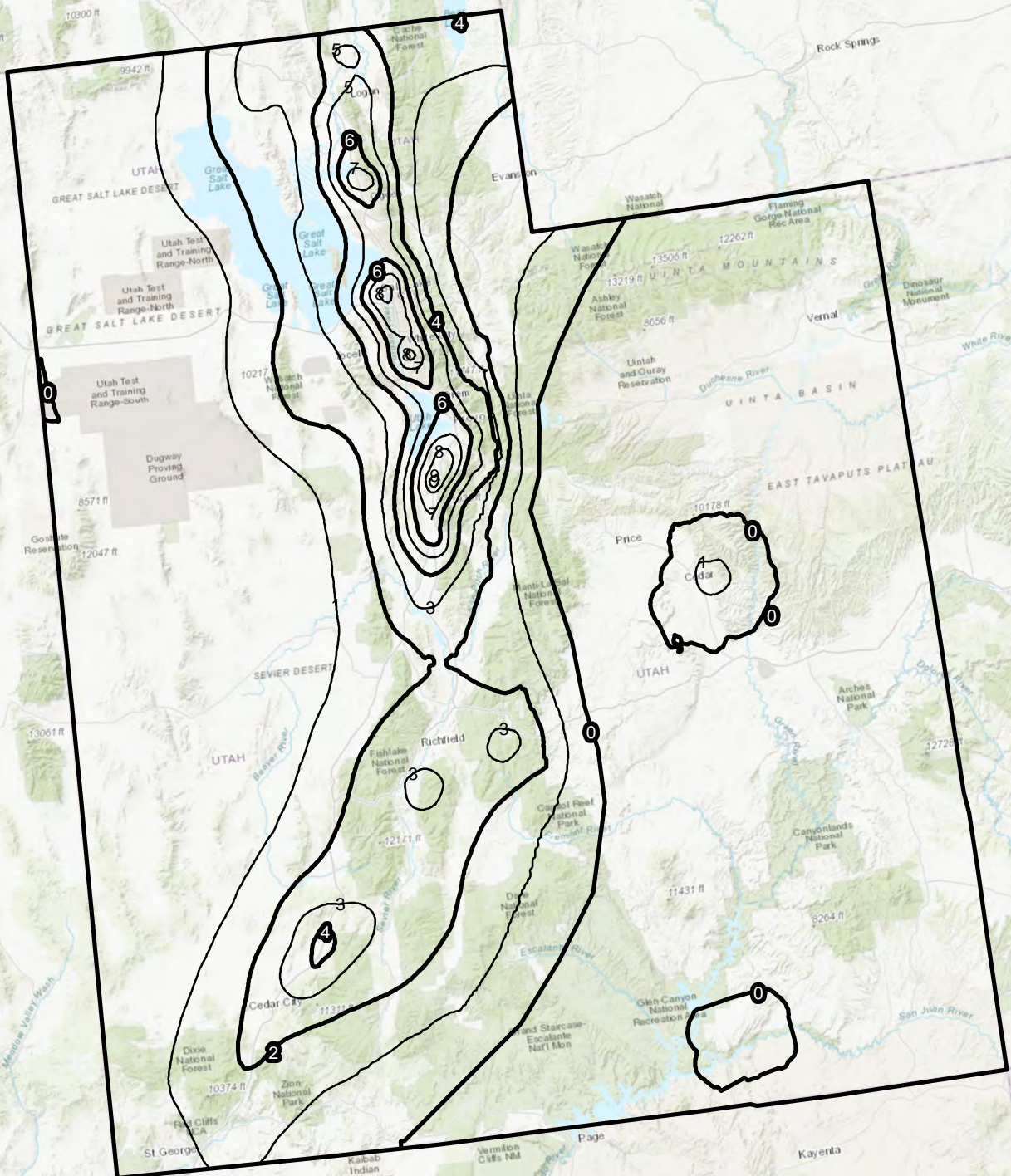
Service Layer Credits: Sources: Esri, HERE, Garmin, Intermap, increment P Corp., GEBCO, USGS, FAO, NPS, NRCAN, GeoBase, IGN, Kadaster NL, Ordnance Survey, Esri Japan, METI, Esri China (Hong Kong), swisstopo, © OpenStreetMap

**Reference Horizontal Strain
Boulanger and Idriss 2014
1033 Year Return Period
Contour Interval: 1 Contour = 2 (%)**



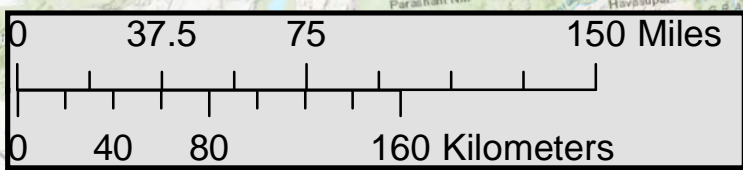
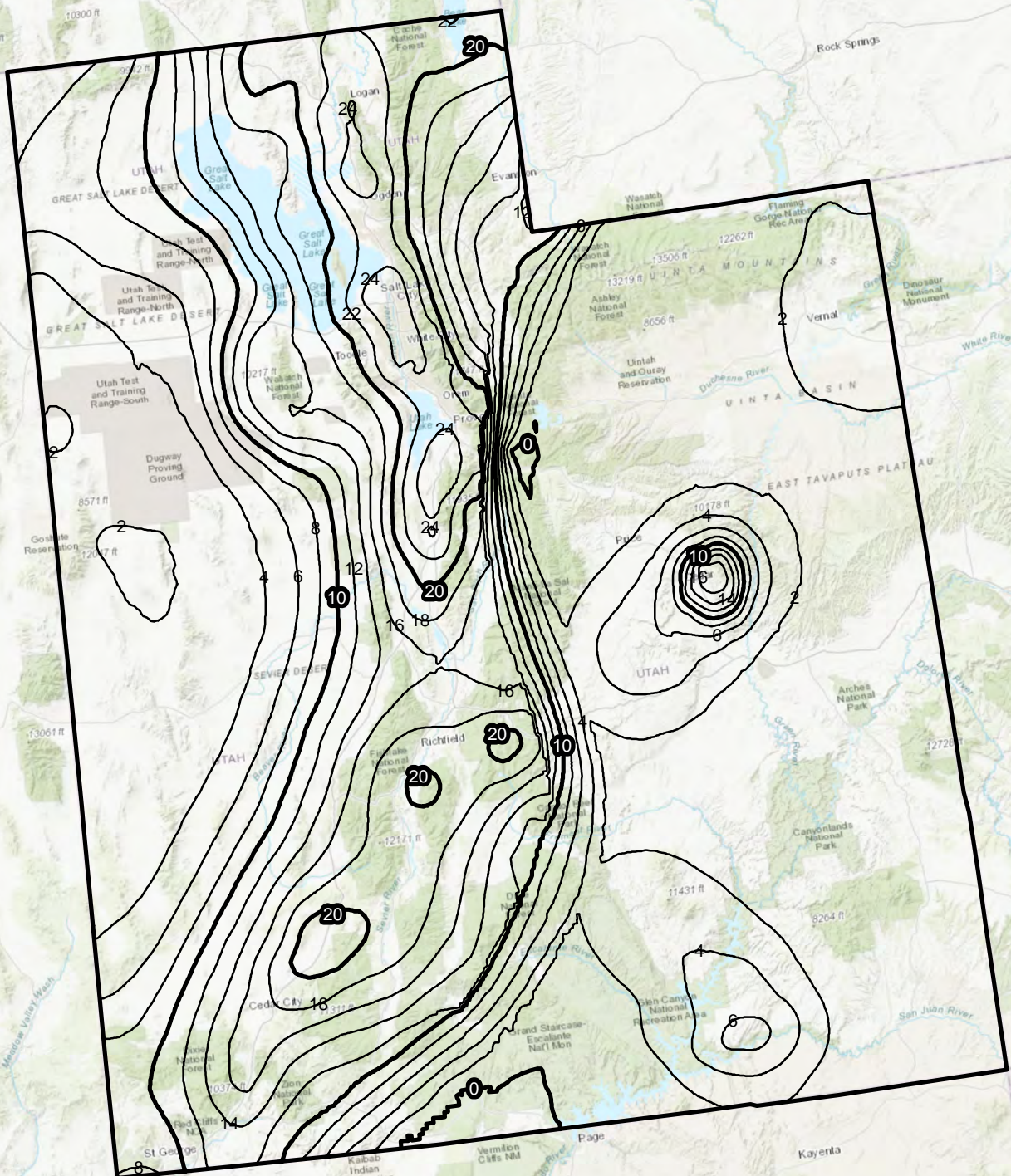
Service Layer Credits: Sources: Esri, HERE, Garmin, Intermap, increment P Corp., GEBCO, USGS, FAO, NPS, NRCAN, GeoBase, IGN, Kadaster NL, Ordnance Survey, Esri Japan, METI, Esri China (Hong Kong), swisstopo, © OpenStreetMap

**Reference Horizontal Strain
Ku et al. 2012
1033 Year Return Period
Contour Interval: 1 Contour = 1 (%)**



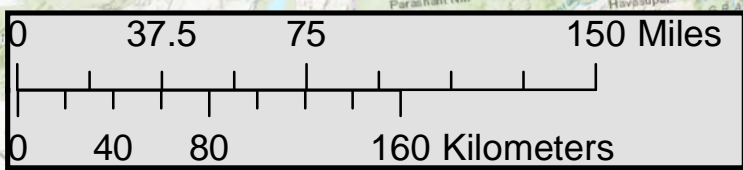
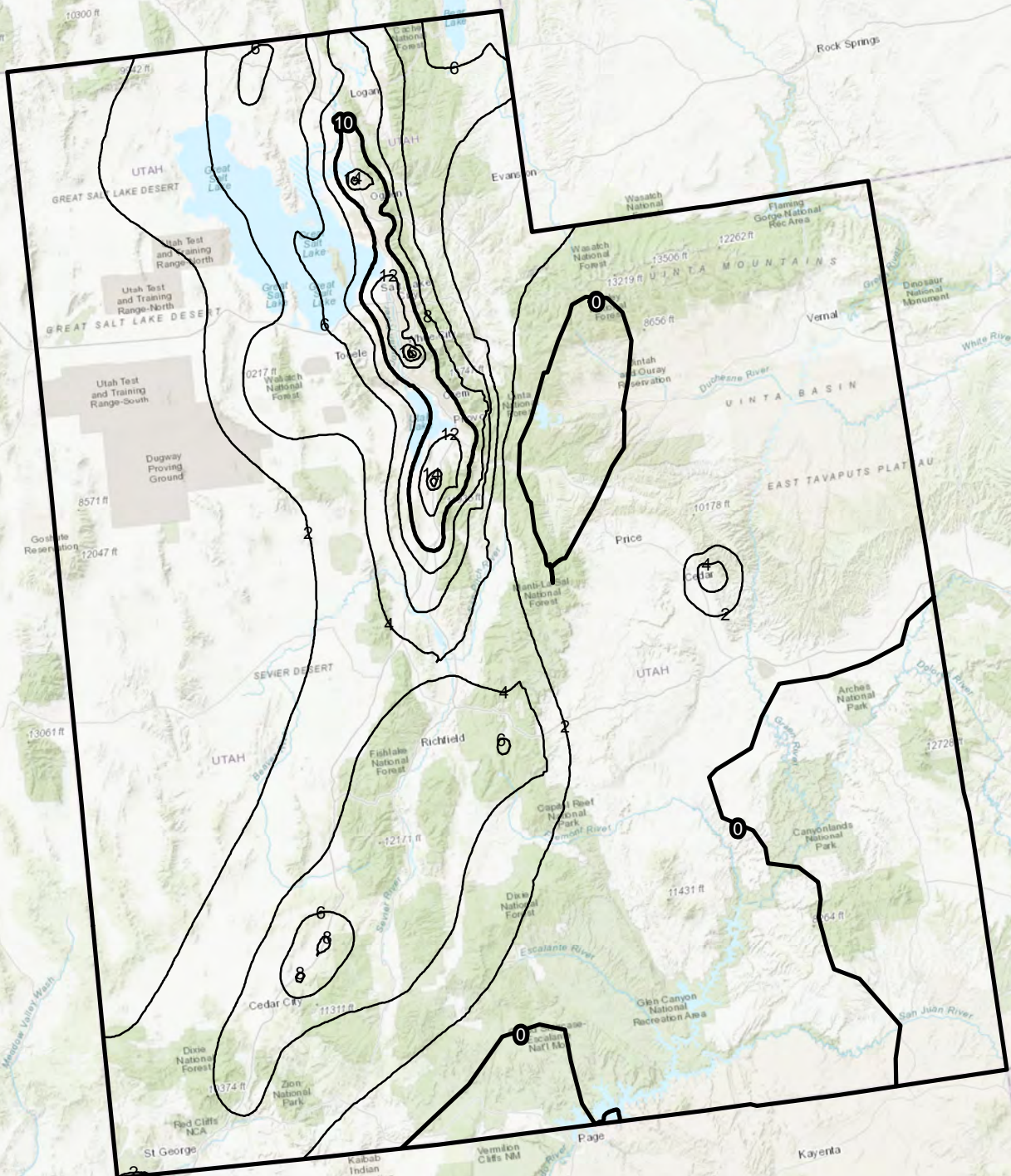
Service Layer Credits: Sources: Esri, HERE, Garmin, Intermap, increment P Corp., GEBCO, USGS, FAO, NPS, NRCAN, GeoBase, IGN, Kadaster NL, Ordnance Survey, Esri Japan, METI, Esri China (Hong Kong), swisstopo, © OpenStreetMap

**Reference Horizontal Strain
Boulanger and Idriss 2014
2475 Year Return Period
Contour Interval: 1 Contour = 2 (%)**

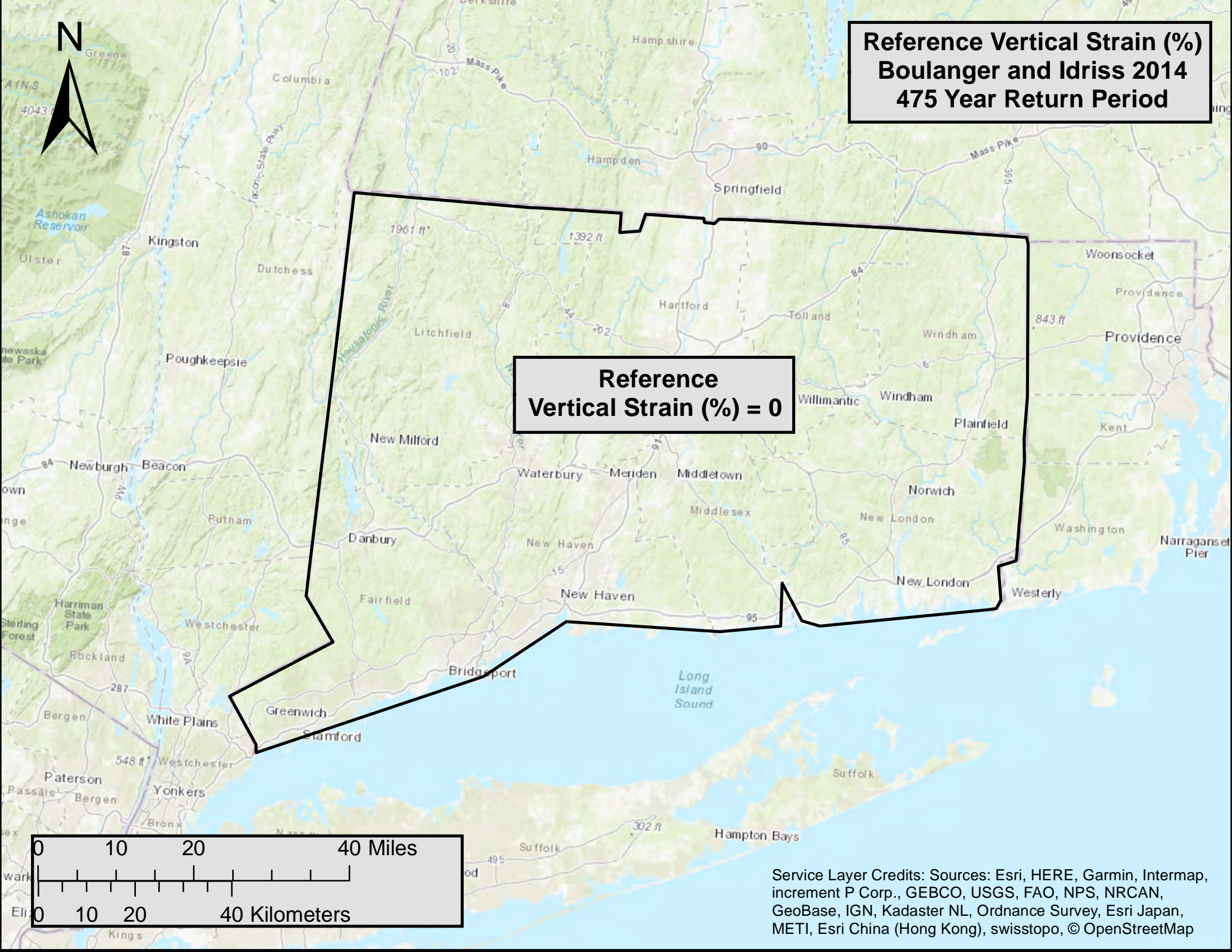


Service Layer Credits: Sources: Esri, HERE, Garmin, Intermap, increment P Corp., GEBCO, USGS, FAO, NPS, NRCAN, GeoBase, IGN, Kadaster NL, Ordnance Survey, Esri Japan, METI, Esri China (Hong Kong), swisstopo, © OpenStreetMap

**Reference Horizontal Strain
 Ku et al. 2012
 2475 Year Return Period
 Contour Interval: 1 Contour = 2 (%)**

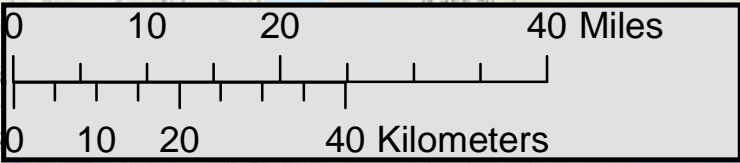


Service Layer Credits: Sources: Esri, HERE, Garmin, Intermap, increment P Corp., GEBCO, USGS, FAO, NPS, NRCAN, GeoBase, IGN, Kadaster NL, Ordnance Survey, Esri Japan, METI, Esri China (Hong Kong), swisstopo, © OpenStreetMap

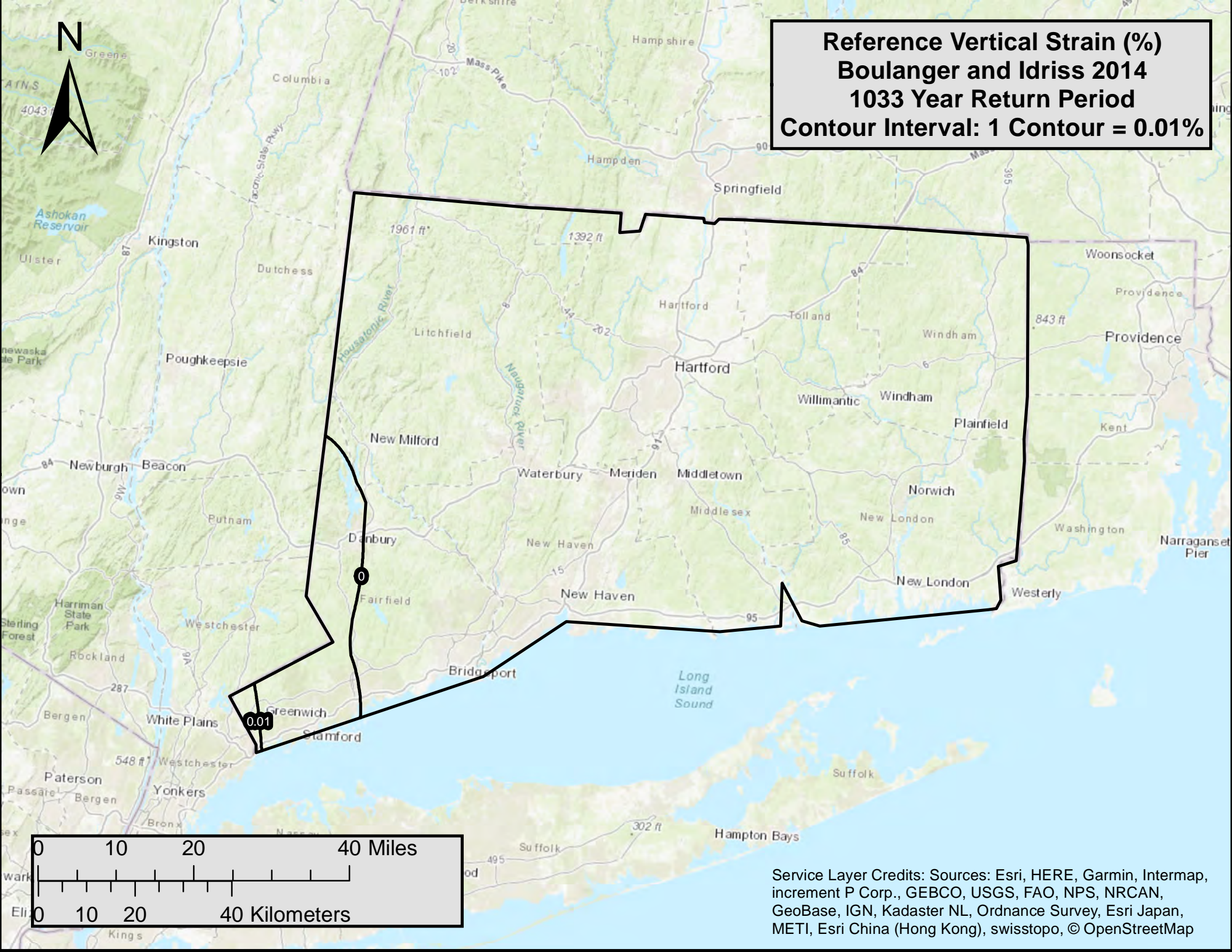


**Reference Vertical Strain (%)
Boulanger and Idriss 2014
475 Year Return Period**

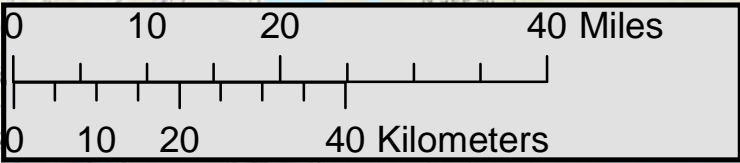
**Reference
Vertical Strain (%) = 0**



Service Layer Credits: Sources: Esri, HERE, Garmin, Intermap, increment P Corp., GEBCO, USGS, FAO, NPS, NRCAN, GeoBase, IGN, Kadaster NL, Ordnance Survey, Esri Japan, METI, Esri China (Hong Kong), swisstopo, © OpenStreetMap

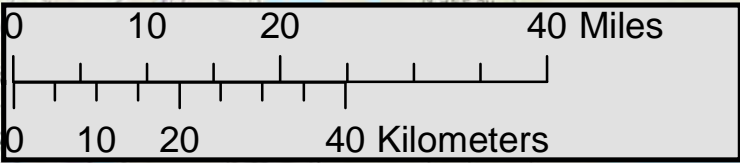
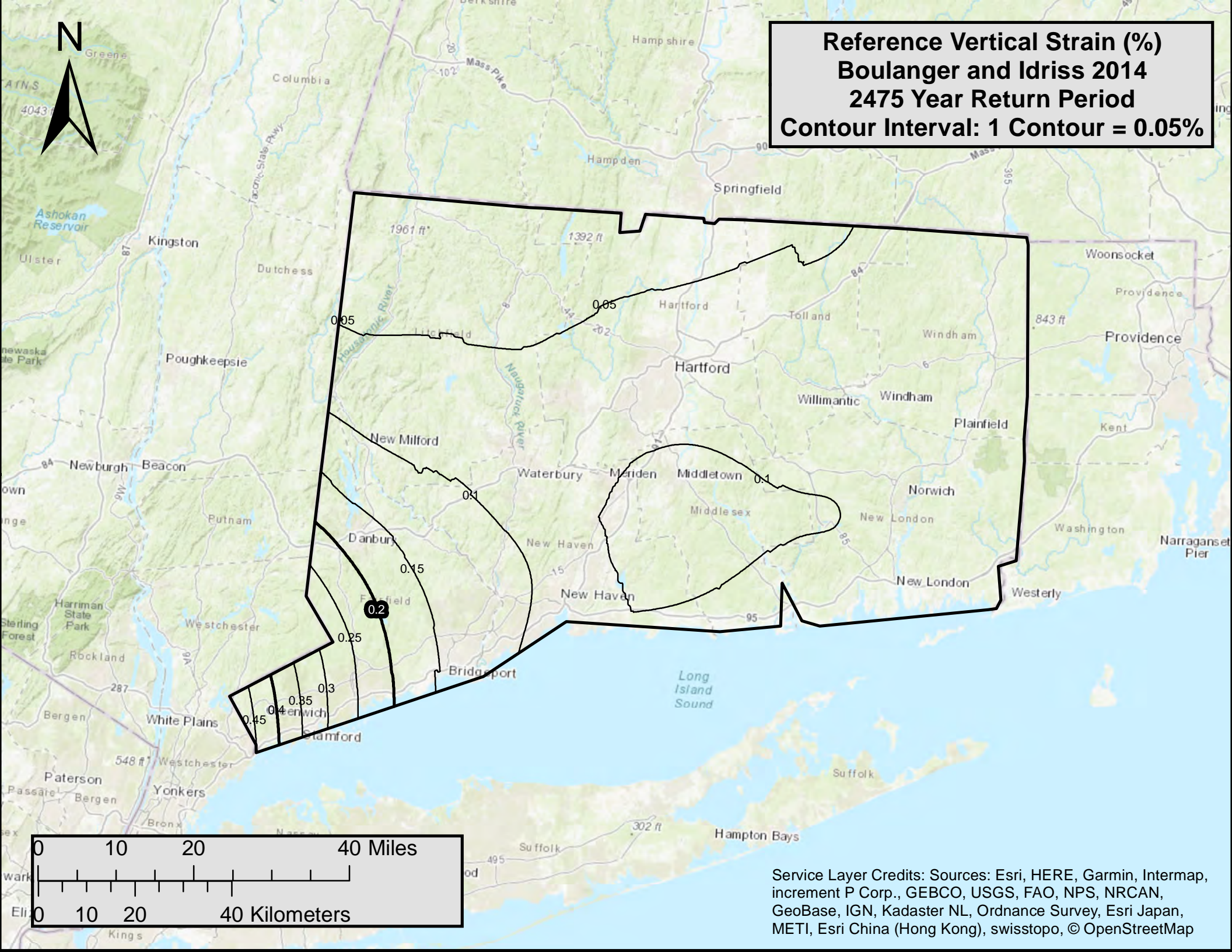


Reference Vertical Strain (%)
Boulangier and Idriss 2014
1033 Year Return Period
Contour Interval: 1 Contour = 0.01%

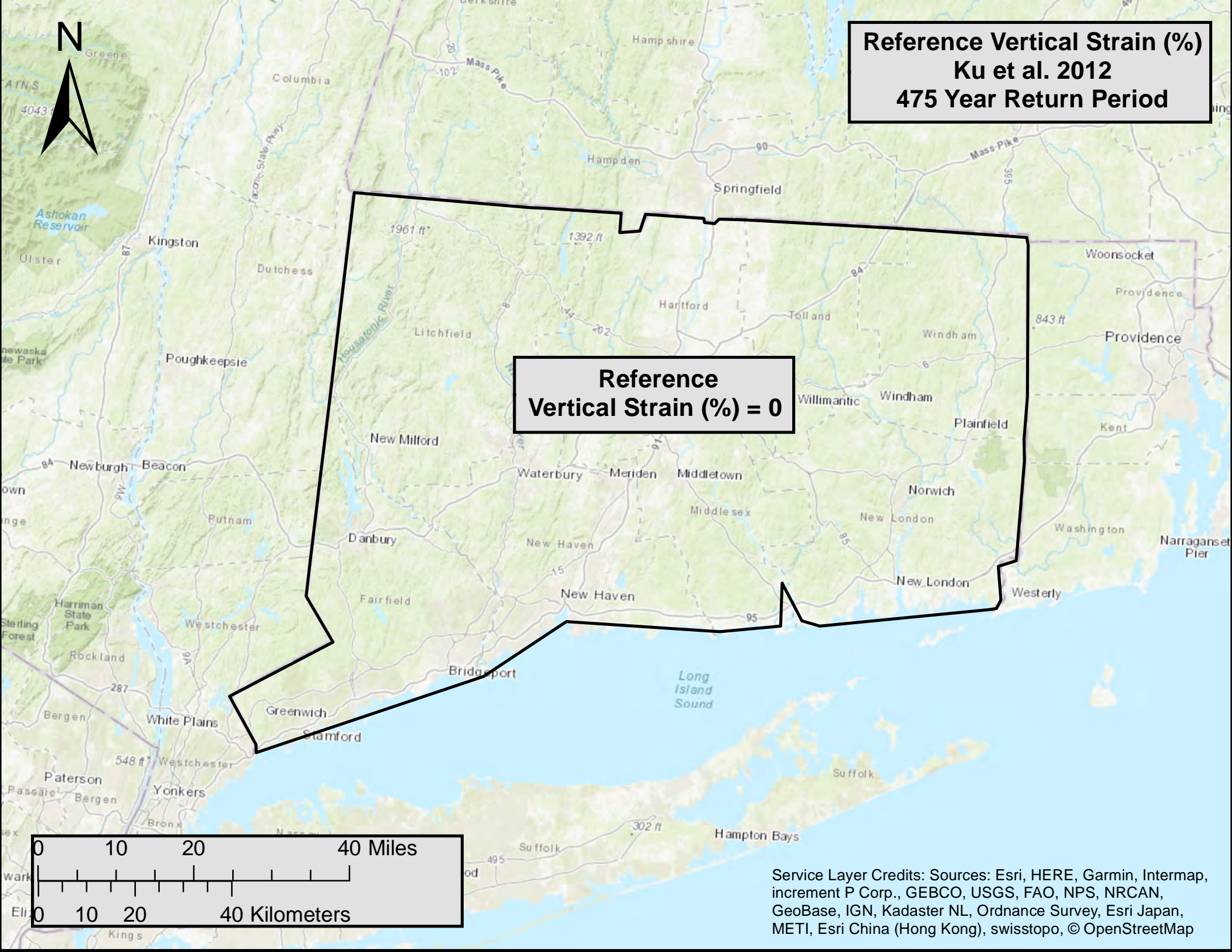


Service Layer Credits: Sources: Esri, HERE, Garmin, Intermap, increment P Corp., GEBCO, USGS, FAO, NPS, NRCAN, GeoBase, IGN, Kadaster NL, Ordnance Survey, Esri Japan, METI, Esri China (Hong Kong), swisstopo, © OpenStreetMap

Reference Vertical Strain (%)
Boulanger and Idriss 2014
2475 Year Return Period
Contour Interval: 1 Contour = 0.05%

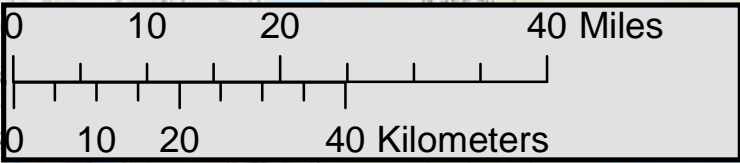


Service Layer Credits: Sources: Esri, HERE, Garmin, Intermap, increment P Corp., GEBCO, USGS, FAO, NPS, NRCAN, GeoBase, IGN, Kadaster NL, Ordnance Survey, Esri Japan, METI, Esri China (Hong Kong), swisstopo, © OpenStreetMap

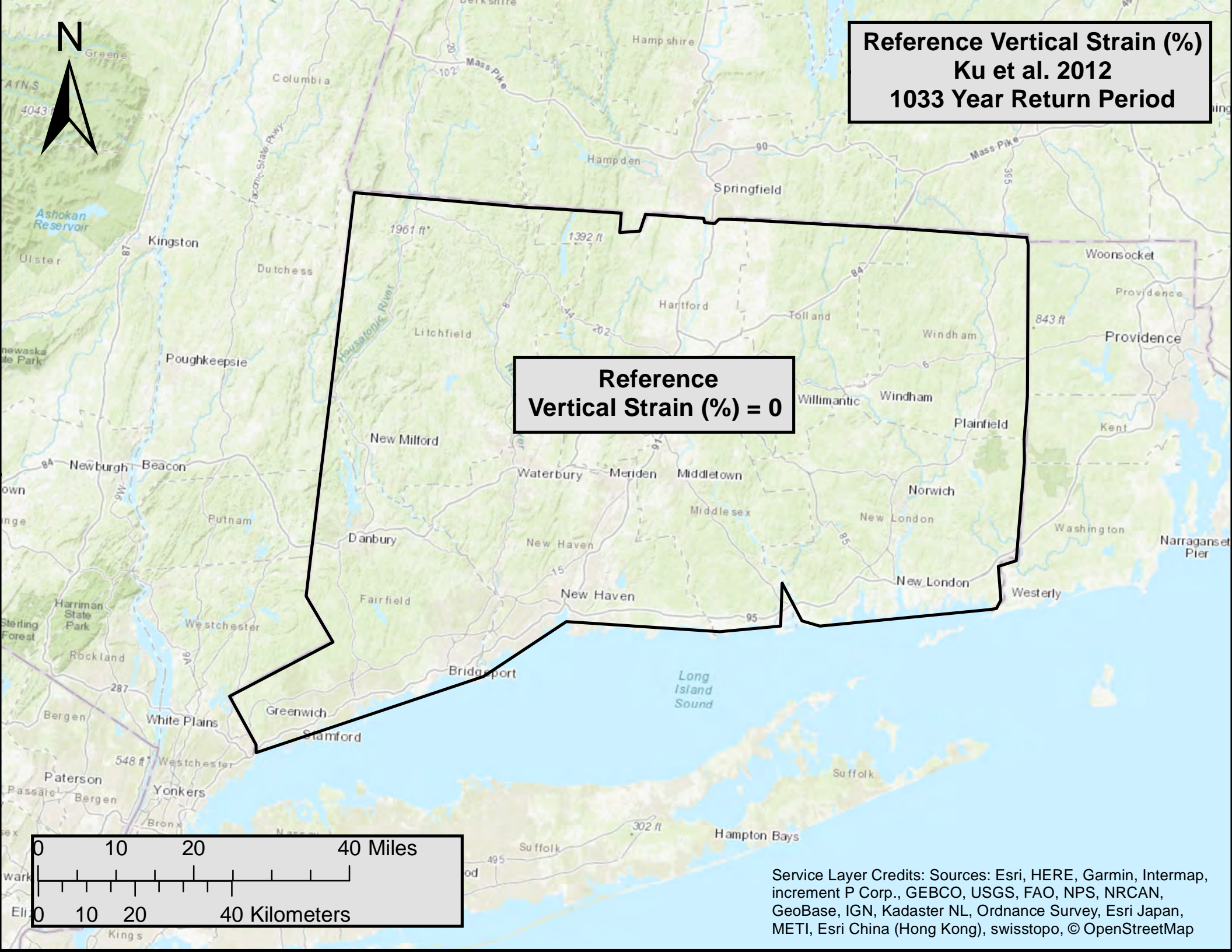


Reference Vertical Strain (%)
Ku et al. 2012
475 Year Return Period

Reference
Vertical Strain (%) = 0

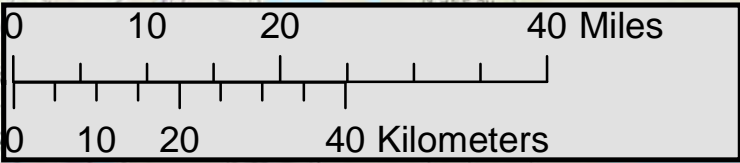


Service Layer Credits: Sources: Esri, HERE, Garmin, Intermap, increment P Corp., GEBCO, USGS, FAO, NPS, NRCAN, GeoBase, IGN, Kadaster NL, Ordnance Survey, Esri Japan, METI, Esri China (Hong Kong), swisstopo, © OpenStreetMap



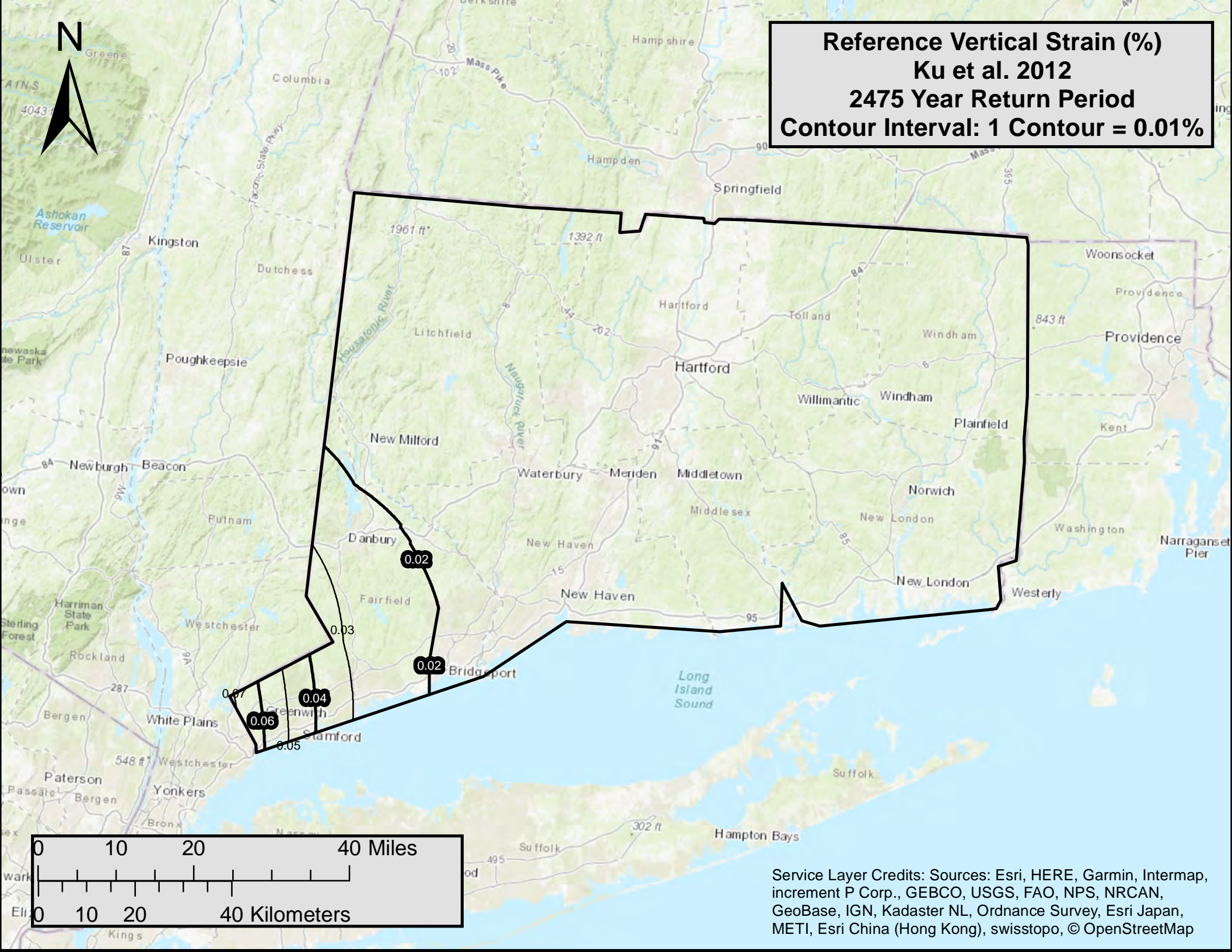
Reference Vertical Strain (%)
Ku et al. 2012
1033 Year Return Period

Reference
Vertical Strain (%) = 0



Service Layer Credits: Sources: Esri, HERE, Garmin, Intermap, increment P Corp., GEBCO, USGS, FAO, NPS, NRCAN, GeoBase, IGN, Kadaster NL, Ordnance Survey, Esri Japan, METI, Esri China (Hong Kong), swisstopo, © OpenStreetMap

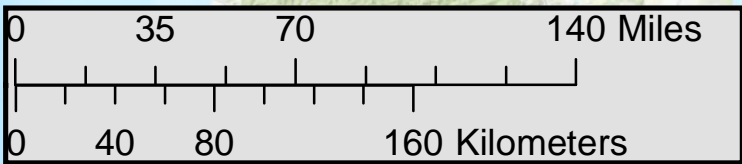
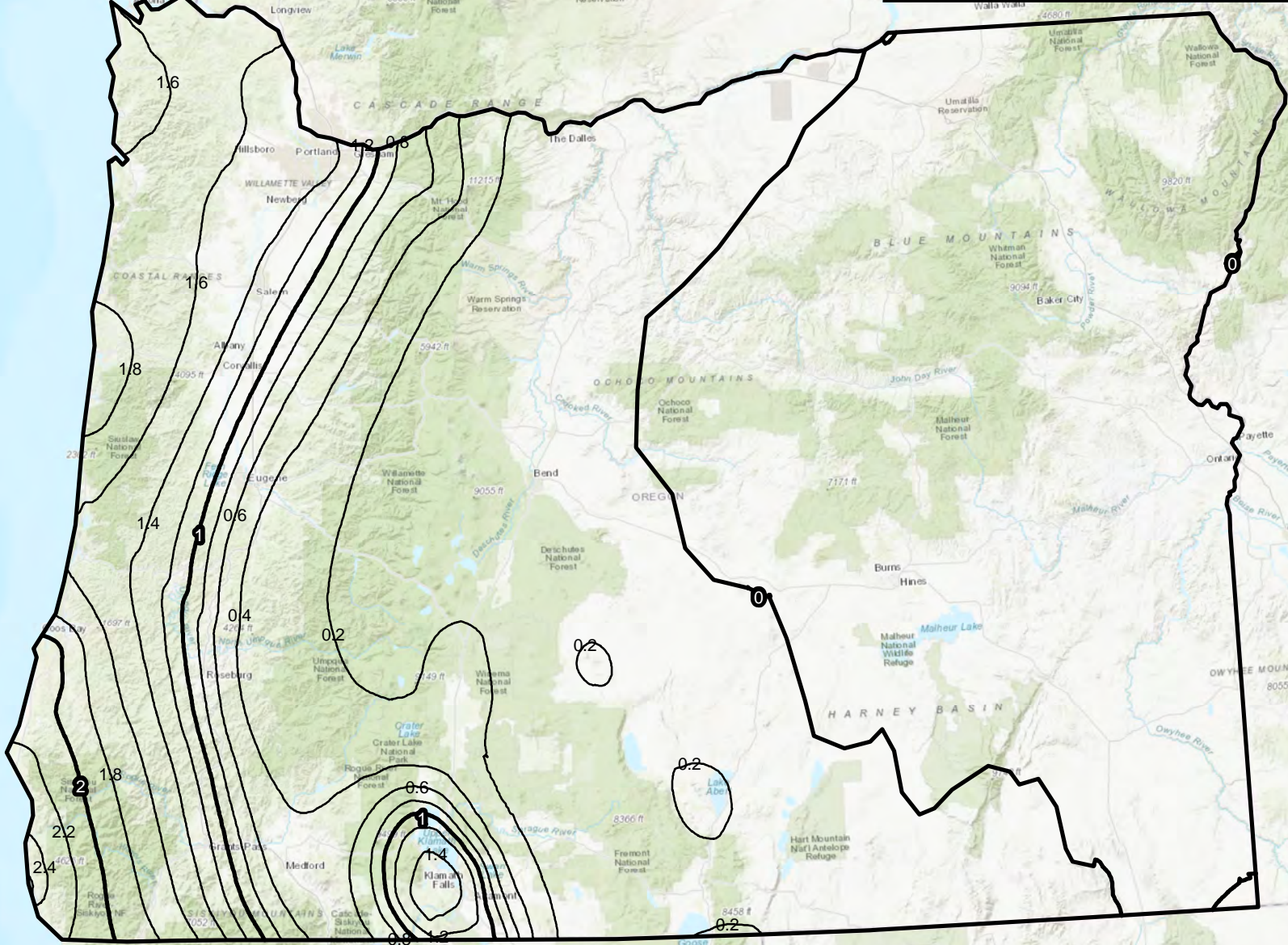
Reference Vertical Strain (%)
Ku et al. 2012
2475 Year Return Period
Contour Interval: 1 Contour = 0.01%



Service Layer Credits: Sources: Esri, HERE, Garmin, Intermap, increment P Corp., GEBCO, USGS, FAO, NPS, NRCAN, GeoBase, IGN, Kadaster NL, Ordnance Survey, Esri Japan, METI, Esri China (Hong Kong), swisstopo, © OpenStreetMap



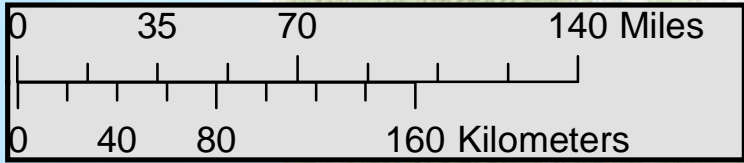
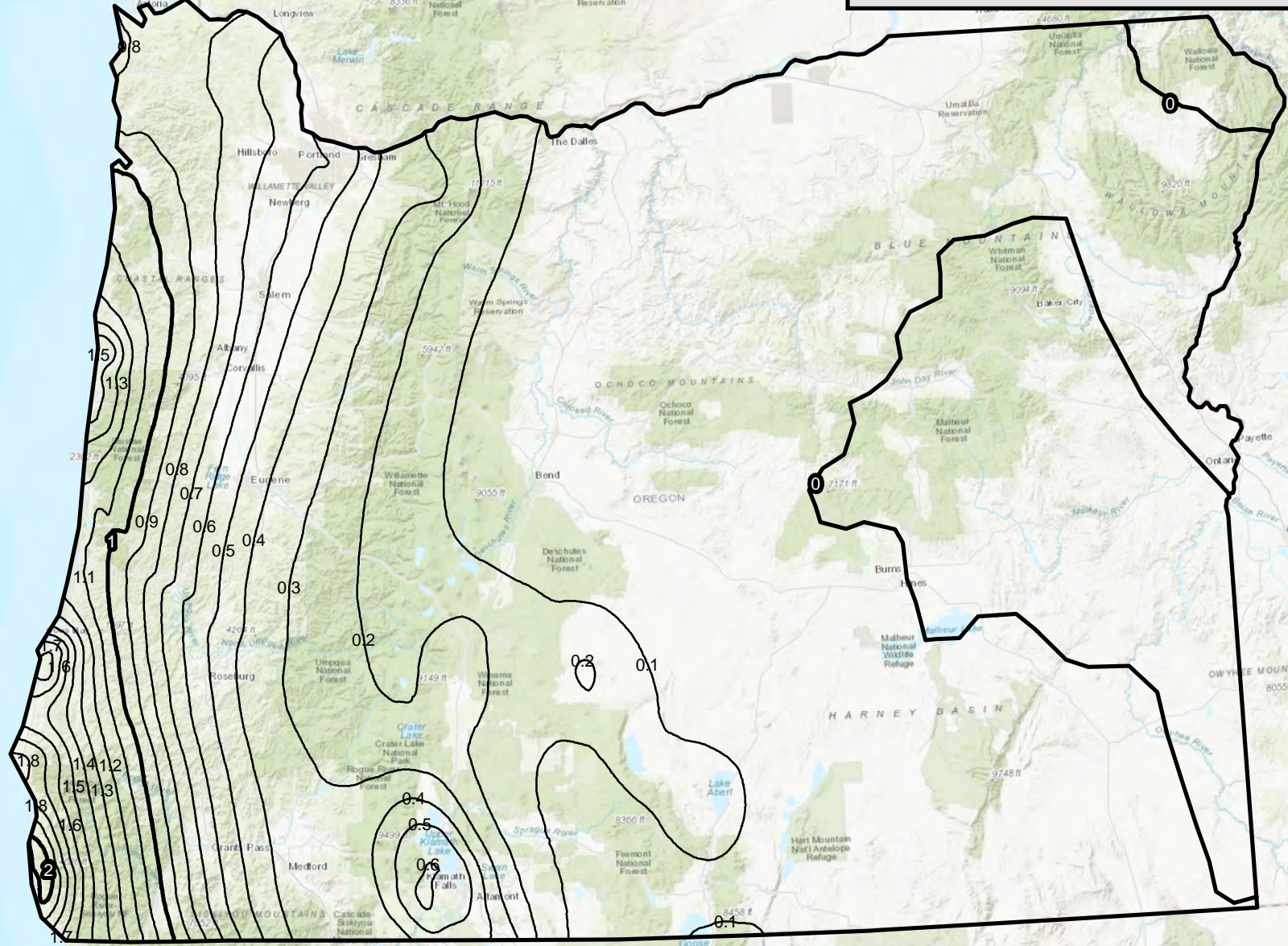
**Reference Vertical Strain
Boulanger and Idriss 2014
475 Year Return Period
Contour Interval: 1 Contour = 0.2 (%)**



Service Layer Credits: Sources: Esri, HERE, Garmin, Intermap, increment P Corp., GEBCO, USGS, FAO, NPS, NRCAN, GeoBase, IGN, Kadaster NL, Ordnance Survey, Esri Japan, METI, Esri China (Hong Kong), swisstopo, © OpenStreetMap



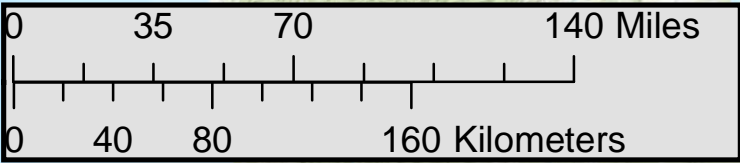
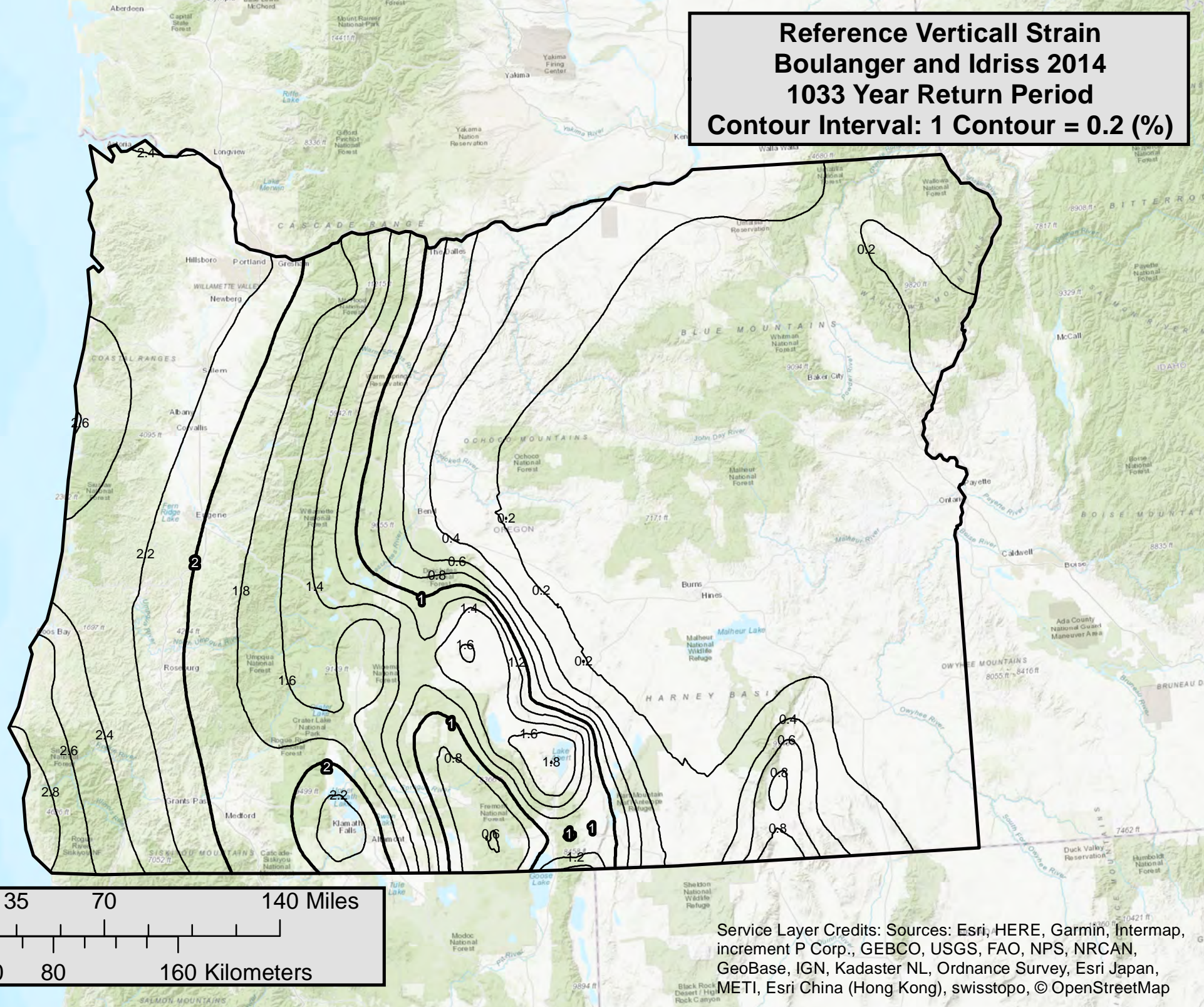
Reference Vertical Strain
Ku et al. 2012
475 Year Return Period
Contour Interval: 1 Contour = 0.1 (%)



Service Layer Credits: Sources: Esri, HERE, Garmin, Intermap, increment P Corp., GEBCO, USGS, FAO, NPS, NRCAN, GeoBase, IGN, Kadaster NL, Ordnance Survey, Esri Japan, METI, Esri China (Hong Kong), swisstopo, © OpenStreetMap



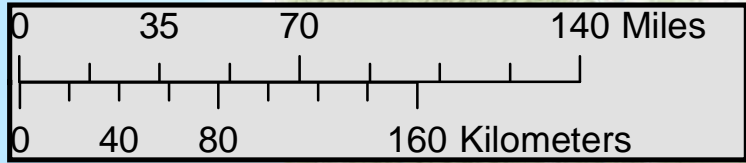
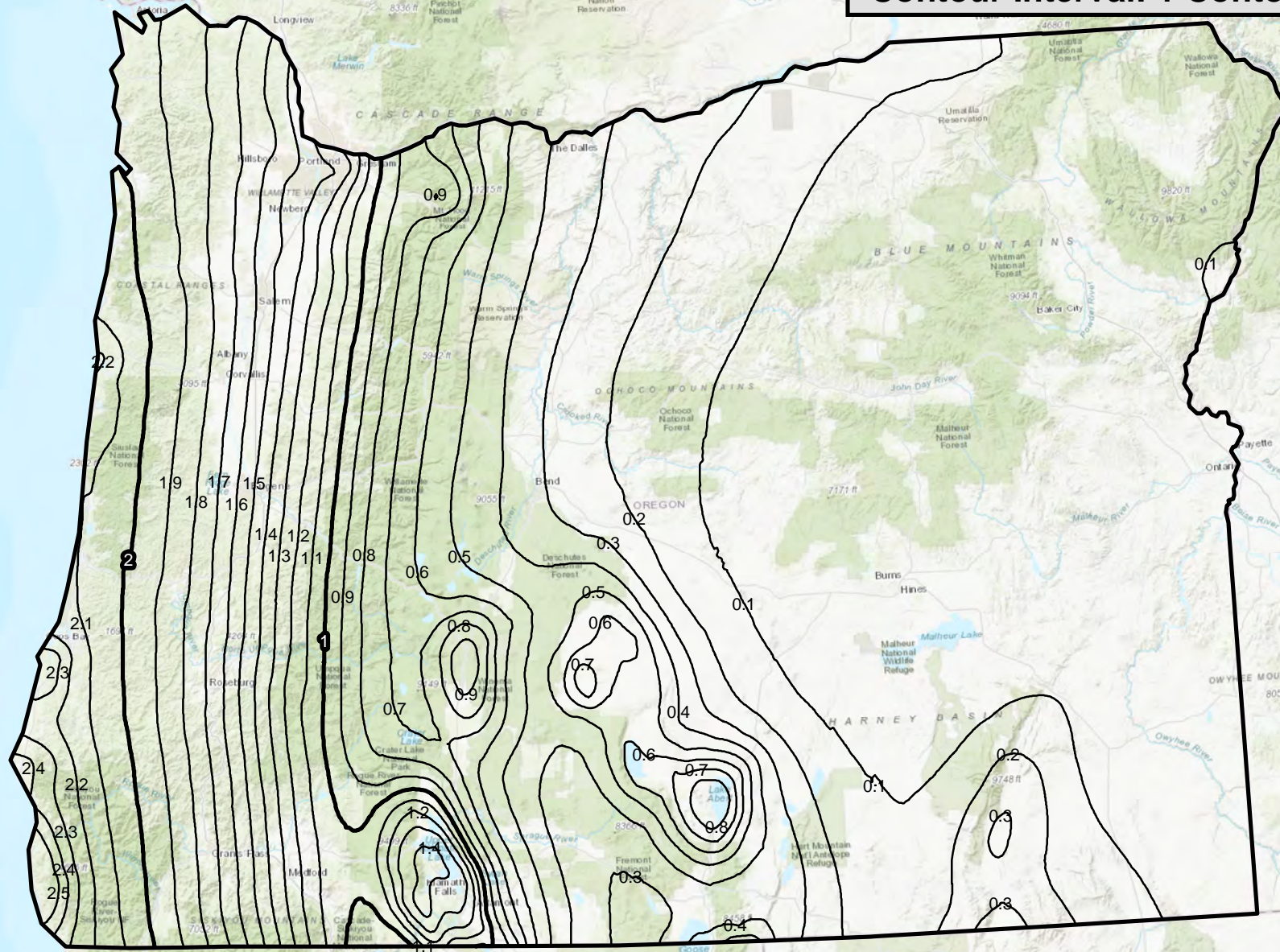
**Reference Vertical Strain
Boulanger and Idriss 2014
1033 Year Return Period
Contour Interval: 1 Contour = 0.2 (%)**



Service Layer Credits: Sources: Esri, HERE, Garmin, Intermap, increment P Corp., GEBCO, USGS, FAO, NPS, NRCAN, GeoBase, IGN, Kadaster NL, Ordnance Survey, Esri Japan, METI, Esri China (Hong Kong), swisstopo, © OpenStreetMap



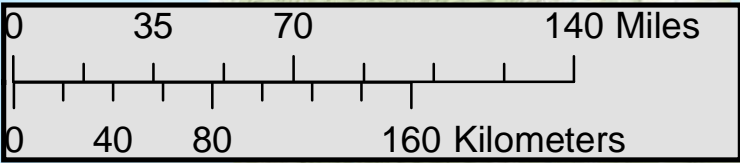
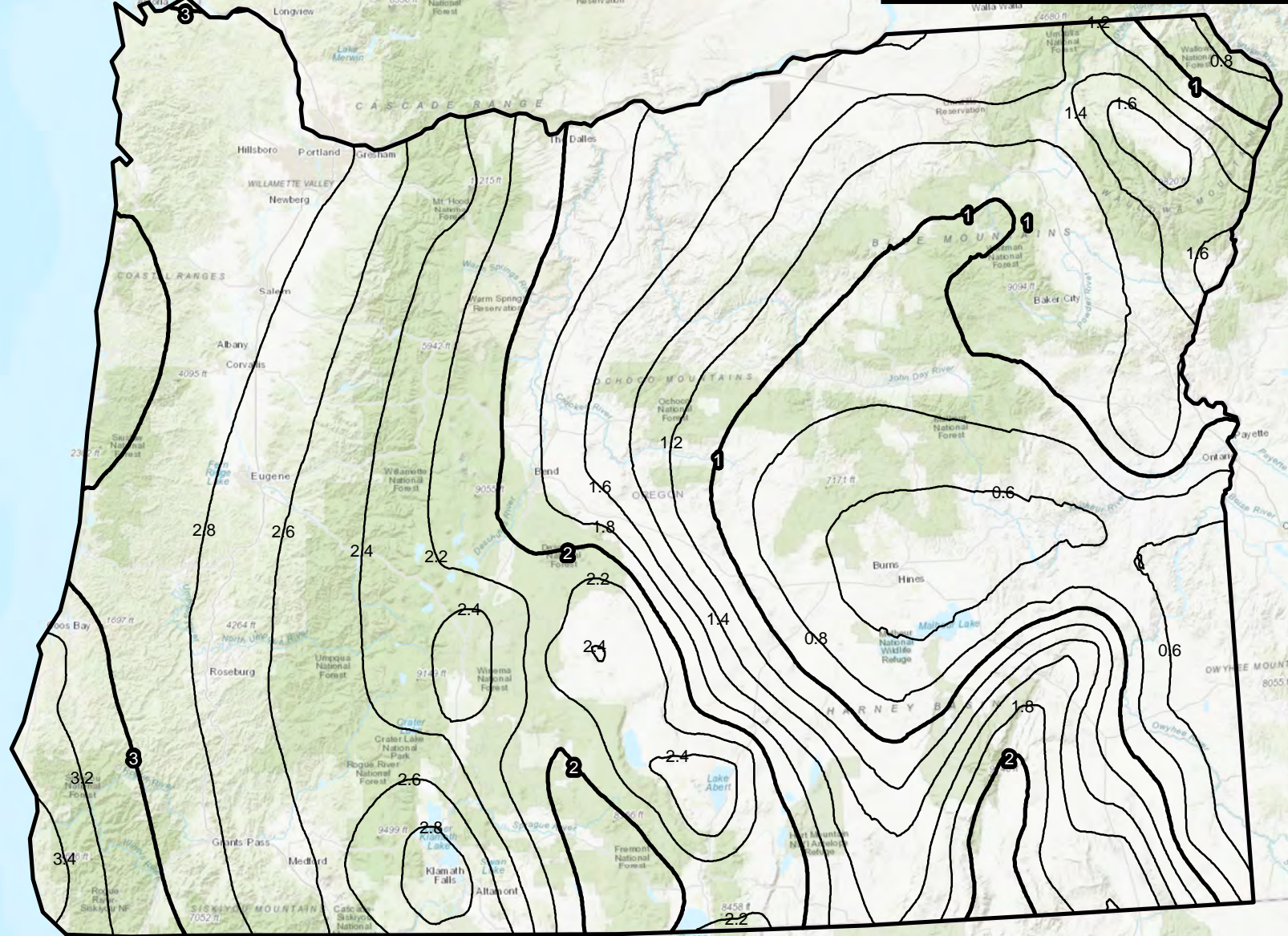
Reference Vertical Strain
Ku et al. 2012
1033 Year Return Period
Contour Interval: 1 Contour = 0.1 (%)



Service Layer Credits: Sources: Esri, HERE, Garmin, Intermap, increment P Corp., GEBCO, USGS, FAO, NPS, NRCAN, GeoBase, IGN, Kadaster NL, Ordnance Survey, Esri Japan, METI, Esri China (Hong Kong), swisstopo, © OpenStreetMap



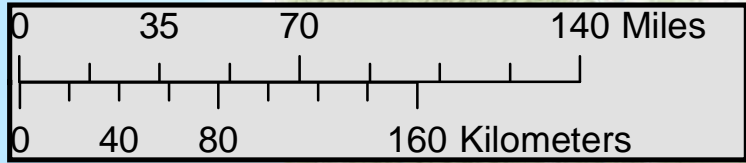
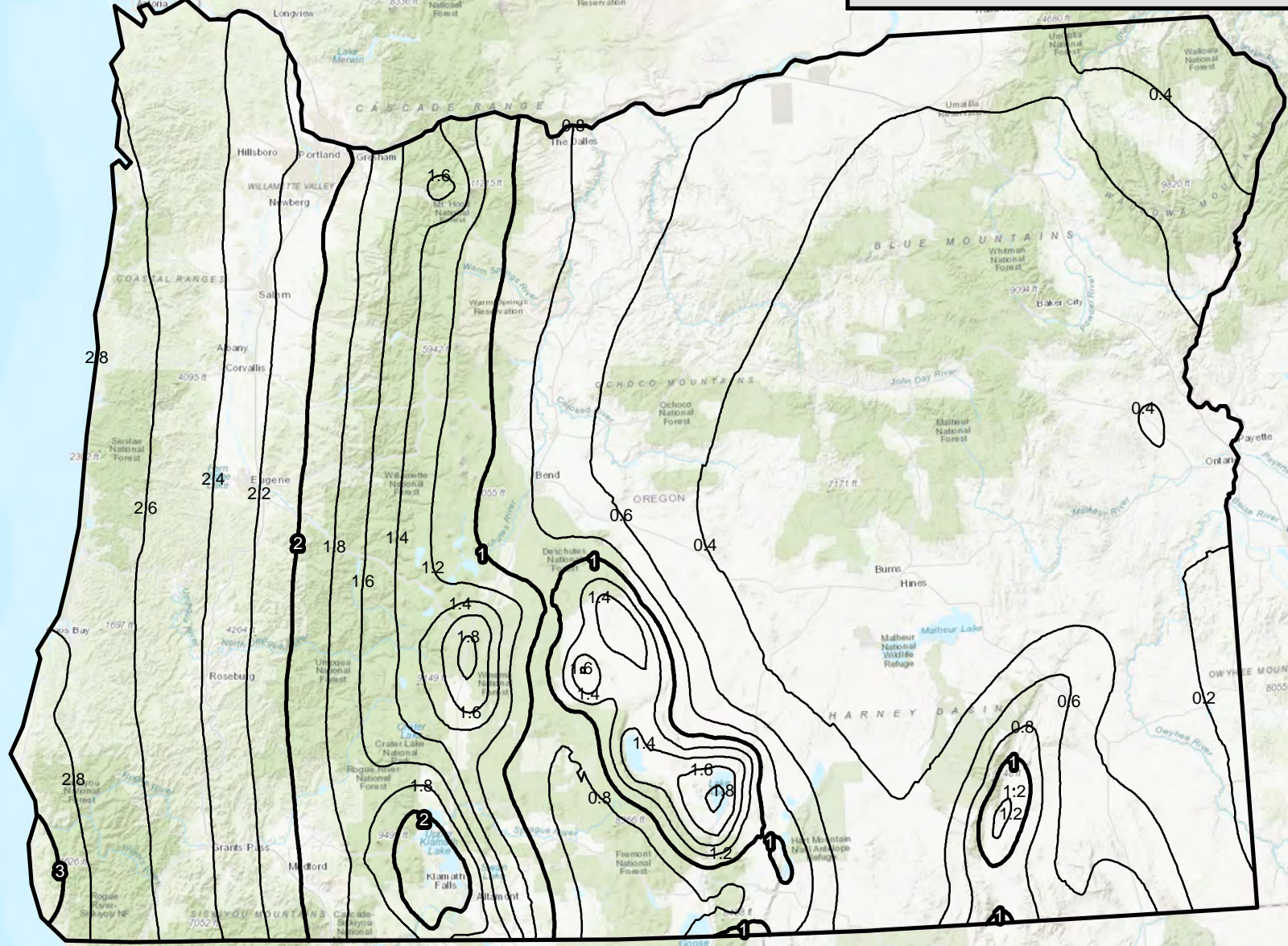
**Reference Vertical Strain
Boulanger and Idriss 2014
2475 Year Return Period
Contour Interval: 1 Contour = 0.2 (%)**



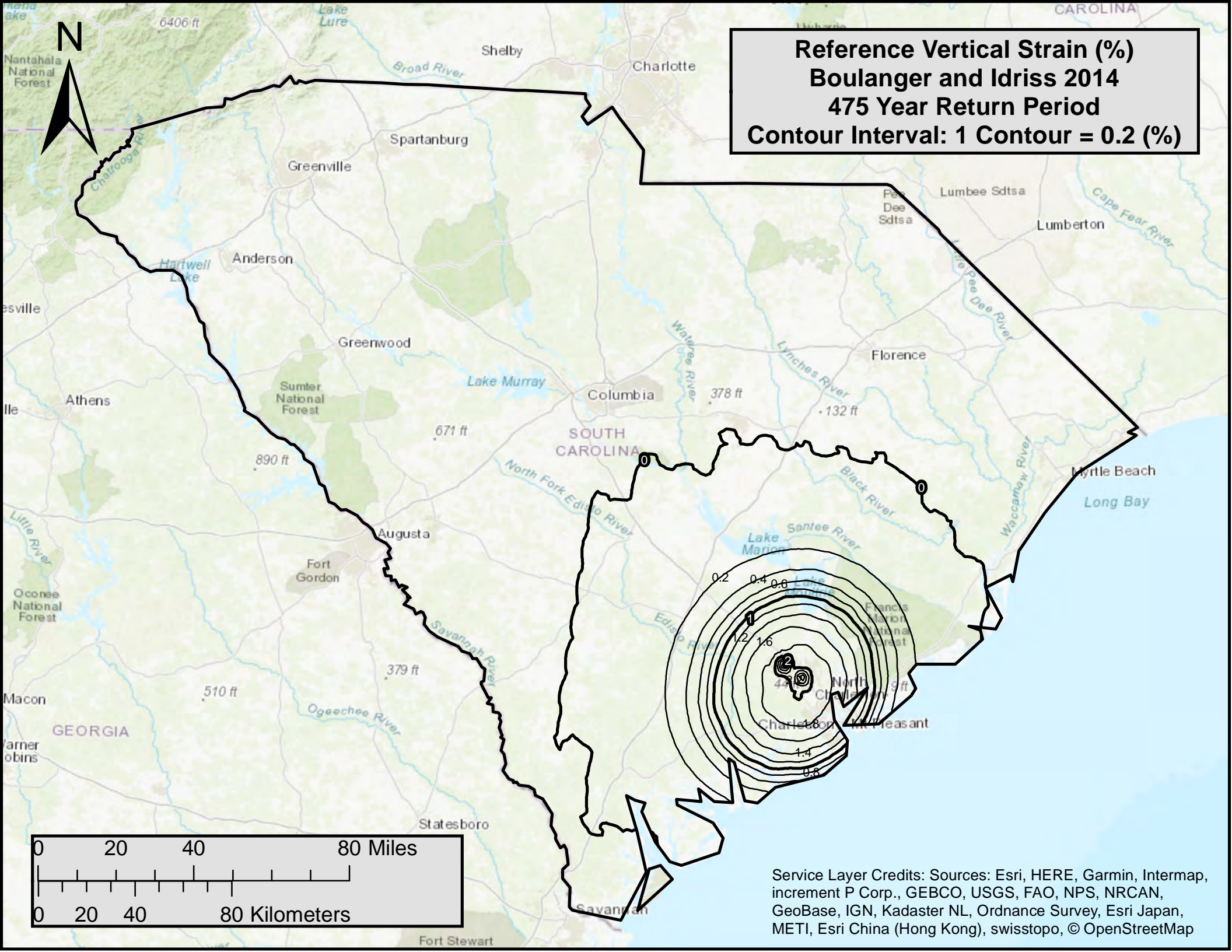
Service Layer Credits: Sources: Esri, HERE, Garmin, Intermap, increment P Corp., GEBCO, USGS, FAO, NPS, NRCAN, GeoBase, IGN, Kadaster NL, Ordnance Survey, Esri Japan, METI, Esri China (Hong Kong), swisstopo, © OpenStreetMap



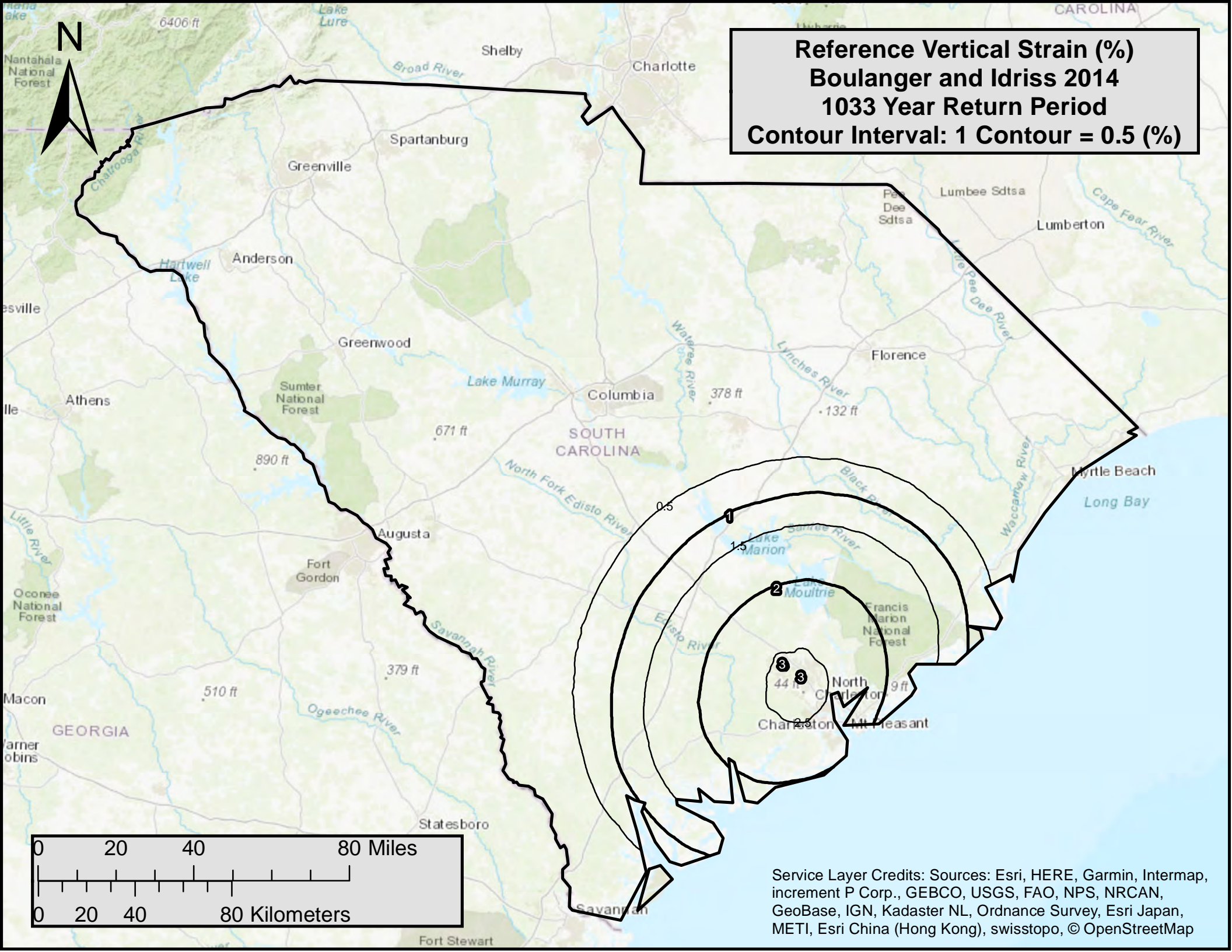
Reference Vertical Strain
Ku et al. 2012
2475 Year Return Period
Contour Interval: 1 Contour = 0.2 (%)

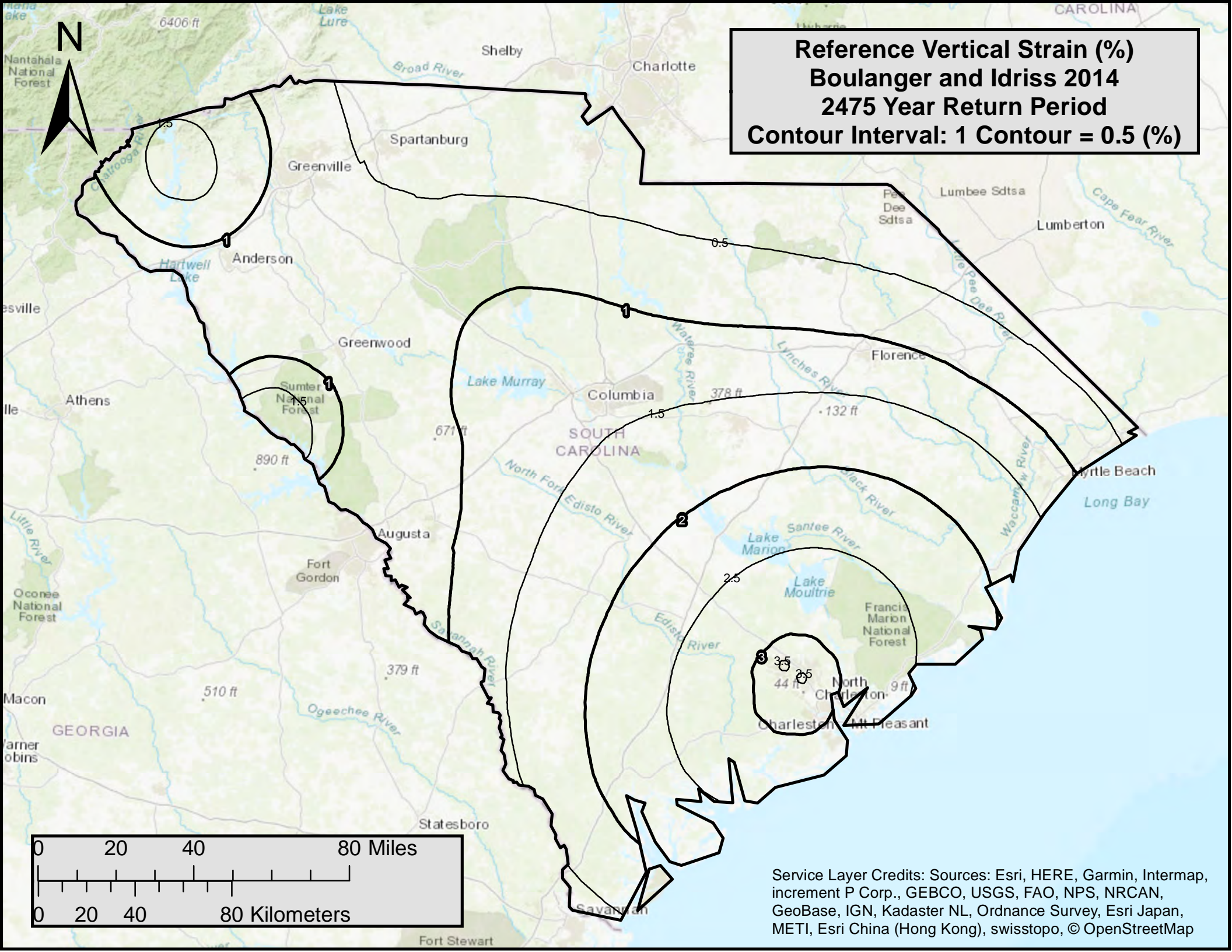


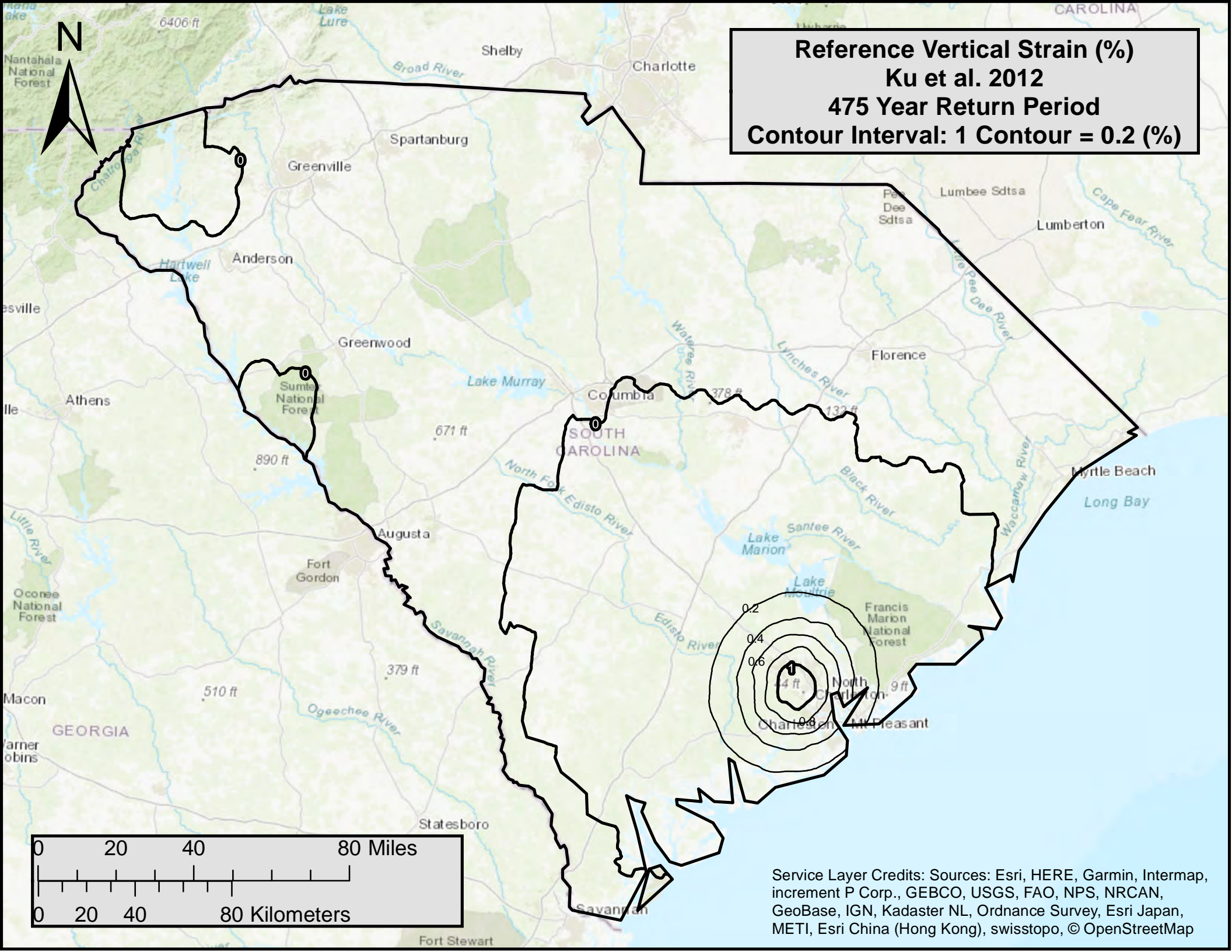
Service Layer Credits: Sources: Esri, HERE, Garmin, Intermap, increment P Corp., GEBCO, USGS, FAO, NPS, NRCAN, GeoBase, IGN, Kadaster NL, Ordnance Survey, Esri Japan, METI, Esri China (Hong Kong), swisstopo, © OpenStreetMap

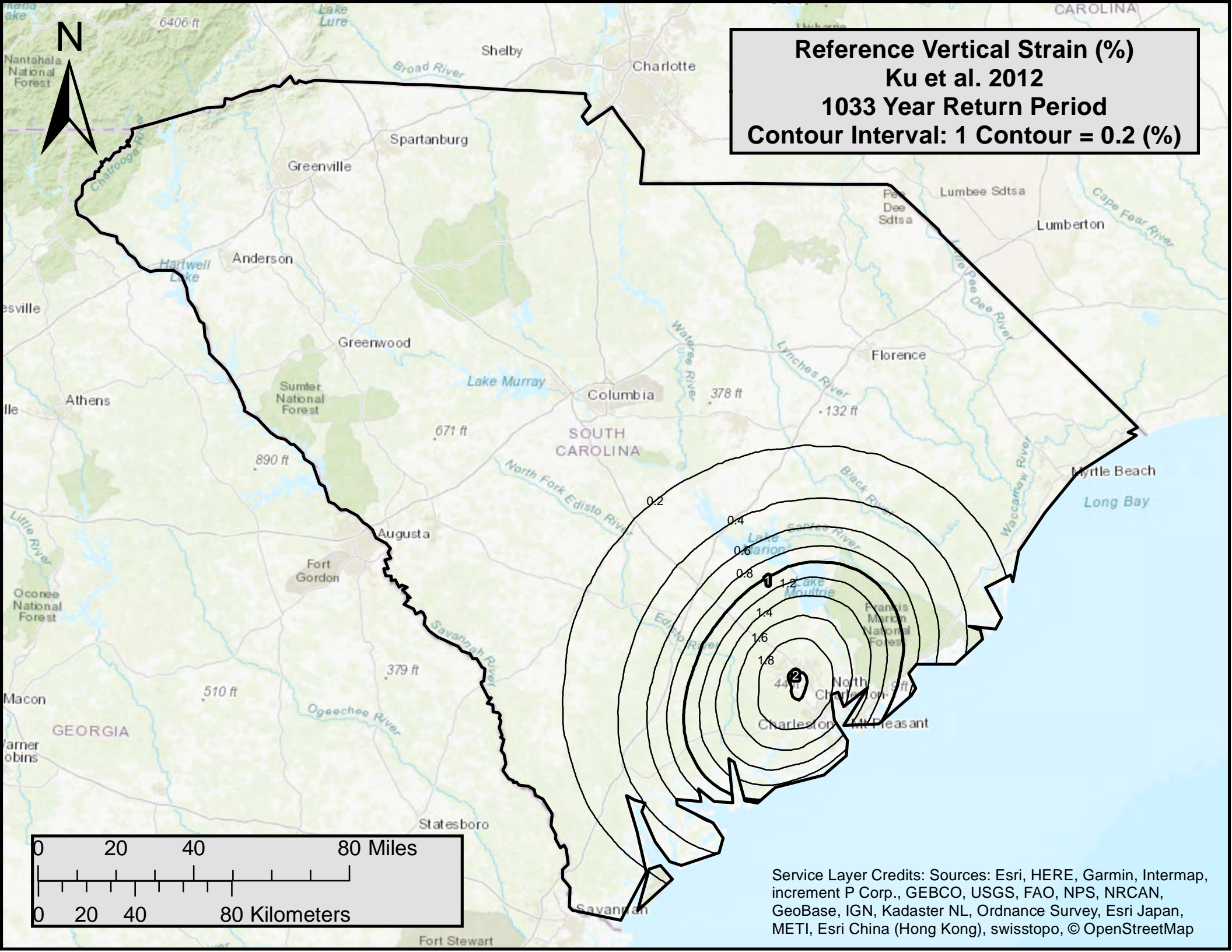


Service Layer Credits: Sources: Esri, HERE, Garmin, Intermap, increment P Corp., GEBCO, USGS, FAO, NPS, NRCAN, GeoBase, IGN, Kadaster NL, Ordnance Survey, Esri Japan, METI, Esri China (Hong Kong), swisstopo, © OpenStreetMap

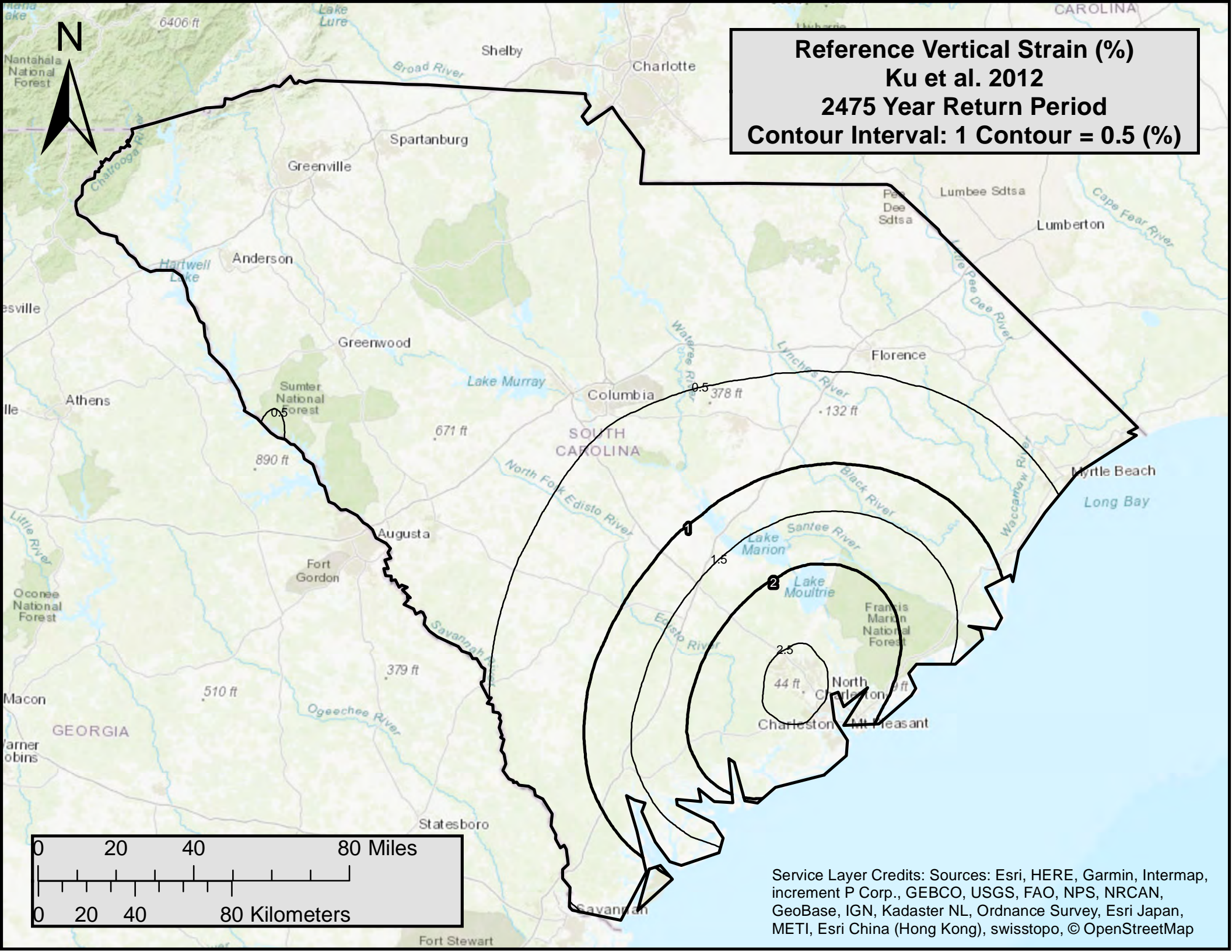




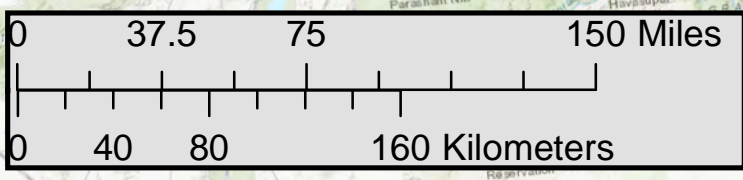
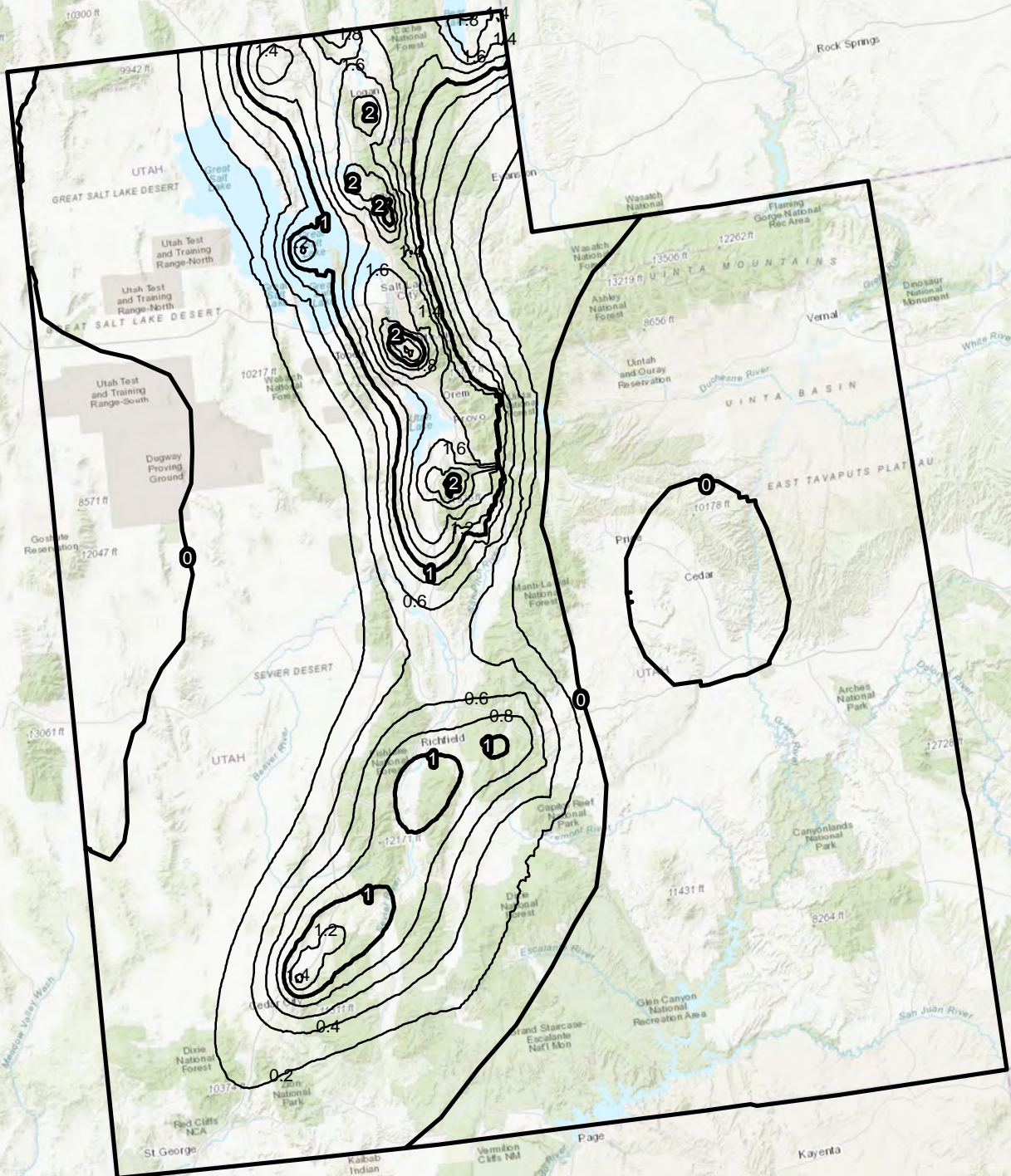




Service Layer Credits: Sources: Esri, HERE, Garmin, Intermap, increment P Corp., GEBCO, USGS, FAO, NPS, NRCAN, GeoBase, IGN, Kadaster NL, Ordnance Survey, Esri Japan, METI, Esri China (Hong Kong), swisstopo, © OpenStreetMap

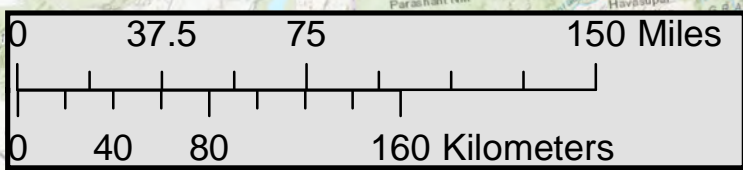
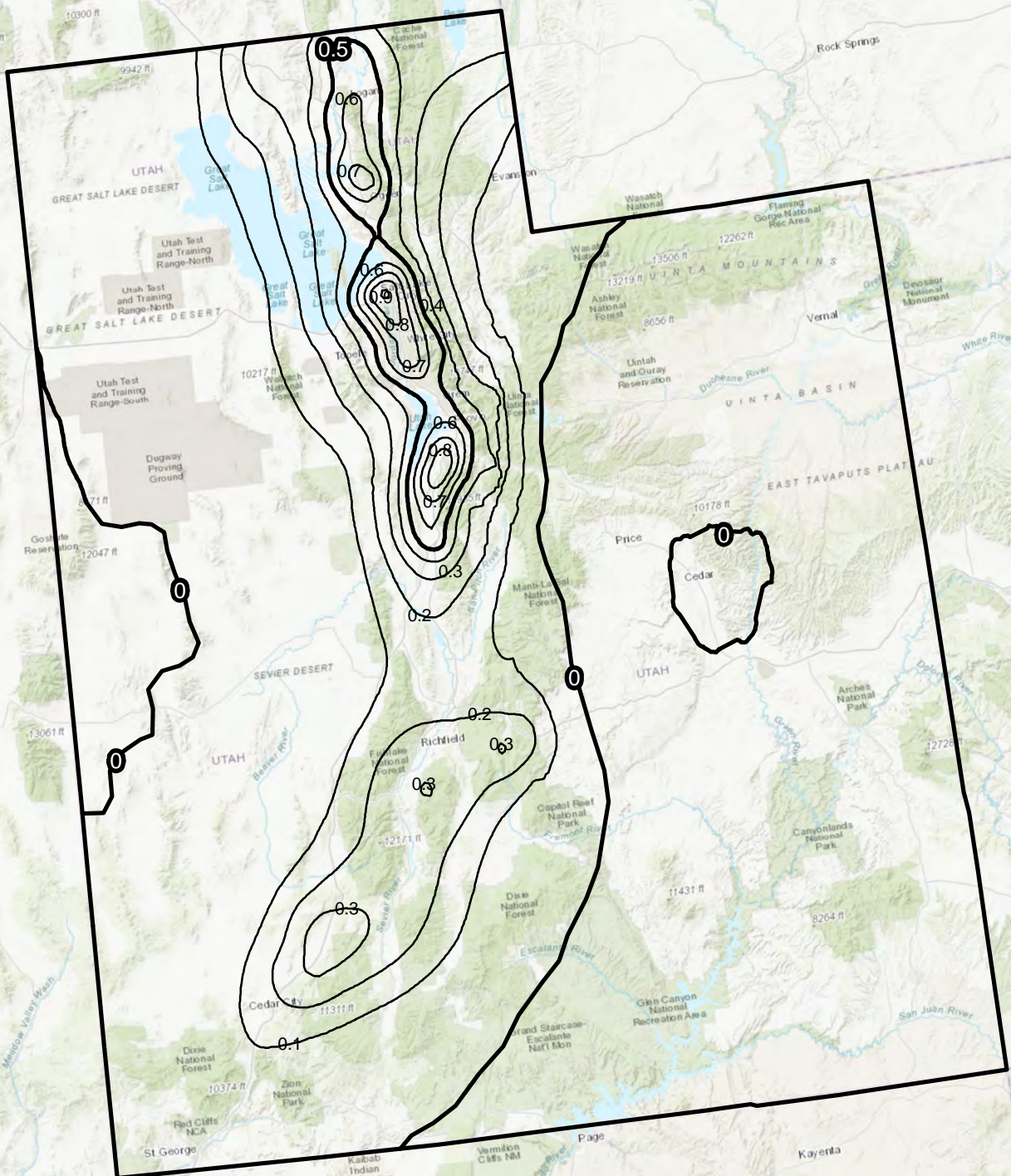


**Reference Vertical Strain
Boulanger and Idriss 2014
475 Year Return Period
Contour Interval: 1 Contour = 0.2 (%)**



Service Layer Credits: Sources: Esri, HERE, Garmin, Intermap, increment P Corp., GEBCO, USGS, FAO, NPS, NRCAN, GeoBase, IGN, Kadaster NL, Ordnance Survey, Esri Japan, METI, Esri China (Hong Kong), swisstopo, © OpenStreetMap

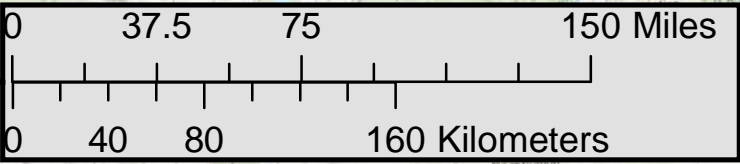
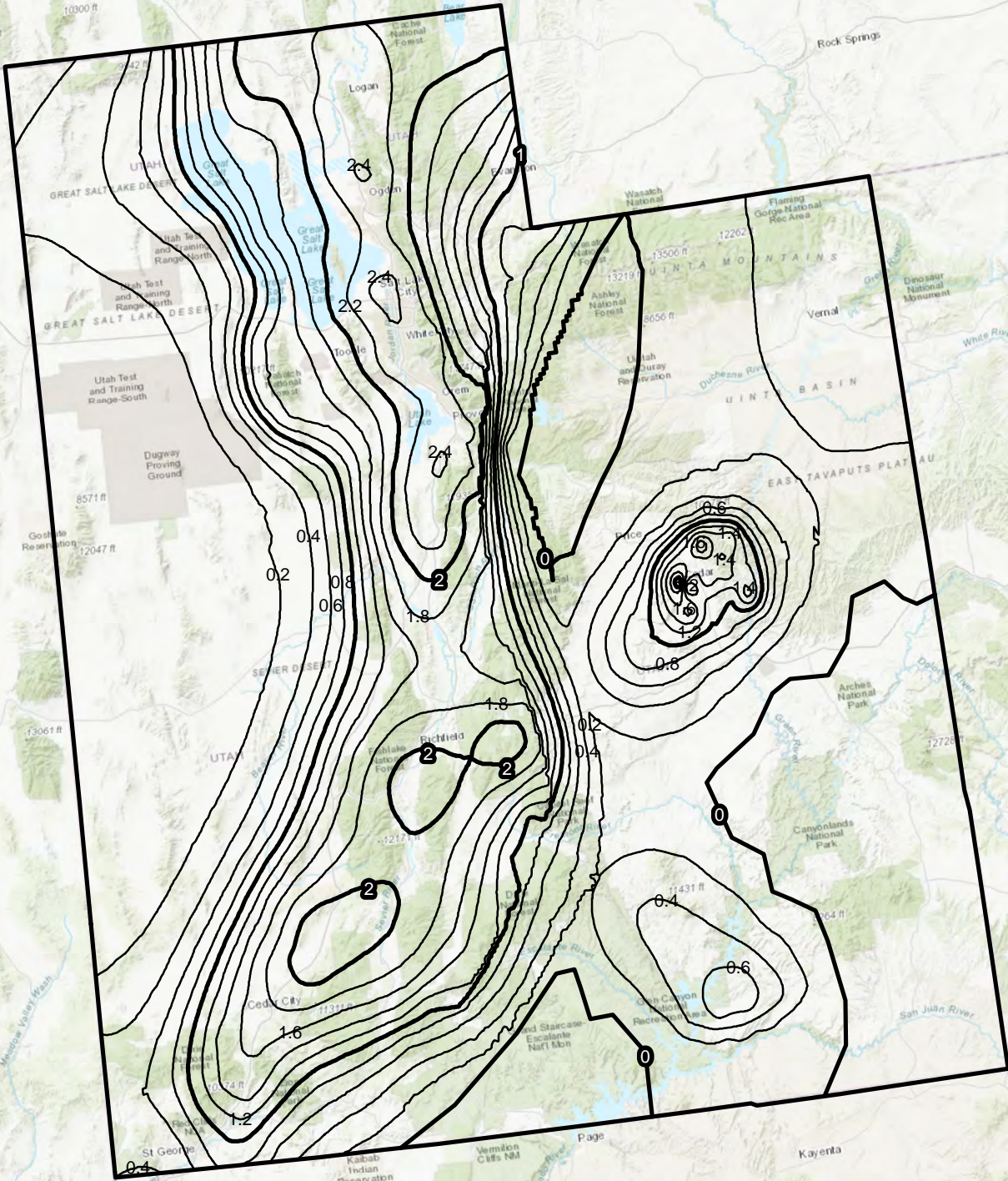
**Reference Vertical Strain
Ku et al. 2012
475 Year Return Period
Contour Interval: 1 Contour = 0.1 (%)**



Service Layer Credits: Sources: Esri, HERE, Garmin, Intermap, increment P Corp., GEBCO, USGS, FAO, NPS, NRCAN, GeoBase, IGN, Kadaster NL, Ordnance Survey, Esri Japan, METI, Esri China (Hong Kong), swisstopo, © OpenStreetMap

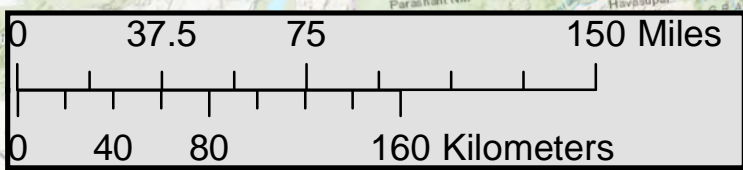
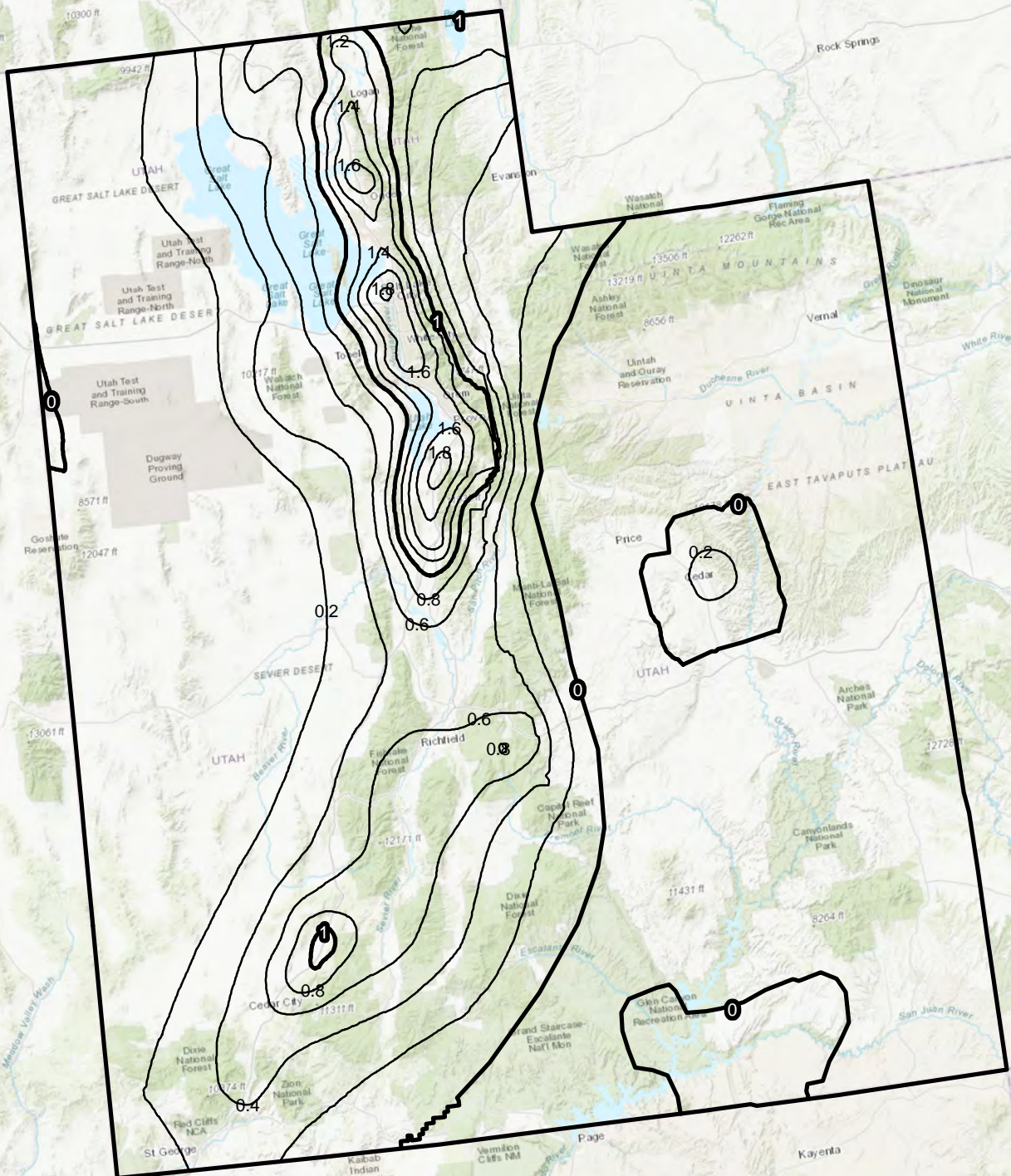


**Reference Vertical Strain
Boulanger and Idriss 2014
1033 Year Return Period
Contour Interval: 1 Contour = 0.2 (%)**



Service Layer Credits: Sources: Esri, HERE, Garmin, Intermap, increment P Corp., GEBCO, USGS, FAO, NPS, NRCAN, GeoBase, IGN, Kadaster NL, Ordnance Survey, Esri Japan, METI, Esri China (Hong Kong), swisstopo, © OpenStreetMap

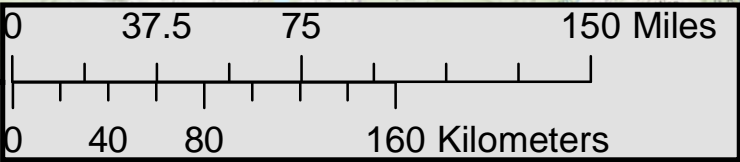
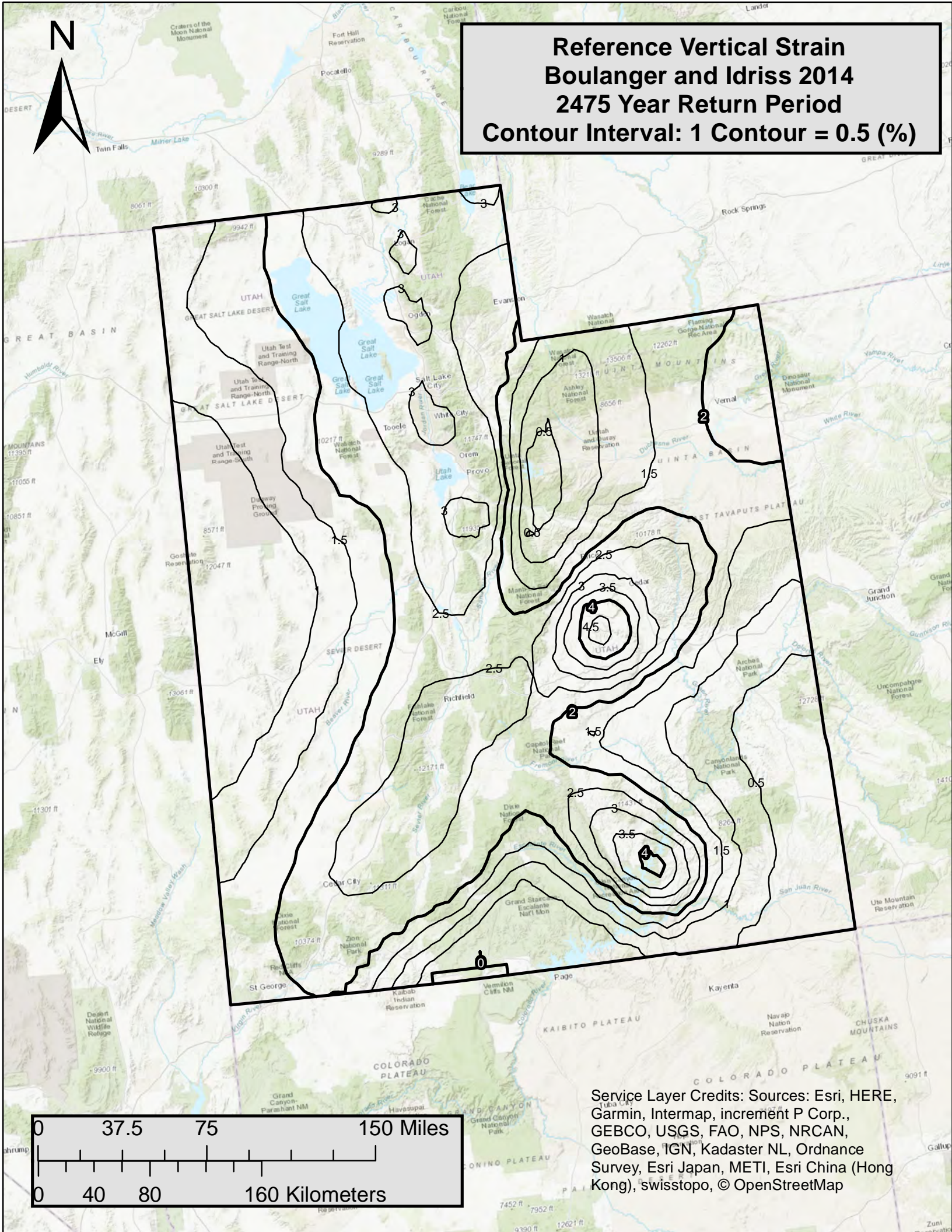
Reference Vertical Strain
Ku et al. 2012
1033 Year Return Period
Contour Interval: 1 Contour = 0.2 (%)



Service Layer Credits: Sources: Esri, HERE, Garmin, Intermap, increment P Corp., GEBCO, USGS, FAO, NPS, NRCAN, GeoBase, IGN, Kadaster NL, Ordnance Survey, Esri Japan, METI, Esri China (Hong Kong), swisstopo, © OpenStreetMap

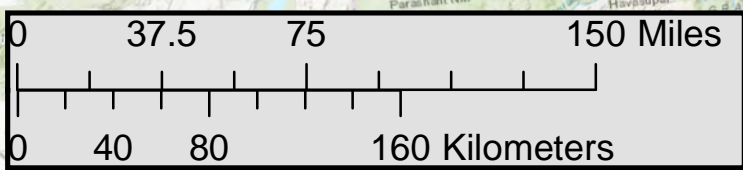
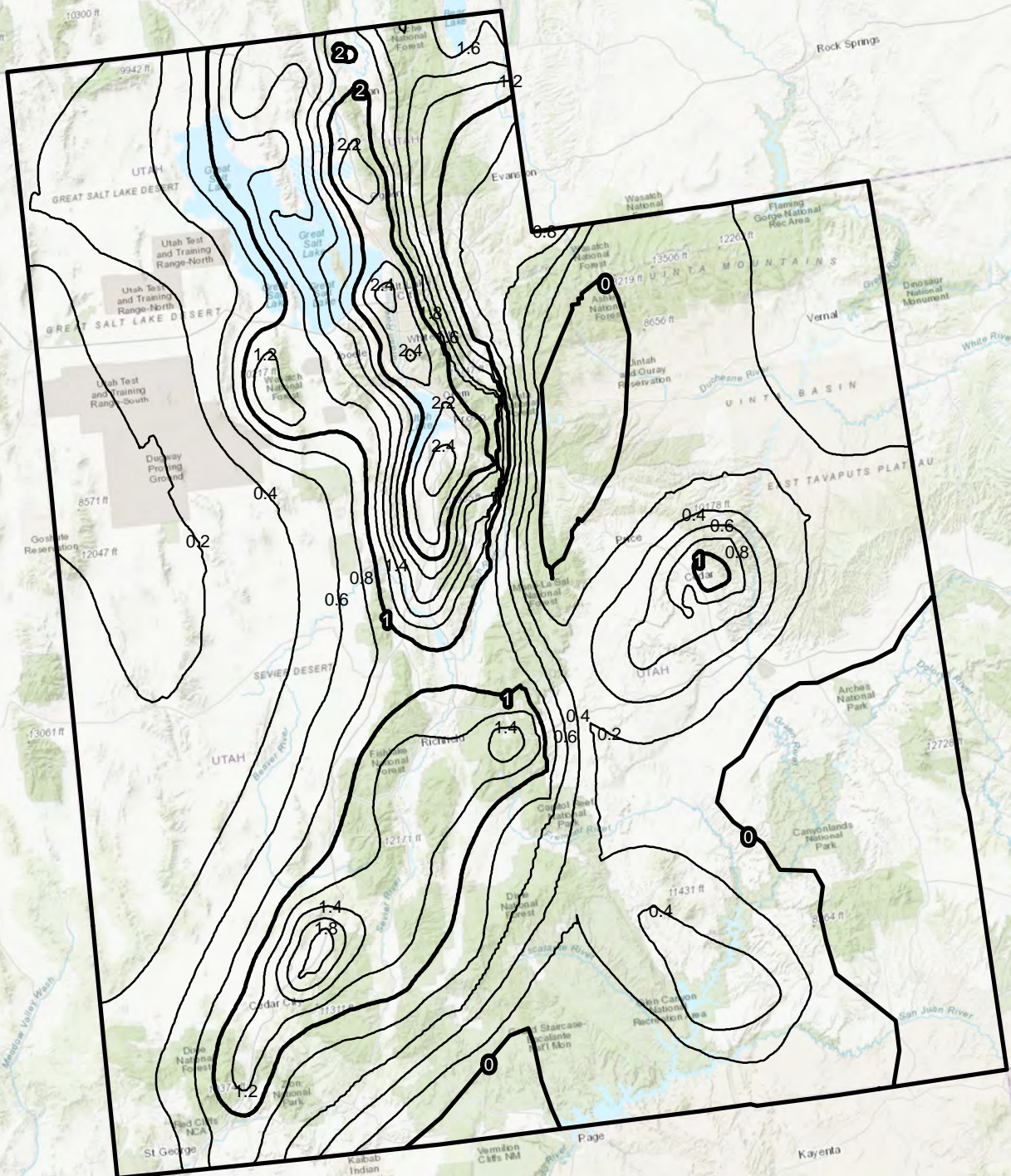


**Reference Vertical Strain
Boulanger and Idriss 2014
2475 Year Return Period
Contour Interval: 1 Contour = 0.5 (%)**



Service Layer Credits: Sources: Esri, HERE, Garmin, Intermap, increment P Corp., GEBCO, USGS, FAO, NPS, NRCAN, GeoBase, IGN, Kadaster NL, Ordnance Survey, Esri Japan, METI, Esri China (Hong Kong), swisstopo, © OpenStreetMap

Reference Vertical Strain
Ku et al. 2012
2475 Year Return Period
Contour Interval: 1 Contour = 0.2 (%)



Service Layer Credits: Sources: Esri, HERE, Garmin, Intermap, increment P Corp., GEBCO, USGS, FAO, NPS, NRCAN, GeoBase, IGN, Kadaster NL, Ordnance Survey, Esri Japan, METI, Esri China (Hong Kong), swisstopo, © OpenStreetMap